Technical Report

DIFFUSION FROM A CONTINUOUS POINT SOURCE INTO THE BOUNDARY LAYER DOWNSTREAM FROM A MODEL HILL

by

E. J. Plate and C. M. Sheih
Fluid Dynamics and Diffusion Laboratory

U. S. Army Research Grant
DA-AMC-28-043-65-G20

Department of Civil Engineering
Colorado State University
Fort Collins, Colorado

December 1965

CER65EJP-CMS60

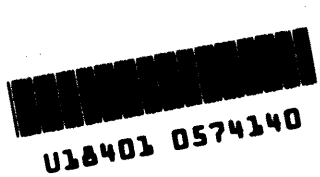

TABLE OF CONTENTS

DIFFUSION FROM A CONTINUOUS POINT SOURCE INTO THE BOUNDARY LAYER DOWNSTREAM FROM A MODEL HILL

by

E. J. Plate* and C. M. Sheih**

1. INTRODUCTION

The problem of diffusion in a disturbed boundary layer is of great importance from a theoretical and a practical point of view. Theoretically, a disturbed boundary layer can be interpreted as a wall boundary layer with a superimposed field of decaying turbulence which is generated by the disturbance. In such a flow field, diffusion solutions for an undisturbed boundary layer are no longer applicable, and the mechanism of turbulent decay must be taken into consideration.

From a practical point of view, a bounday layer which is disturbed by obstacles at the wall is much more common than the ideal case of an undisturbed boundary layer. However, since disturbances can be generated by infinitely many different types of obstructions, it is important to study models which represent the scaled down versions of common type disturbances, with the hope that the results can be used as building blocks from which effects of more general disturbances can be constructed. Therefore, an initial study had been made in which the diffusion cloud emanated from a line source of ammonia located at a distance of 1.5 ft upstream from an "impulse disturbance" formed by a two-dimensional fence. The results of this program have been prepared for publication, and a pre-publication form of the paper is appended to this report.

---

* Associate Professor
** Graduate Research Assistant

In the present study the obstruction consisted of a two-dimensional model of sinusoidal shape which extended over the whole width of a wind tunnel floor. A continuous point source of helium was placed at the crest of the model in the centerline of the wind tunnel. The situation is shown in Fig. 1. Three different models, all shaped like a half sine wave (i.e., described by a curve $z = h \cos \pi \frac{x}{b}$ for $-1/2\,b \leq x \leq +1/2\,b$) were used. The model dimensions are listed in Table 1, in which h denotes the maximum height, b the width at the base of the model, while u_∞ is the nominal velocity of the ambient air determined at a distance of 3 ft. upstream from the model in the center of the wind tunnel.

TABLE 1: Test Cases

Model Shape		Velocity	Source Location	
h(in)	b(in)	u_∞ (fps)	x(in)	z(in)
1	10	20	0	1
2	10	10, 20, 40	0	2
4	20	20	0	4

The experimental data were taken at different distances x. At each distance, four concentration profiles and three velocity profiles were taken. The concentration profiles consisted of a horizontal profile taken at a distance z of 0.125 in. from the wind tunnel floor. On the basis of this profile, the maximum concentration was determined and a vertical profile was measured at the vertical section where the maximum occurred. Then, two more horizontal profiles were taken at distances above the floor at which the concentration of the vertical profile had decreased to one-half and one-quarter of the maximum (usually the ground) concentration. The four profiles are sufficient to map out the diffusion cloud at each distance x.

Velocity profiles were taken at the centerline of the tunnel and at distances of 4 inches to the right and the left of the centerline. The three profiles were augmented by a number of horizontal profiles which are measured to permit an evaluation of three-dimensional effects of the flow on the concentration distribution.

No detailed analysis of the experimental data will be given in this report. Instead, it will be investigated how the data compare with those obtained in the appended paper (which shall henceforth be called paper A). The data of this study have some great advantages over the fence data. They are obtained with a point source. Therefore, conclusions can be drawn on the lateral diffusion of a helium cloud in a disturbed boundary layer. They are taken with a vastly improved sampling system (with a mass spectrometer type leak detector) which permitted not only faster but also more accurate measurements. And finally, they are taken with the obstructing models immersed in a much thicker boundary layer, so that there exists a reasonable hope that results for the intermediate zone discussed in paper A can be obtained from the experimental data.

The disadvantage of developing a thick boundary layer in the wind tunnel is that three-dimensional secondary flows are set up due to the presence of the corners of the wind tunnel. These can, at large distances downstream from the wind tunnel entrance, give rise to a very distinct three-dimensional flow pattern downstream from the models. The three-dimensional flow finds its expression in quite different mean velocity profiles at the three locations for each distance x . Generally, the profiles right and left of the centerline have, at the same elevations, larger velocities than the velocity of the profile at the centerline. Therefore, there must exist a velocity component directed toward the center and upward which can have an effect on the spreading of the diffusion cloud. However, no corrections will be made for the secondary flow, and all velocity distributions which are analyzed consist of averages of the three velocity profiles taken.

2. EXPERIMENTAL EQUIPMENT AND PROCEDURES

The experiments were performed in the large U. S. Army Meteorological Wind Tunnel located in the Fluid Dynamics and Diffusion Laboratory of Colorado State University. The wind tunnel has been described in detail by Plate and Cermak (1963). The instruments used are part of the standard laboratory equipment with the exception of the mass spectrometer leak detector. The wind tunnel and the instruments used are briefly described.

2.1 The Wind Tunnel

The wind tunnel is of recirculating type. It is shown in Fig. 2. The models were placed at a distance of 40 ft downstream from the inlet of the test section. The boundary layers along the walls of the tunnel were artificially tripped to become turbulent by a heavy saw-tooth fence followed by a 4 ft section of 3/8 inch gravel fastened all around the exit portion of the transition section.

The air speed in this wind tunnel is controlled with a variable speed, variable pitch aircraft propellor. The temperature of the ambient air is maintained at a constant level by means of an air conditioning system. The pressure in the test section was kept constant by adjusting the ceiling of the test section before the model was installed. Since the test section has a cross sectional area 6 x 6 ft^2, the blockage offered by the models was considered negligibly small.

2.2 Instrumentation

The measurements consisted of velocity distributions for the mean velocities, and of mean concentrations. Pressure distributions, turbulence quantities, etc. have not been determined for this study, but reference can be made to Plate and Lin (1965) for some measurements of these variables.

2.2.1 Velocity measurements. The velocity distributions were measured with a pitot static tube of standard (Prandtl) design. The two pressure ports of the tube were connected to the two ports of an electronic differential pressure transducer (Transonic Equibar Type 120) which provides a DC output proportional to the differential pressure. This DC-voltage was applied to the Y - axis of an X - Y plotter (Moseley Type 135). To the other axis of the plotter, a voltage was applied which was obtained across a potentiometer. The potentiometer was geared to the drive screw of a motor driven positioning device and, thus, provided a resistance proportional to the distance of the probe from the ground. In this manner, continuous profiles were obtained of the dynamic pressure.

The pressure transducer was calibrated about once a week against a water manometer which was used as primary standard. The position potentiometer and the amplifier of the X - Y plotter X- axis were calibrated against measured distances before each run, or before each set of runs, if no interruption of the test sequence was required.

2.2.2 Concentration measurements. The gas feed and sampling system is shown schematically in Fig. 3. The continuous point source was supplied with helium directly from the pressurized bottle. The flow rate of helium was controlled by using a pressure regulator at the bottle outlet and by passing the gas through a sensitive flow meter. The exit velocity of the gas was set at approximately 20 fps regardless of velocity conditions in the air surrounding the source.

The air was sampled continuously by means of a probe to which a vacuum pump applied negative pressure. The suction line was connected through a T - section to the inlet leak of the mass spectrometer. The leak detector continuously sampled the helium content of the gas - air flow and gave an electrical (dc-volt) output which is applied to the X - axis of an

X - Y plotter. The Y - axis of the recorder is calibrated against distance as for the velocity measurements. However, because of the slow response of the mass spectrometer, continuous profiles could not be taken. Instead X - amplifier of the plotter was switched to time base, and a plot of output voltage from the mass spectrometer vs. time was obtained for selected elevations. A typical result is shown in Fig. 4. The experimental results in output volts of the mass spectrometer were converted into concentrations by means of a calibration chart.

An example of the calibration is shown in Fig. 5. It had been found during an initial study that a drift in the mass spectrometer output due to dirtying of the filament of the mass spectrometer tube caused a change in the magnitude of the concentration measurements which resulted in a perfect parallel shift of the calibration curve on double logarithmic paper. Therefore, before each data point was taken, a one-point calibration was made with a helium-nitrogen mixture of known helium concentration (0.05, 0.2, or 0.5 %). The calibration curves were extended to lower than the calibrated concentrations by extending the calibration curves parallel to the original calibration curve supplied by the manufacturer. No error analysis has been made, because the data were found to be almost completely reproducible. Any discrepancies between data obtained at different days could be attributed to slight differences in feed rates or sampling probe position. The data are considered to be precise within 5% .

3. RESULTS

The results consist of mean velocity and concentration distributions. They are tabulated in Tables 2 to 5.

3.1 Velocity Distribution Data

The velocity distribution data show the typical behavior of a disturbed boundary layer as was discussed extensively by Plate (1966). At some

distance downstream from the hill model, the disturbed boundary layer consists of two portions: an inner boundary layer, which develops along the wall in agreement with laws applicable to smooth flat plates, and an outer boundary layer which reflects the effect of the hill model on the profile. Both profiles are connected through a suitable blending region.

However, in contrast to the data in paper 1, the ranges of initial boundary layer thickness δ_o (i.e., the thickness of the boundary layer at the location of the model crest, but before the model was placed on the wind tunnel floor) to the height h of the model, covers a wide enough range to show the three significantly different types of profile development observed by Plate (1966).

3.1.1 Profile Type 1. The effect of the hill model is not found in the outer portion of the boundary layer which appears as if the hill had not been there at all. This case is best illustrated in Fig. 6. The small hill model of 1-inch height, with its gentle slopes, produced only local profile disturbances in the lower layer of the boundary layer. It appears possible to analyze this condition by a small perturbation method, in which the small perturbations are set up by the hill model. Such an analysis shall be tried in the near future.

3.1.2 Profile Type 2. This profile type, which is illustrated in Figs. 7, 8, and 9, corresponds to moderate ratios of δ_o/h. The profile consists of two well defined logarithmic profiles. The inner profile obeys the law of the wall, i.e., its slope is determined by the shear stress at the wall. The outer profile differs from the outer profile of a boundary layer along a smooth wall. It assumes the shape of a straight line on the logarithmic plot, but the slope of this line is not given by the wall conditions, but

by the hill model -- in a manner which has not yet been fully clarified. It seems, as is discussed in paper A, that the hill induces a shear stress near the separation streamline which is larger than that found on the wall of a smooth plate. It appears that a constant stress layer is formed in the outer flow of the boundary layer, which is joined to the second constant stress layer near the wall. The difference in shear stresses in the two layers results in a transition region of shear stresses between the two layers which broadens. Ultimately, the shear transition layer covers the whole outer boundary layer. This is evident in Fig. 9, where, at x = 180 inches, the profile has assumed again a shape which is typical of a velocity profile in the undisturbed boundary layer along a smooth flat plate.

3.1.3 Profile Type 3. The third profile type occurs when the ratio of the model height to the height of the boundary layer becomes large. In such cases, the shear stress in the outer layer appears to be still constant for a given distance from the hill crest x , but it is so large that it cannot be preserved. Consequently, the shear stress is reduced with distance, and this implies that the slope of the logarithmic outer profile changes with distance. Or, another explanation might be that the difference between the shear stress in the inner boundary layer and in the outer boundary layer is so large that the transition zone between the two boundary layers grows much more rapidly than in the cases of Profile Type 2. An analysis of this situation with a two layer model consisting of two equilibrium profiles, along the lines suggested by Townsend (1965) might be fruitful, but has as yet not been attempted.

3.1.4 The development of the boundary layer thickness. The boundary layers which are disturbed by a fence show a significant increase of boundary layer thickness with fence height, as is shown in paper A. This behavior is not found for the bounday layers in the Army Wind Tunnel which were disturbed by the sinusoidal hill models, as is evident in Fig. 11. Also, the boundary

layer thickness increases with velocity u_∞ (see Fig. 12). It is at present not certain whether this can be attributed to lack of two-dimensionality due to the development of the corner eddies in the test section, whether this is induced by the coarse gravel at the inlet section, or whether this is a real phenomenon which would occur for any very long smooth flat plate.

The boundary layers thicknesses δ shown in Figs. 11 and 12 were defined as that distance from the wall at which the local mean air velocity had reached a value of $0.99\ u_\infty$. Small adjustments for the values thus found were made in order to obtain best coincidence of the velocity profiles in Fig. 6 to 10.

3.2 The Concentration Profiles

The investigation of the concentration profiles is directed towards determination of the similarity law for both the vertical and the horizontal concentration distributions. Furthermore, it is determined how the similarity parameters for the profiles vary with distance x, with velocity u_∞, and with height of the model hill. The similarity parameters are tabulated in Table 4. The experimental data for the vertical concentration distributions are given in Table 5. In Table 6 the experimental data for the horizontal concentration measurements are summarized.

3.2.1 Similarity profiles for the concentration distributions. Typical examples of concentration distributions are given in Figs. 13 and 14. Fig. 13 shows vertical concentration distributions, and Fig. 14 horizontal concentrations. Apart from indicating the impressive accuracy of the experimental data, they suggest representing the profiles in a unifying non-dimensional form.

Vertical concentration distributions have been non-dimensionalized by dividing the distances z through the values λ, and the concentrations

c by c_{max} . The length scale λ was defined as that distance from the wall at which the local concentration has decreased to half the value at the ground level. The ground level concentration is usually the largest concentration and is designated with c_{max} .

Non-dimensional vertical distributions of concentrations are shown in Figs. 15 and 16. They reveal the remarkable result that, for low velocities and for the small hill models, the concentration distribution is almost linear. Only at large velocities, or for the high hill model (2" x 20") do the non-dimensional profiles show significant curvature. Near the outer edge of the profile, the concentrations decrease more gradual than would be required by a linear profile, but for most of the other profiles, linearity seems to be well established. Of course, the fact that any concentration profile would have to have a point of inflection contributes to make the profiles appear linear, but if the data of this study are compared with the data of paper A, the difference is still remarkable.

If one concentrates on the development of the profiles with distance, it is noticeable that a marked deviation from a "universal" distribution law occurs only very near the models where most of the concentration is found near the ground, and a very rapid decrease takes place shortly above $y = \lambda$. This behavior near the model is expected because in the separation bubble which exists shortly downstream from the model, only small vertical concentration gradients are possible, while the strong turbulence which is generated near the separation stream line will develop only after a short distance, so that vertical spreading of the concentration cloud is limited.

Fig. 17 shows examples of lateral concentration profiles which have been non-dimensionalized by dividing the lateral distance y

(measured from the centerline of the wind tunnel) through the distance η, measured from the centerline, at which the concentration has decreased to one-half its value at the centerline c_c. The profile shapes are independent of both distance from the wall and distance downstream from the hill models. Also, no change in profile shape with model type can be recognized. Therefore, Fig. 16 shows only one case, which corresponds to the 4 x 20 sinusoidal hill model.

Horizontal and vertical concentration profiles can be combined into isoconcentration maps for different distances x, as is shown in two examples in Figs. 18 and 19. The examples show the good consistency of vertical and horizontal data. But they show also a rather larger growth in the vertical direction of the concentration cloud than to the sides. The possibility cannot be disregarded that this is an effect of the three-dimensionality of the mean velocity distribution field, as has been discussed previously.

3.2.2 The similarity parameters. There remains to show the development of the similarity parameter in space. The vertical length parameter λ is shown in Fig. 20 as function of x with hill sizes as third variables. Also, given in Fig. 20 is the growth of a diffusion cloud which has been emitted from a continuous ground level point source into the boundary layer along a smooth flat plate without distortion. The latter case had been studied previously by Malhotra and Cermak (1963). Our data lie consistently higher than those of Malhotra and Cermak which must be attributed again to the updraft velocity in the center of the wind tunnel. In fact, it appears that a possible way of correcting for the vertical velocity induced by the corner eddies of the wind tunnel might be found from this difference between our data and those of Malhotra and Cermak (1963).

The data for the 1-inch hill follow the trends set by the smooth flat plate. There seems to be no difference whatsoever. This result is in agreement

with the velocity distribution development shown in Fig. 6. Only the innermost portion of the boundary layer "feels" the presence of the hill, and since in this inner layer the concentration gradients are very small, the effect of the hill on the concentration profile can easily be covered up by the random variations of the data caused by experimental error.

Perhaps the most remarkable result of the study is the confirmation of the growth law for for λ which was found for the fence-disturbed boundary layer of paper A . For hill models which might be suspected of having separation occurring near their crests, the value of λ increases approximately according to a power law with $\lambda \propto x^{0.5}$. As had been pointed out previously by Plate and Lin (1965), this corresponds to the spreading of a wake in free shear flow, in contrast to the 0.8 power which is valid for a boundary layer, or an internal boundary layer, as is discussed in paper A . The 0.5-power law for the growth of λ is therefore a feature which is peculiar to the flow, and which is not induced by the presence of the boundary layer edge, as could have been reasoned for the case of the fence-disturbed boundary layer.

For the data of this study, λ increases slightly with velocity, as shown in Fig. 21.

The horizontal width parameter η is shown in Fig. 22 as function of distance x, at $z = 1/8$-inch, with u_∞ as third variable. The y values can be presented by a power law of the form

$$\eta \propto x^{0.3}$$

where the factor of proportionality decreases with increase in velocity.

If the variation of η with x and model type is studied, which is shown in Fig. 23, it is noticed that again the 1 x 10 sinusoidal hill does not introduce any significant disturbance. The higher hills, on the other hand, have η-values which initially grow much more rapidly than the flat plate data. But for larger distances both the 2 x 10 and the 4 x 20 hill follow the same power laws.

4. CONCLUSION

In this report, experimental data are given which pertain to the diffusion from an elevated continuous point source into a boundary layer along a smooth flat plate which has been distorted by a sinusoidally shaped model hill. No analysis of the data beyond consistency plots has been given. The consistency plots confirm earlier conclusions in a paper by Plate (1965) which is appended to the present report.

The velocity profiles in the disturbed boundary layer show three different types of redevelopment of the boundary layer. Apparently, it is necessary that separation occurs on the model if the outer part of the mean velocity profile is to be affected by the presence of the model. This is confirmed by the diffusion data which showed that the diffusion characteristics do not differ for the case of a smooth flat plate and the case with the 1 x 10 sinusoidal model.

If separation occurs at the model, then a significantly more rapid increase in the concentration plume height and width is obtained in the neighborhood of the model. But further downstream, the rate of growth of the plume dimensions is decreased, so that at some large distance downstream the plume in an undisturbed boundary layer might have the same geometry as the plume of a disturbed boundary layer.

The many interesting results give some illuminating insights into diffusion processes in disturbed boundary layers. The detailed analysis of the data, which shall follow this report, might furthermore produce quantitative answers. A first step towards such a goal is made in the appended paper by Plate (1965).

REFERENCES

Malhotra, R. C., and J. E. Cermak (1964), "Mass diffusion in neutral and unstably stratified boundary-layer flows," Int. J. Heat Mass Transfer, Vol. 7, pp. 169-186.

Plate, E. J. (1966), "Ein Beitrag zur Berechnung von Austaus chvorgängen in der durch eine Wand gestörten bodennahen Lufts chicht." Dissertation submitted to the Department of Civil Engineering, Technische Hochschule Stuttgart, Stuttgart, Germany.

Plate, E. J., and J. E. Cermak (1963), "Micrometeorological wind tunnel facility description and characteristics." Final report on Contract No. DA-36-039-SC-80371, U. S Army Electronic Proving Ground Procurement office, U. S. Army Signal Supply Agency, Fort Huachuca, Arizona.
CER63EJP-JEC9.

Plate, E. J., and C. W Lin (1965), "The velocity field downstream from a two-dimensional model hill." Final report, Part I. to U. S. Army Materiel Agency under Contract DA-AMC-36-039-63-G7.
CER65EJP-CYL14.

Townsend, A. A. (1965), "Self preserving flow inside a turbulent boundary layer." J. Fluid Mech, Vol. 22, pp. 773-797.

NOTATION

b	= base width of model	(in.)
c	= local concentrations of helium	(ppm)
c_c	= centerline concentration for lateral concentration profiles	(ppm)
c_{max}	= max concentration of a concentration profile	(ppm)
δ	= boundary layer thickness	(in.)
δ_o	= thickness of the undisturbed boundary layer at the model location	(in.)
η	= length scale of horizontal concentration distribution	(in.)
h	= maximum model height	(in.)
λ	= vertical length scale of the concentration profiles	(in.)
u_∞	= ambient reference velocity	(fps)
x	= distance parallel to wind tunnel floor, measured from the model crest	(in.)
y	= coordinate parallel to model axis	
z	= vertical distance from the wind tunnel floor	(in.)

APPENDIX 1

FIGURES

FIGURES

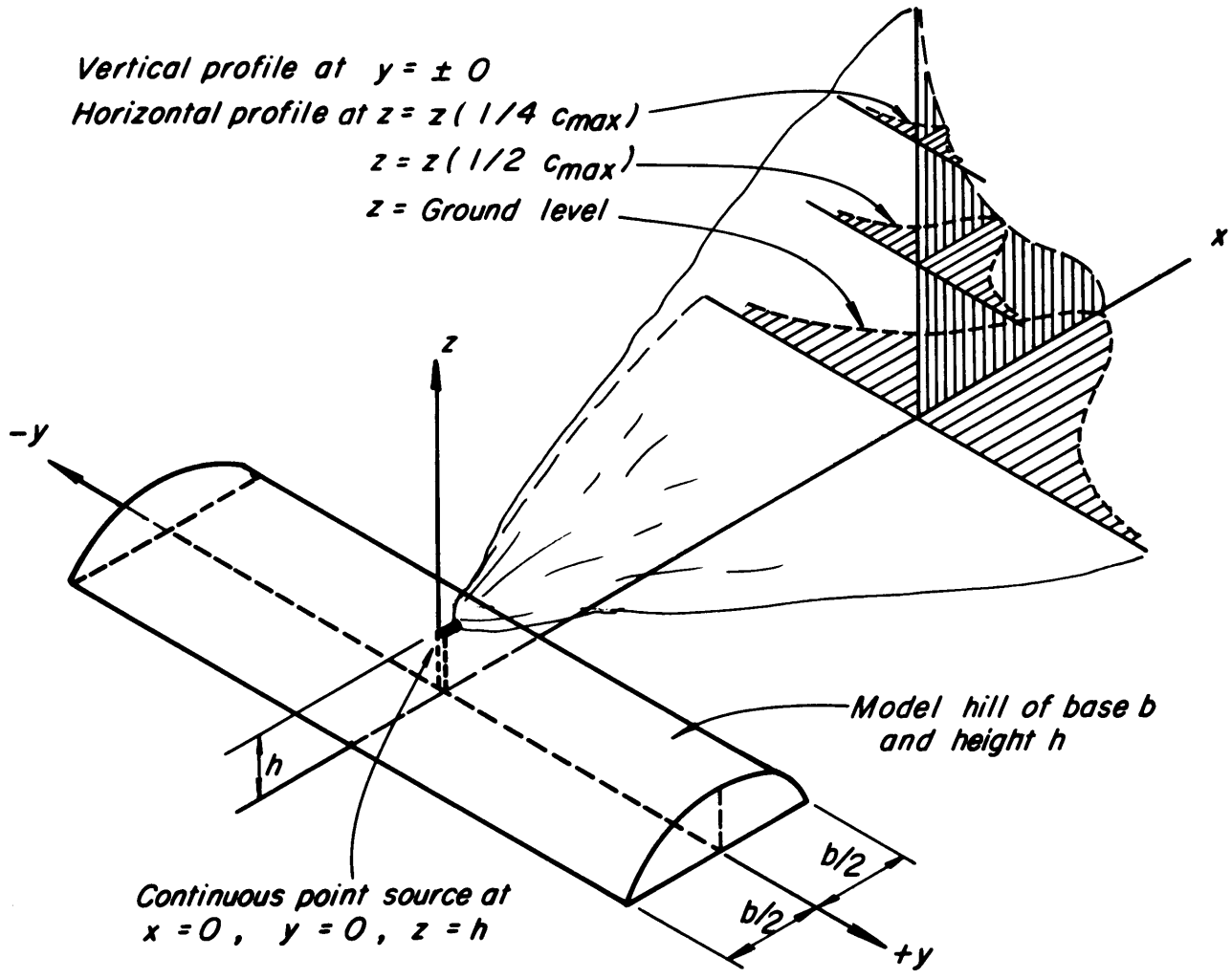

Fig. 1 Definition of problem

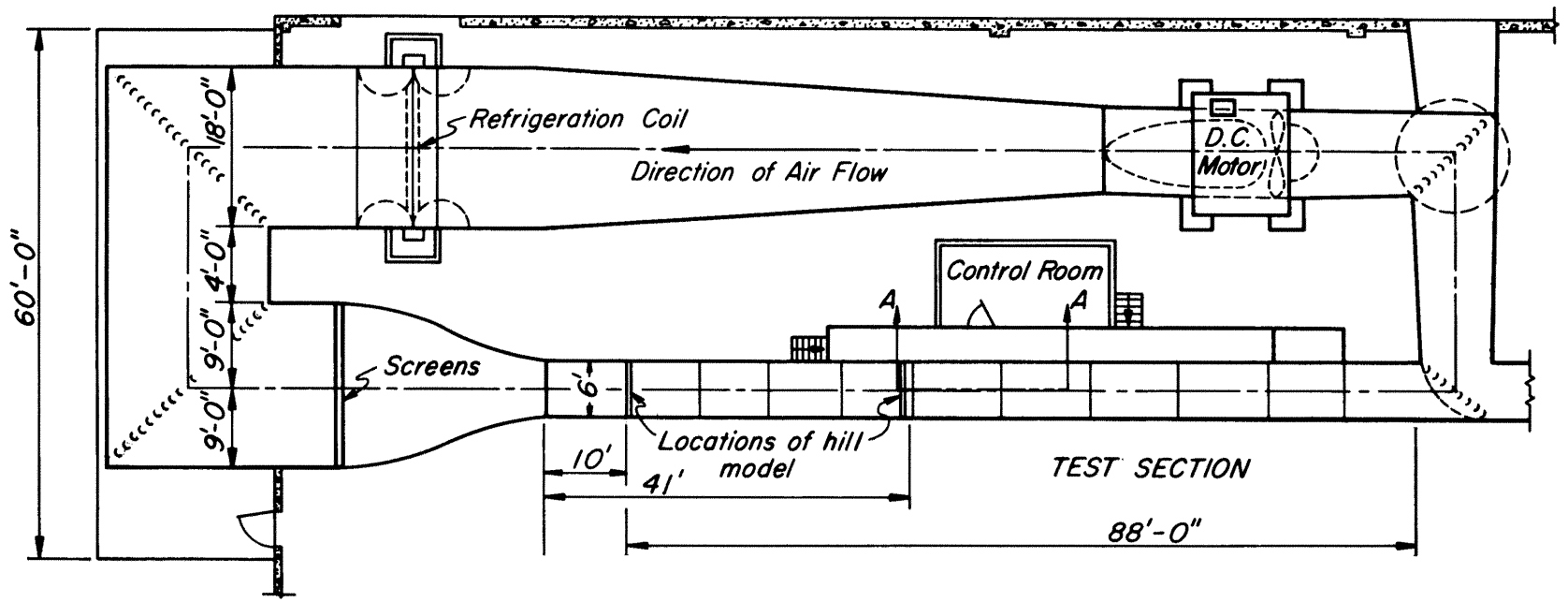

PLAN VIEW

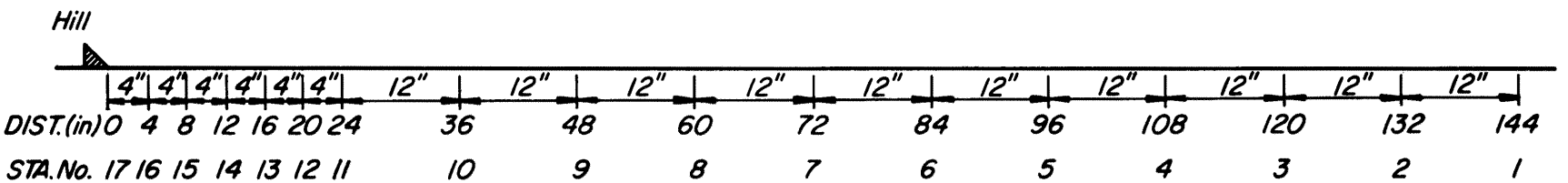

SECTION A—A

Fig. 2 Large wind tunnel.

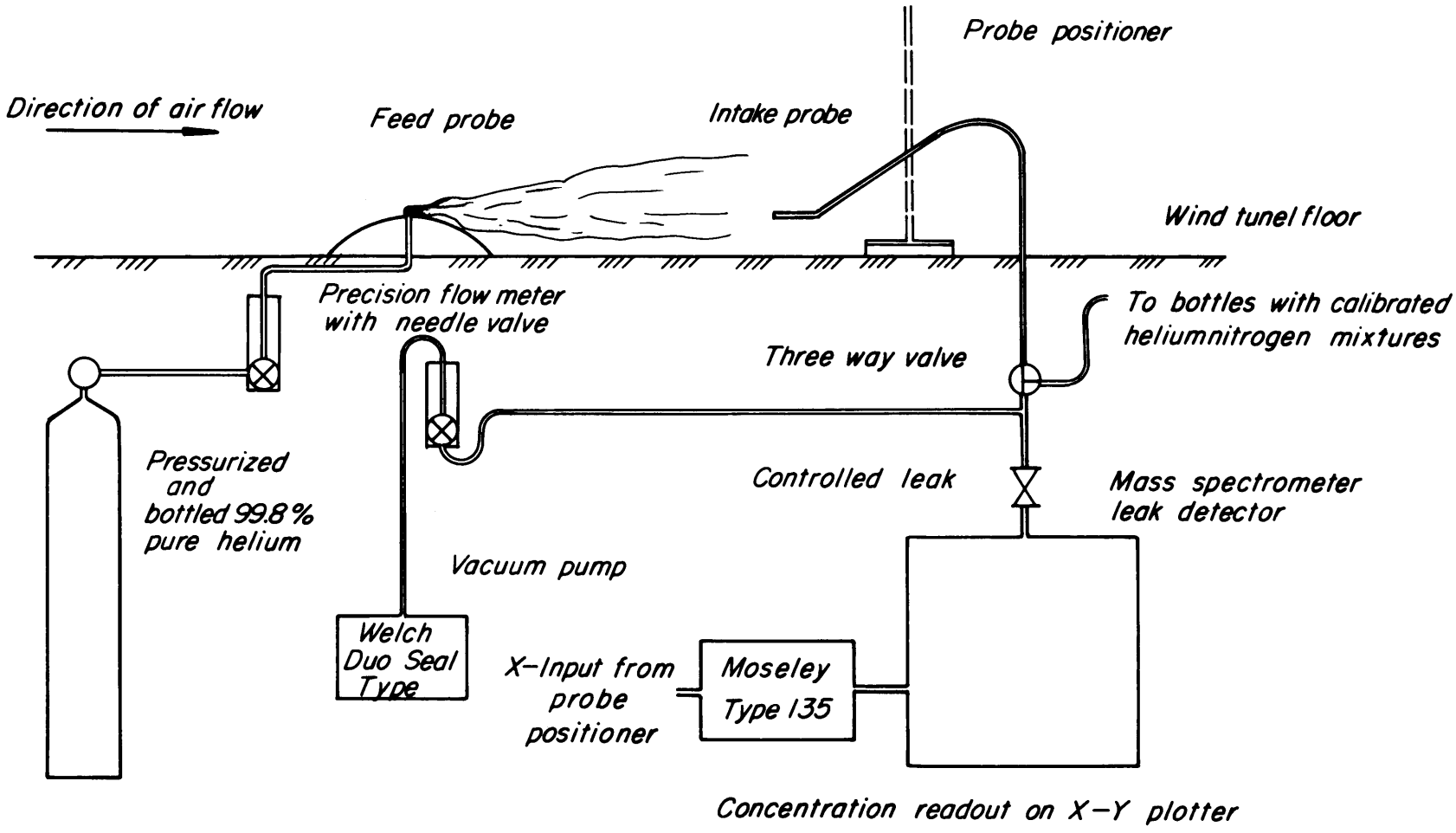

Fig. 3 Schematic view of gas feed and sampling system.

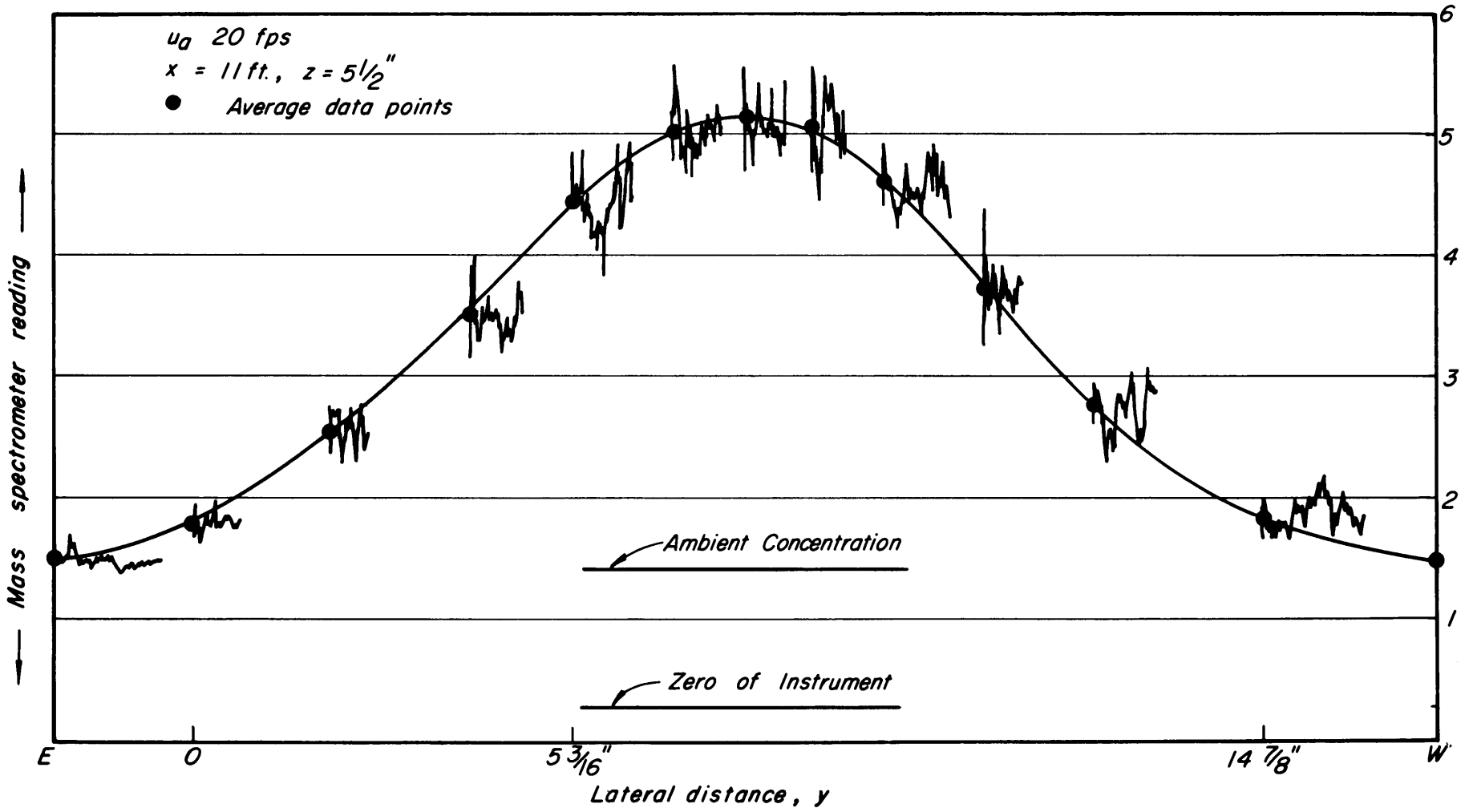

Fig. 4 Example of data recording with mass spectrometer and x-y-recorder.

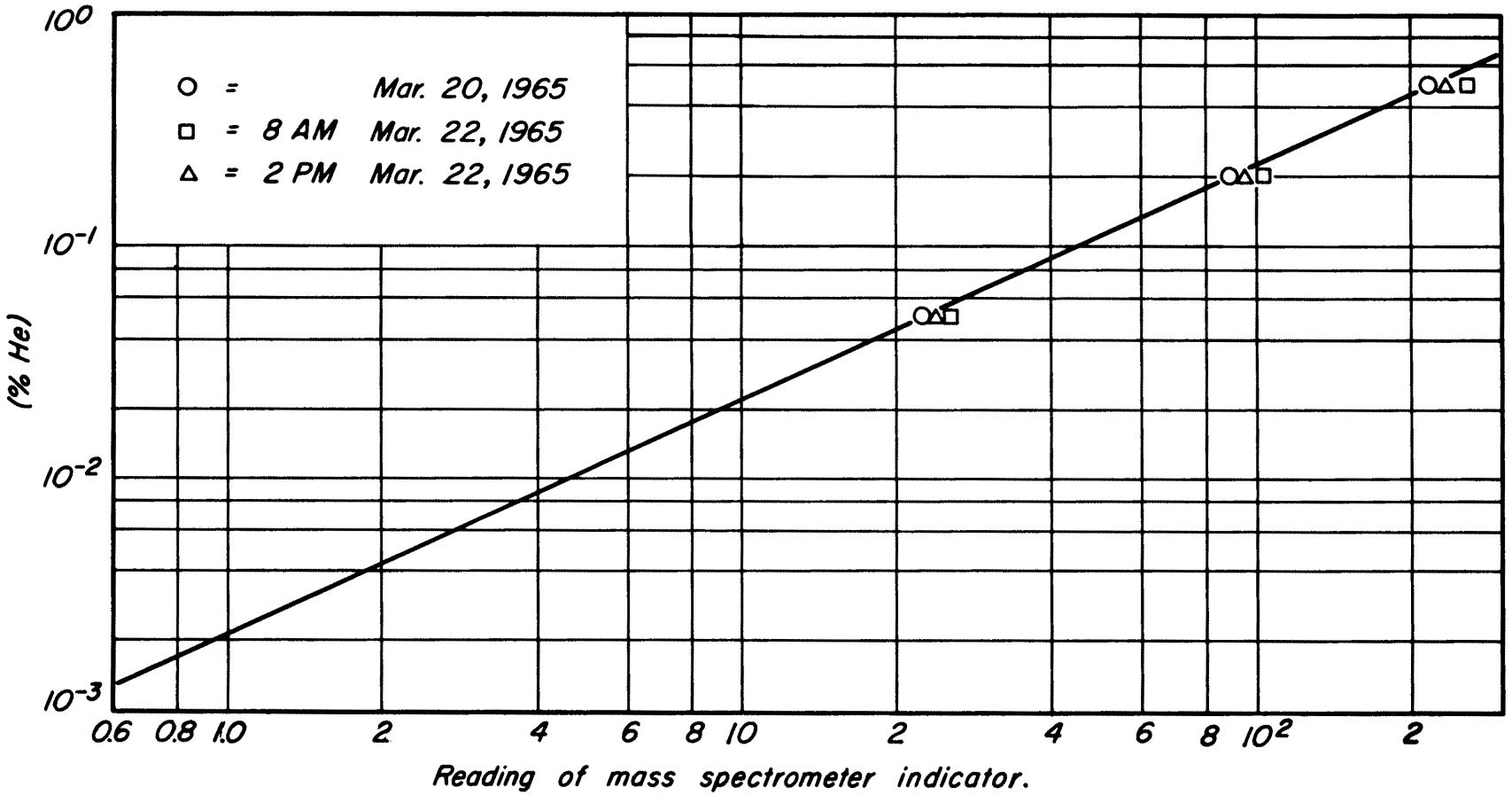

Fig. 5 Typical calibration of mass spectrometer.

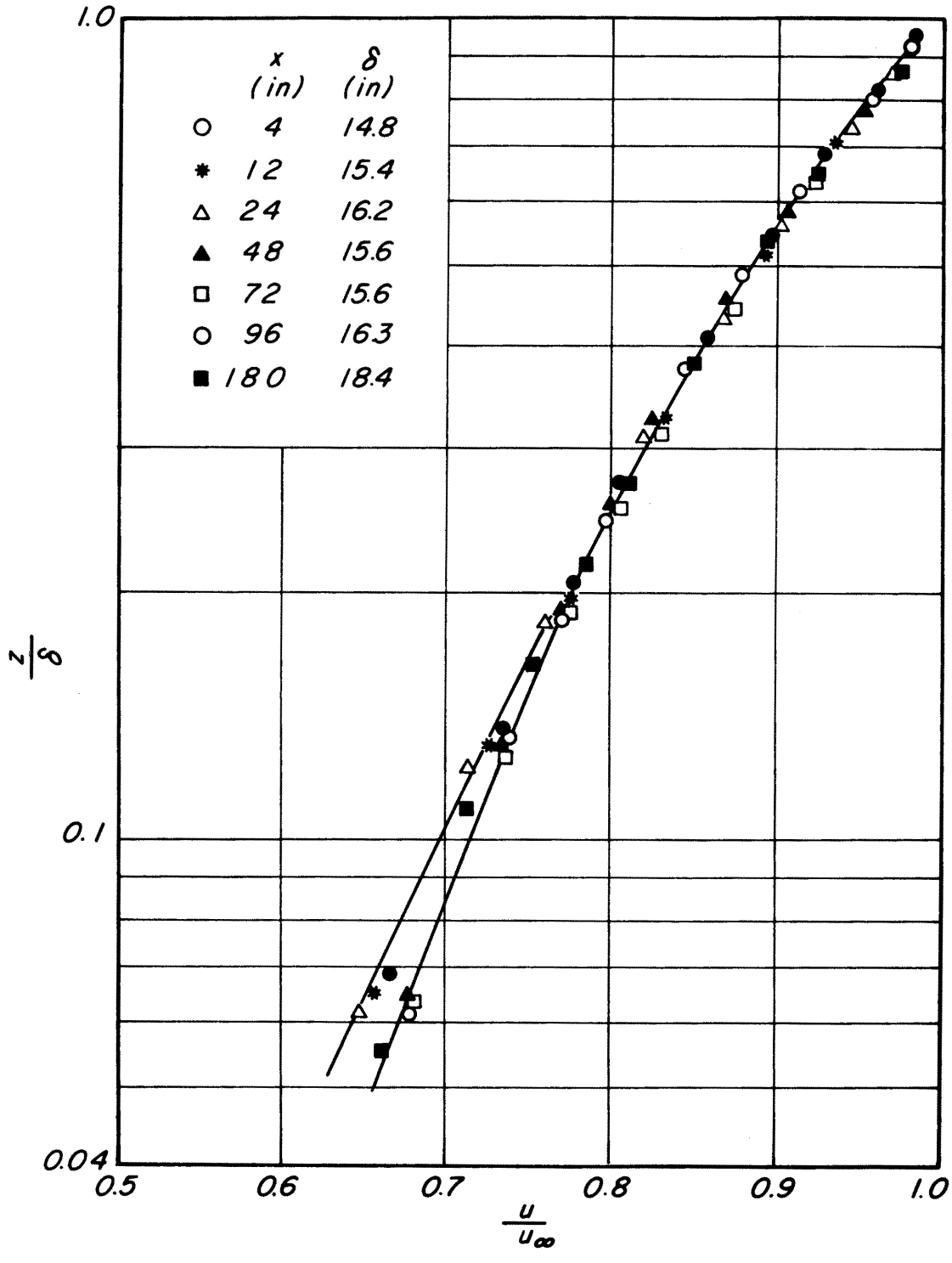

Fig. 6 Dimensionless velocity distributions.

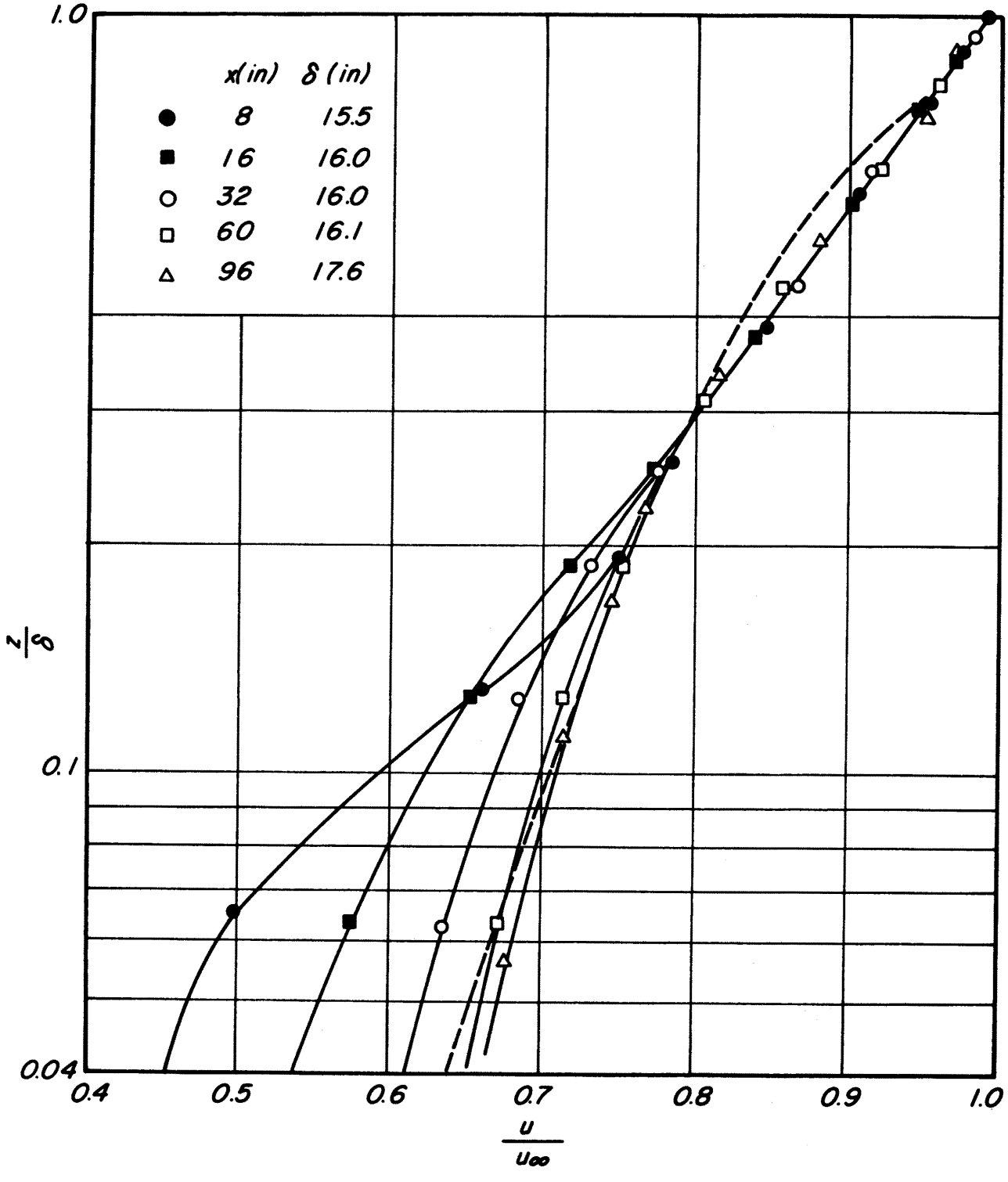

Fig. 7 Dimensionless velocity distributions.

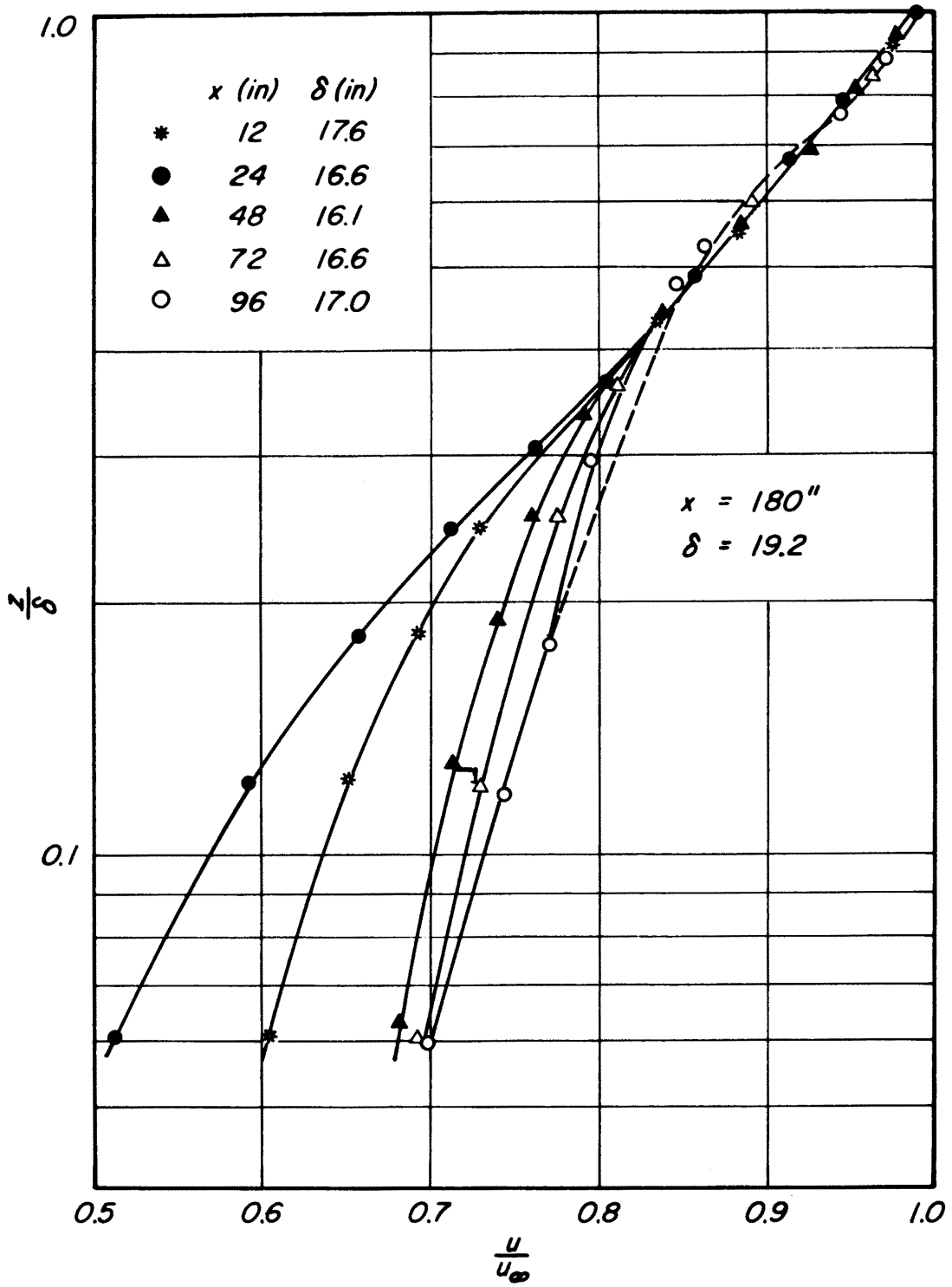

Fig. 8 Dimensionless velocity distributions.

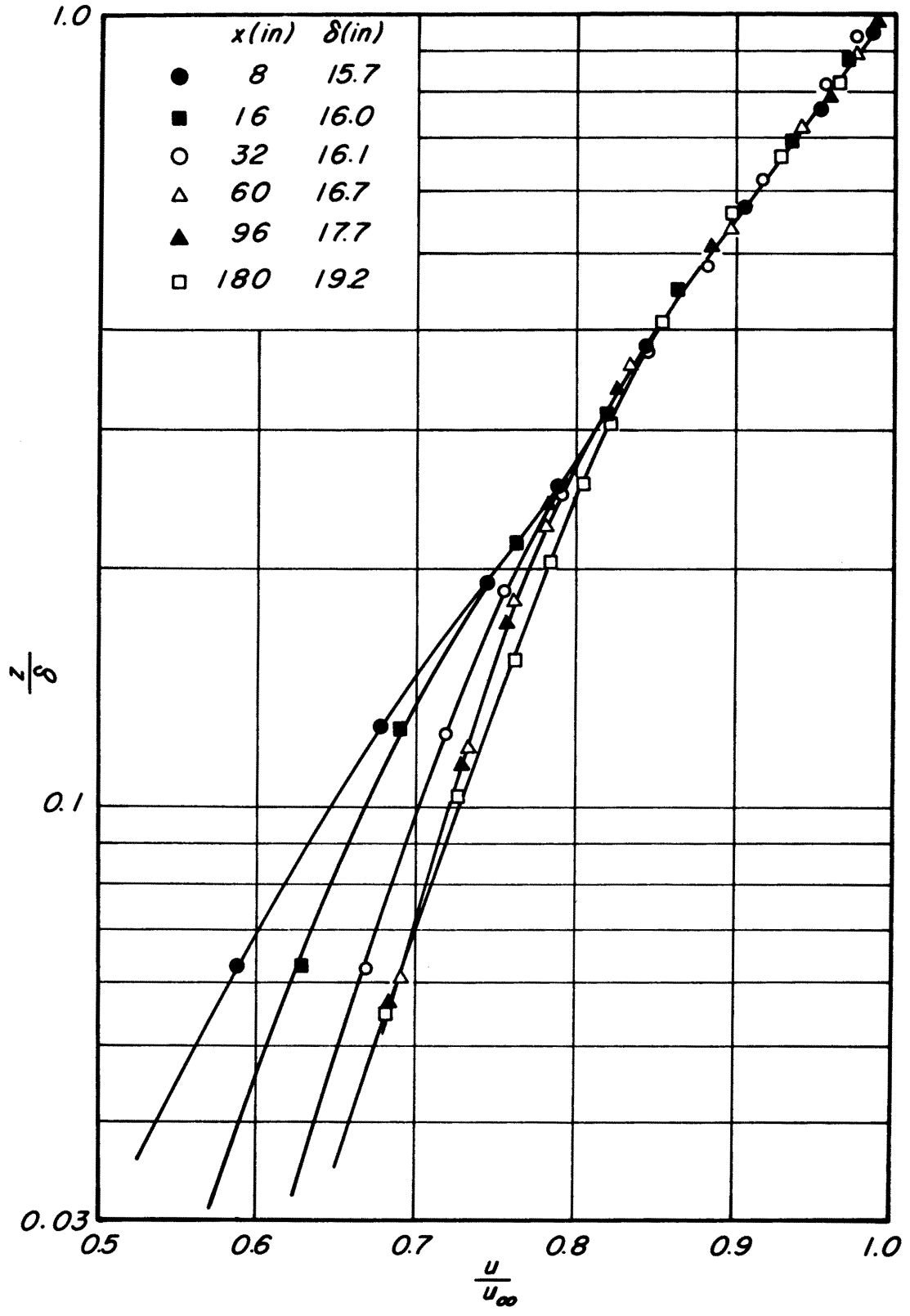

Fig. 9 Dimensionless velocity distributions.

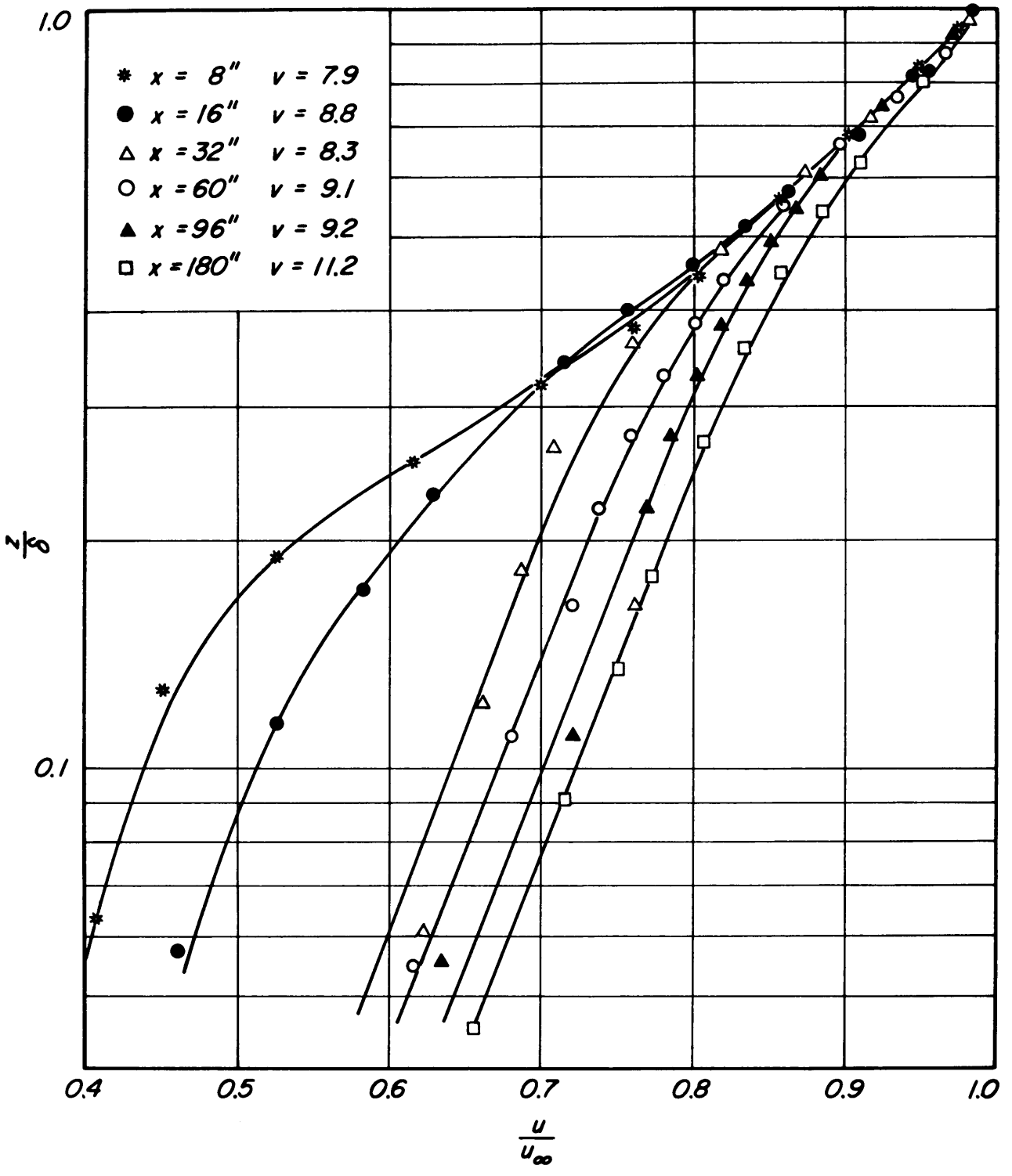

Fig. 10 Dimensionless velocity distributions.

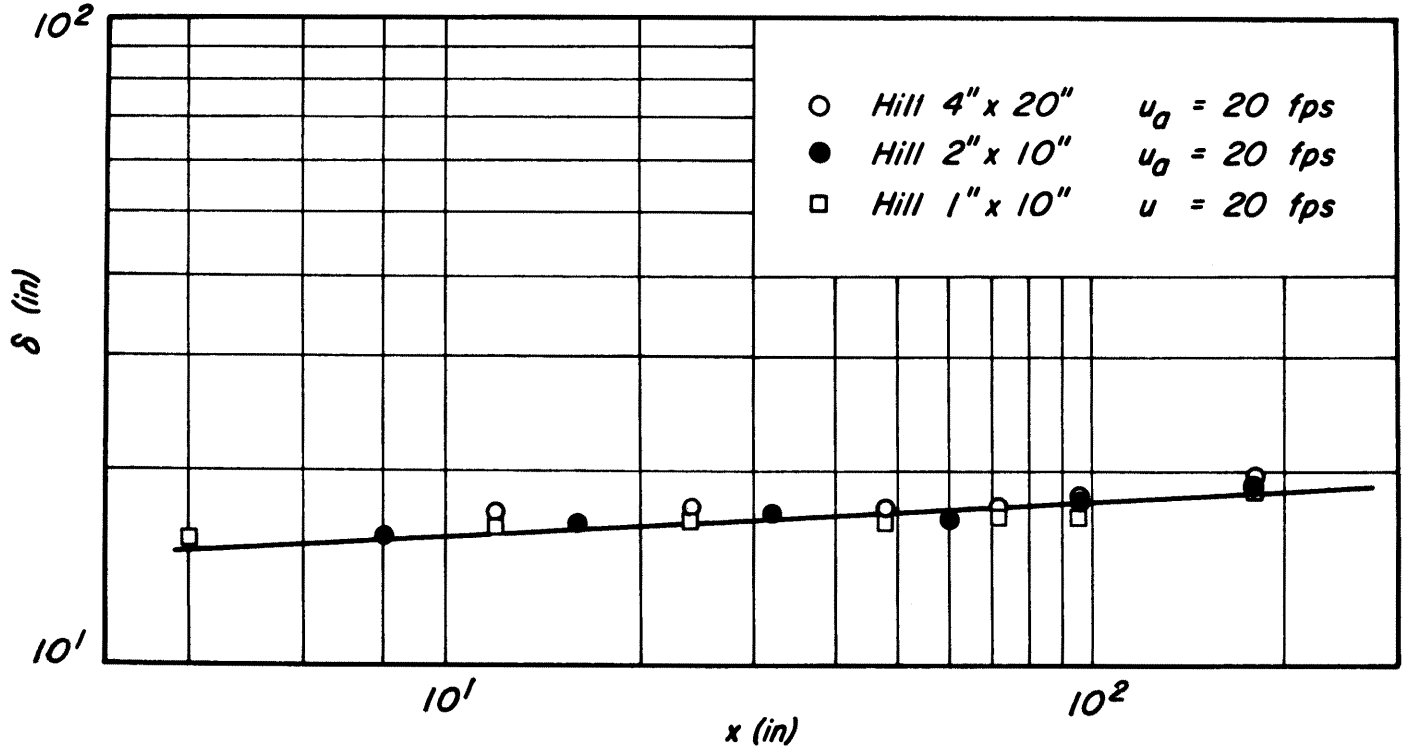

Fig. 11 Development of the boundary layer thickness as function of x for different hill models.

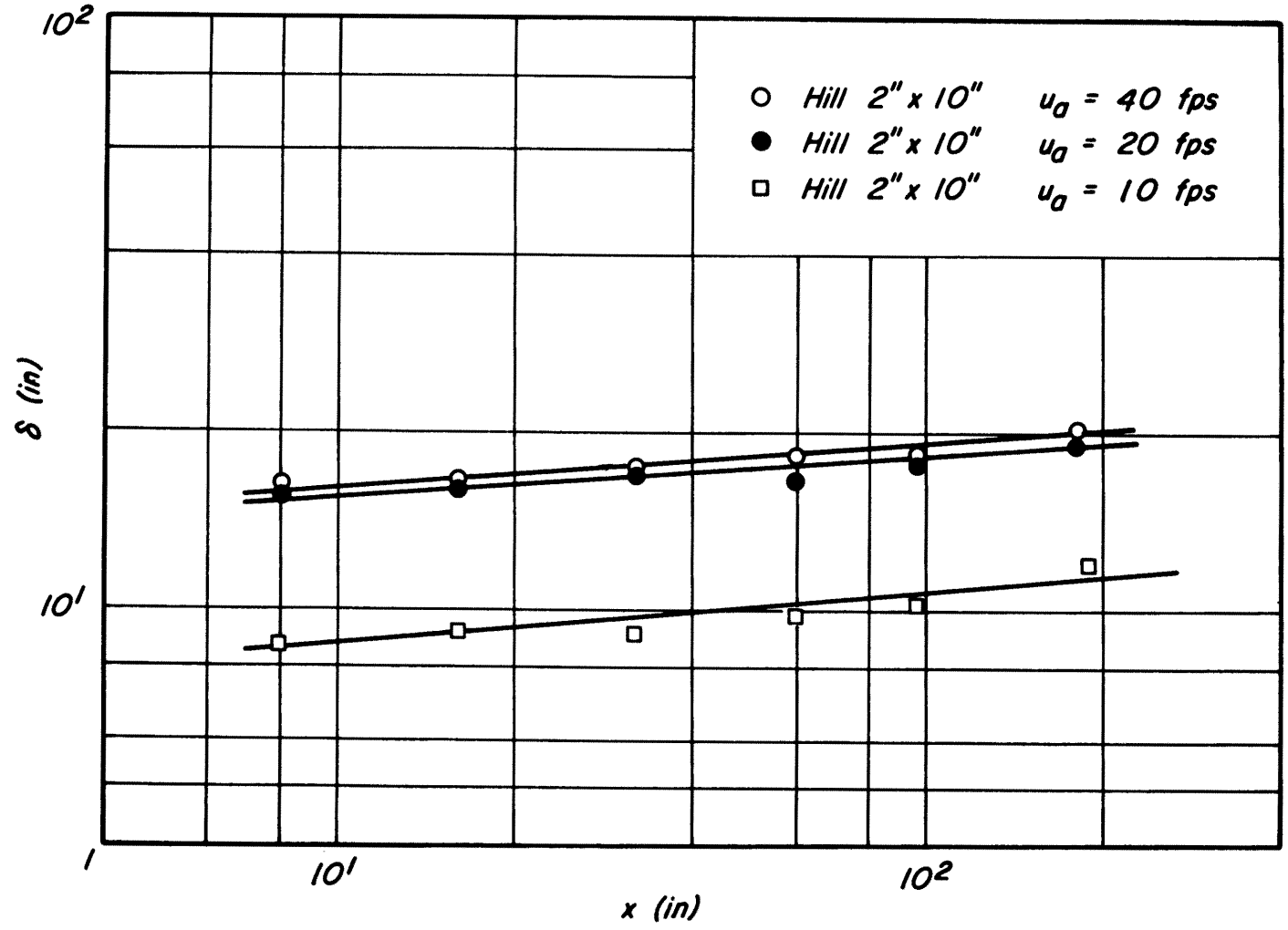

Fig. 12 Development of the boundary layer thickness as function of x for different velocities u_∞.

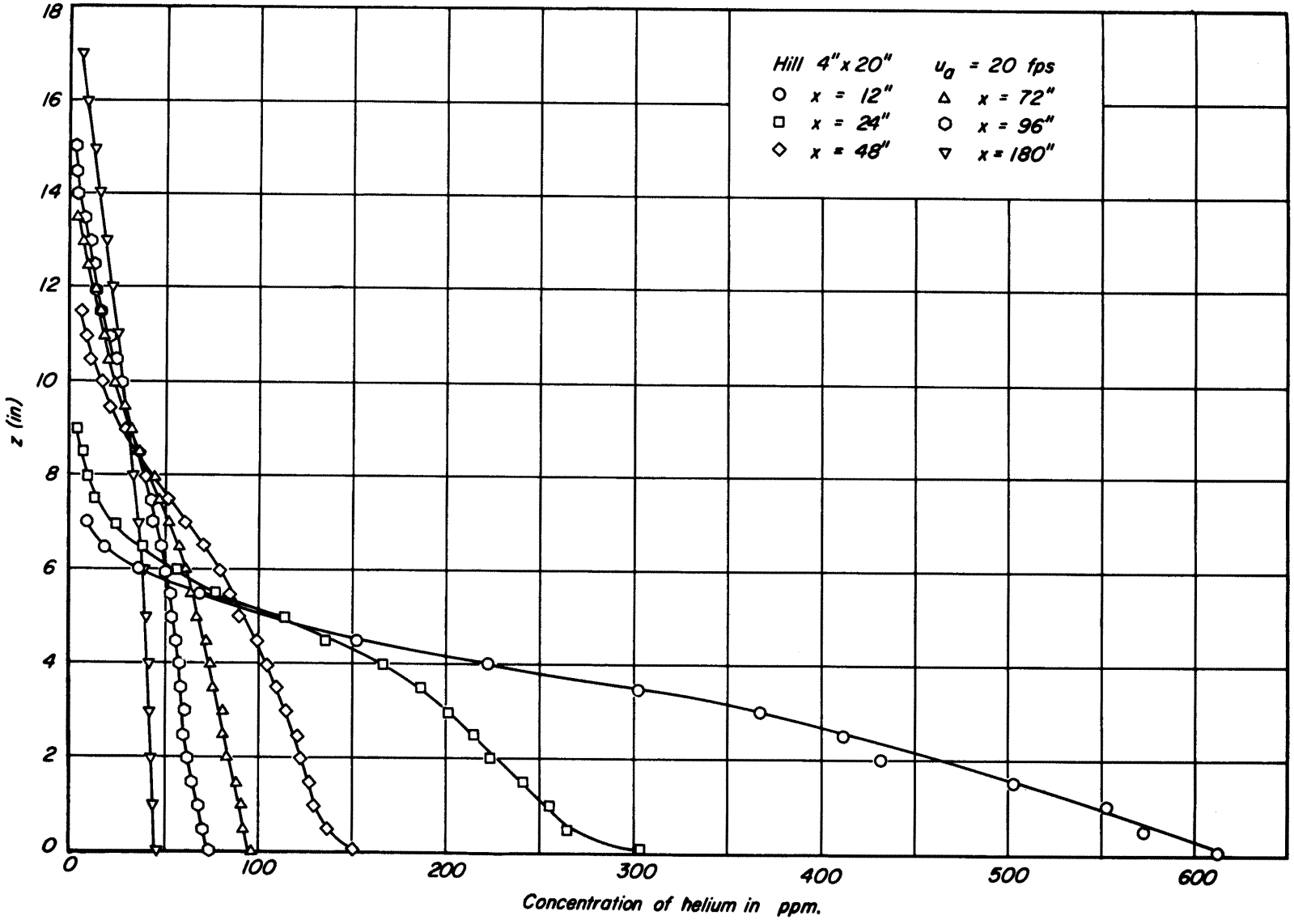

Fig. 13 Example of vertical centerline concentrations.

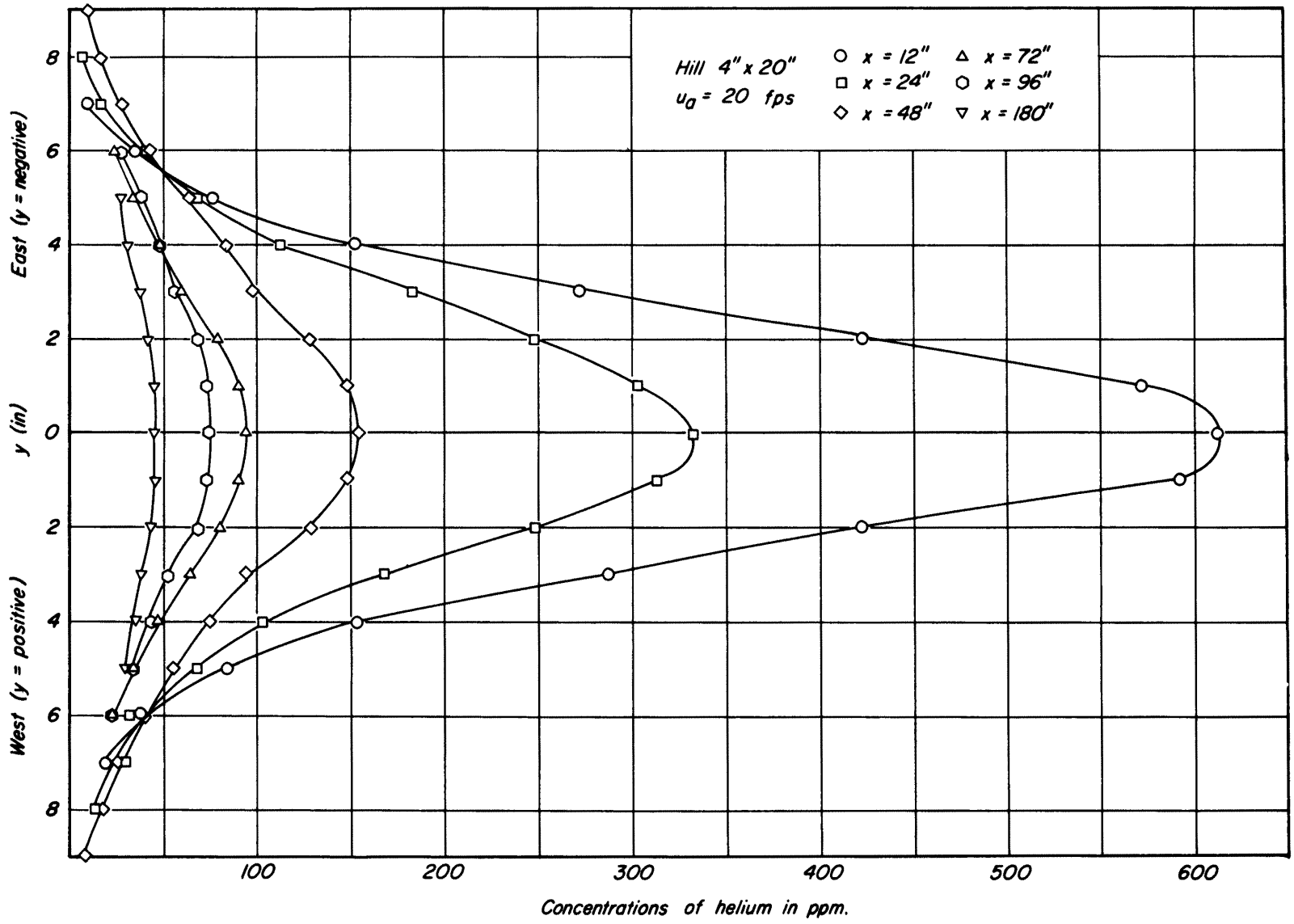

Fig. 14 Example of horizontal concentrations at $z = \frac{1}{8}$".

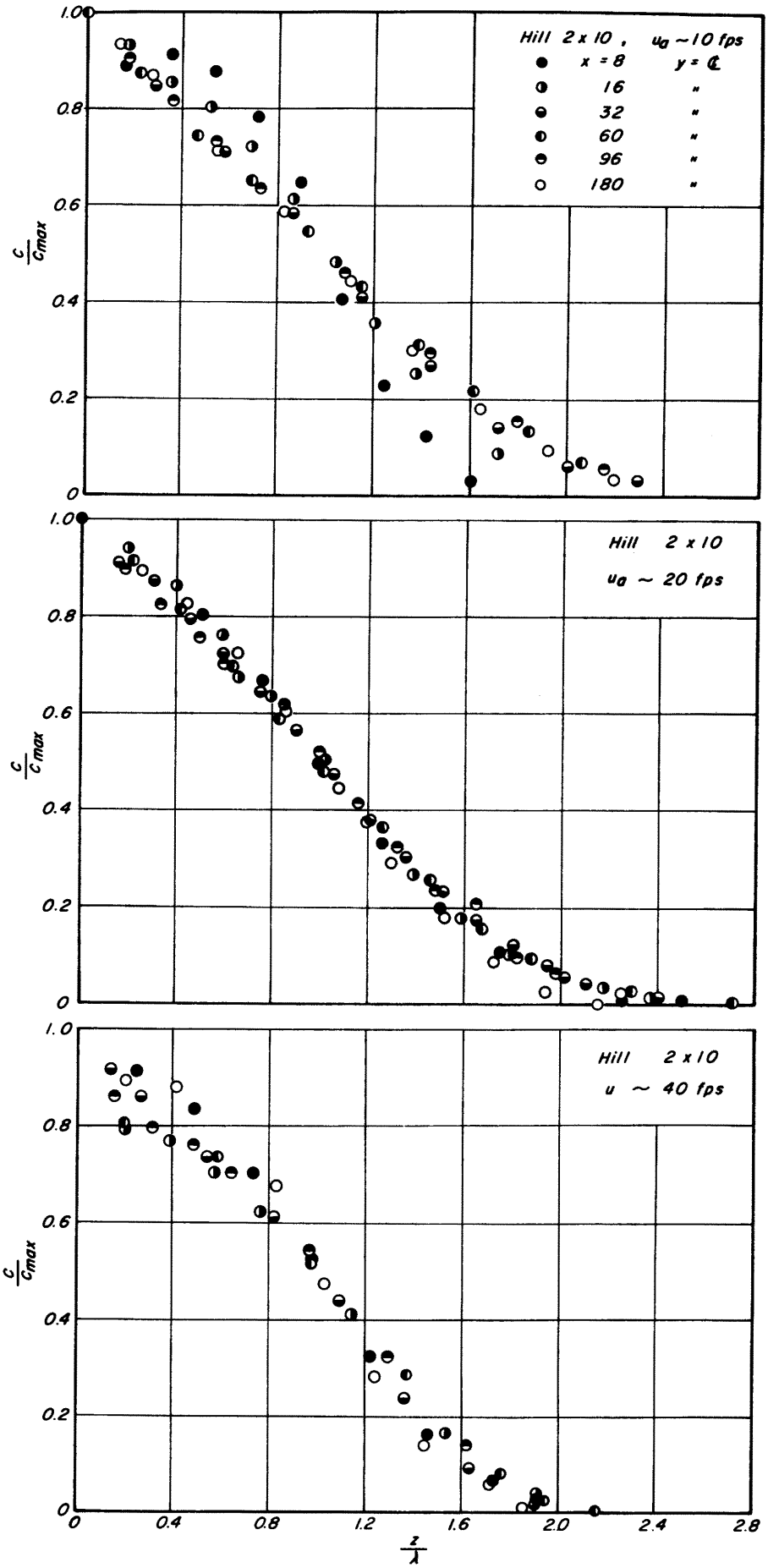

Fig. 15 Non-dimensional vertical concentration distributions for different hill models.

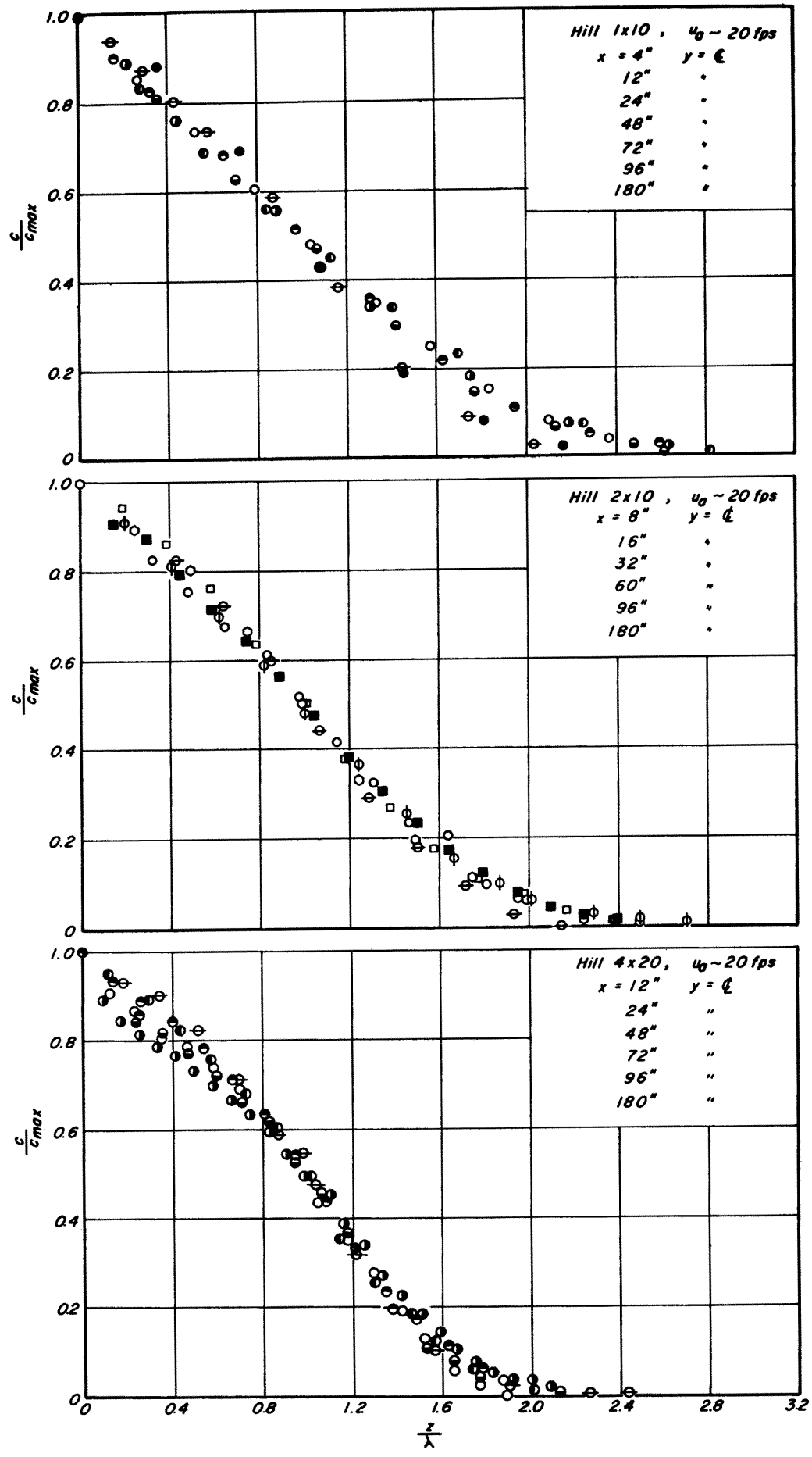

Fig. 16 Non-dimensional vertical concentration distributions for different u_∞.

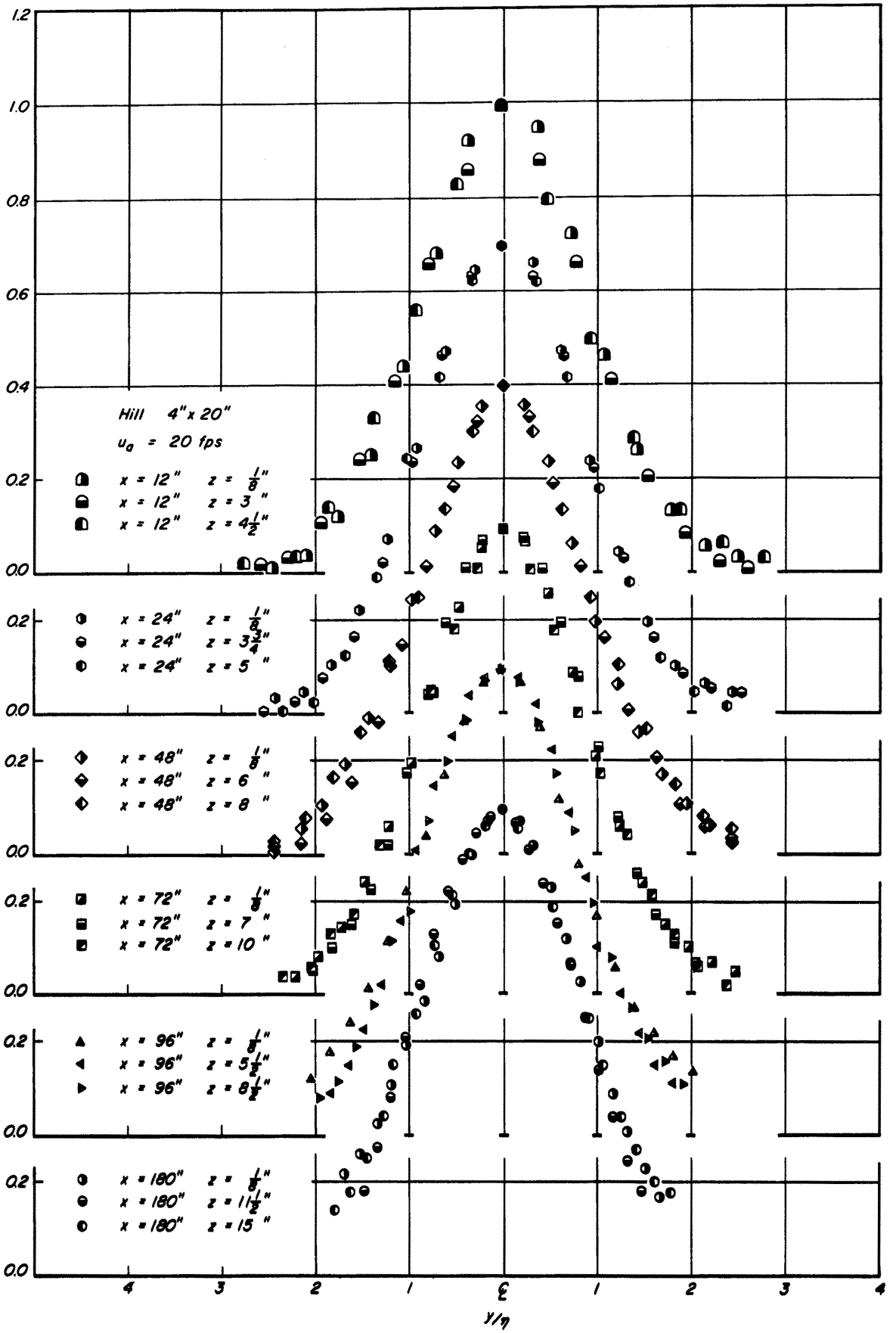

Fig. 17 Non-dimensional horizontal concentration distributions: examples.

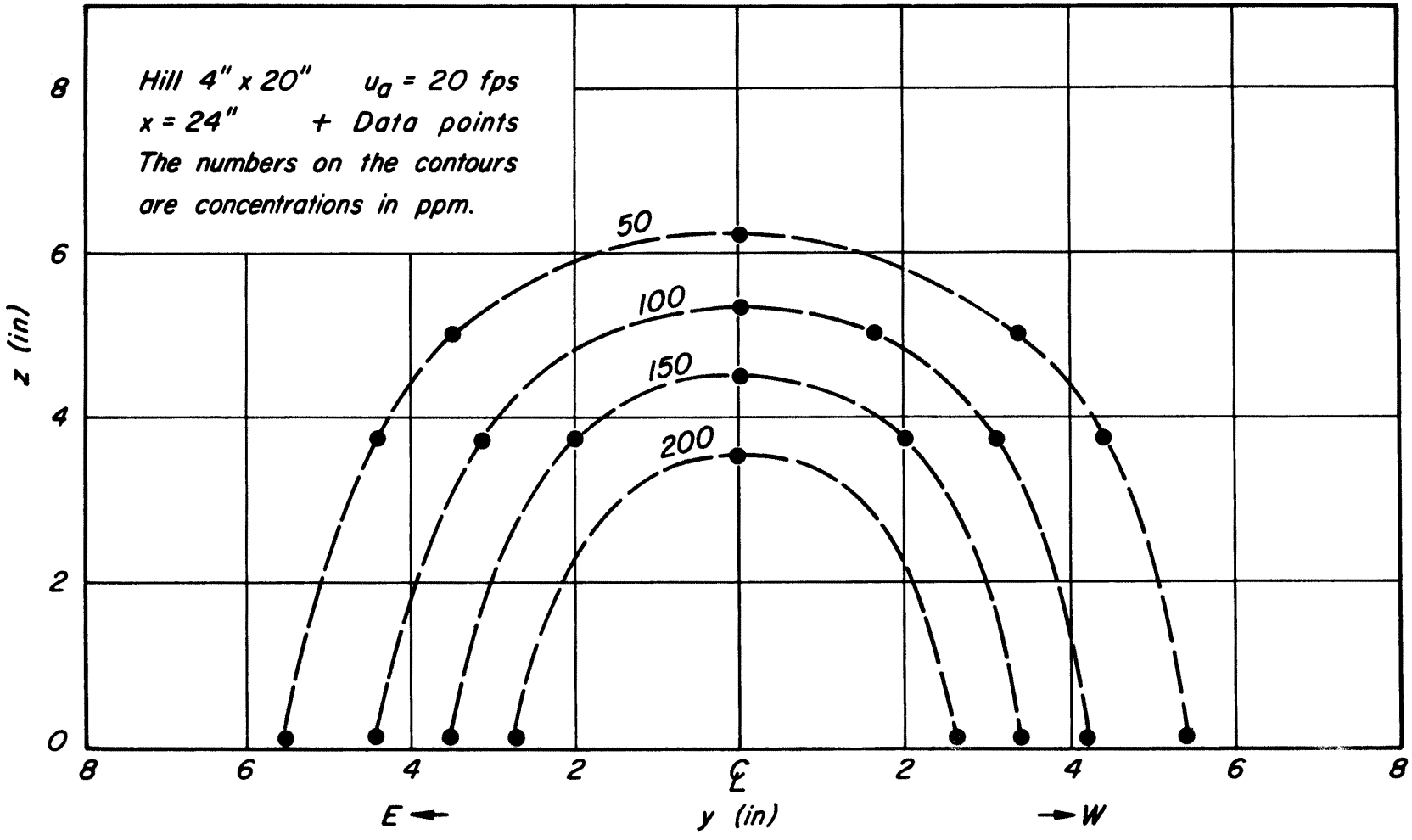

Fig. 18 Examples of isoconcentration contours.

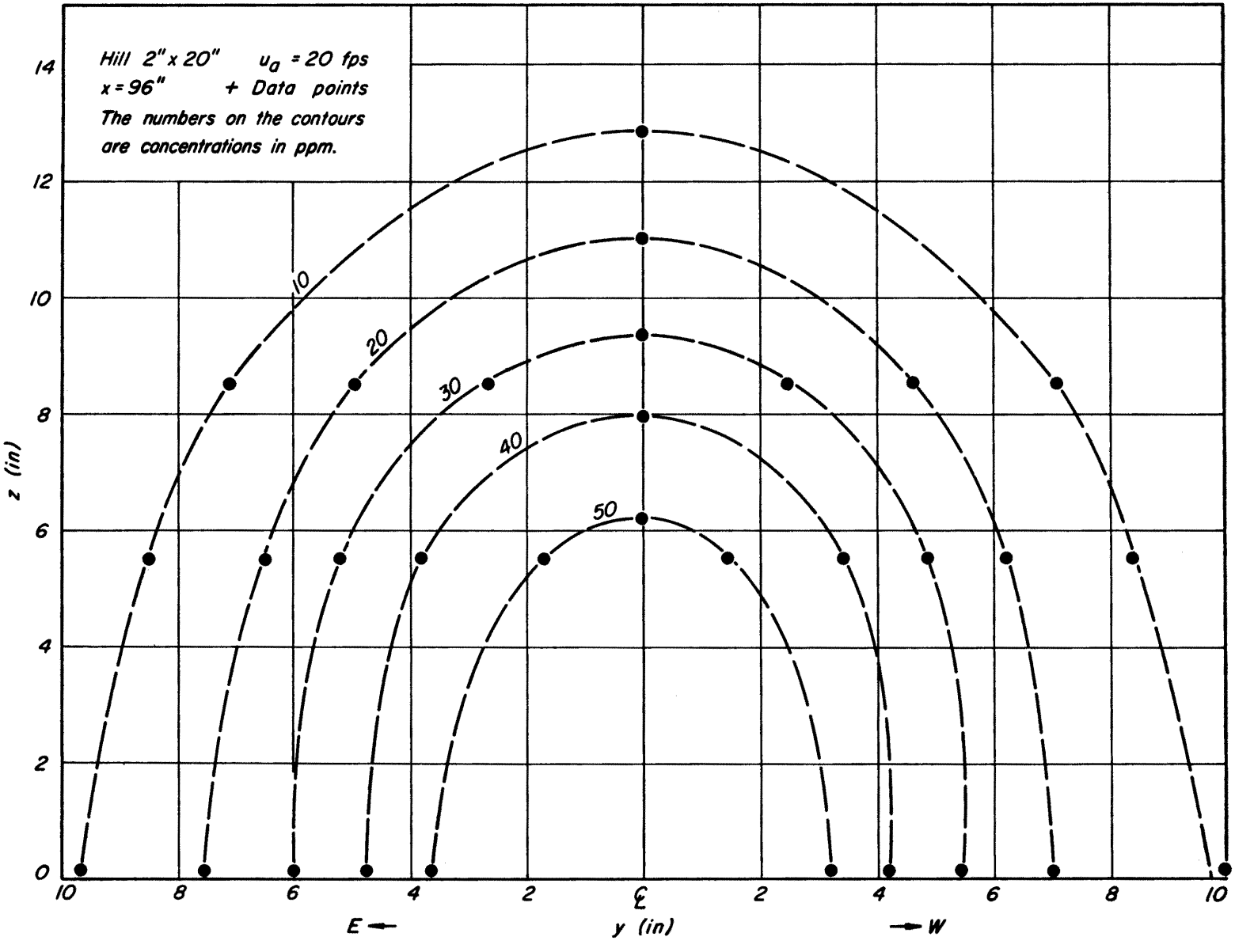

Fig. 19 Examples of isoconcentration contours.

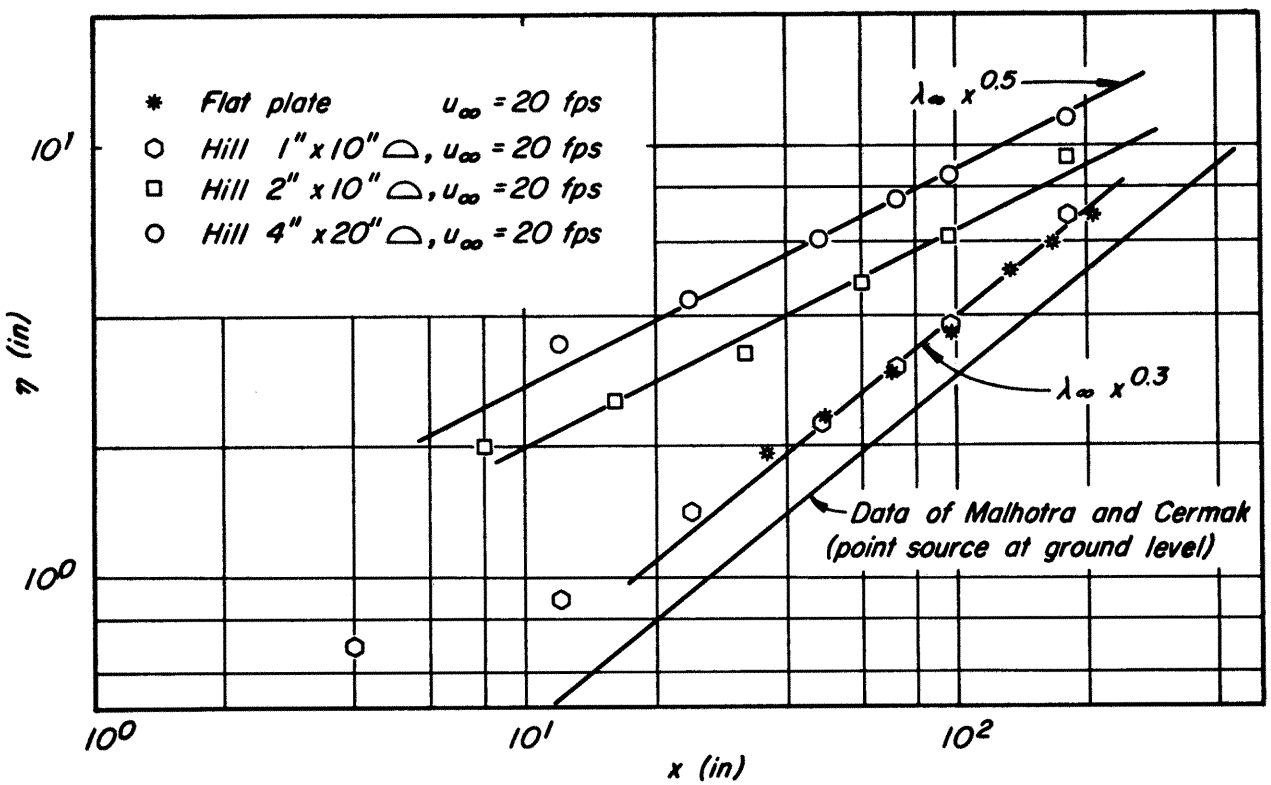

Fig. 20 Growth of λ with x for different hill models.

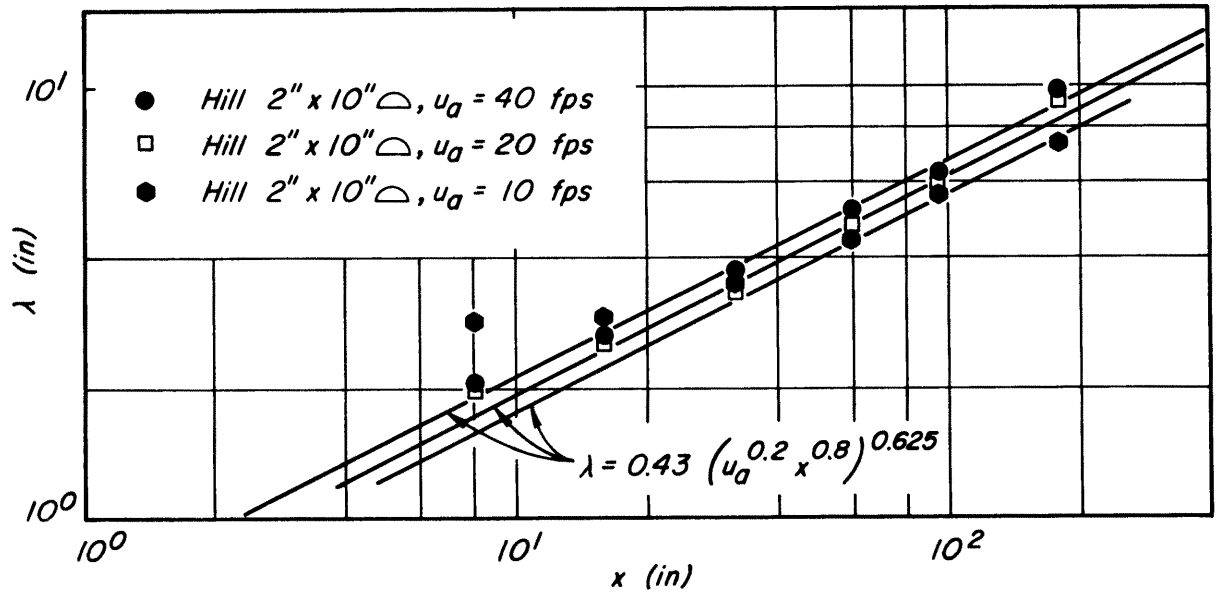

Fig. 21 Growth of λ with x for different u_∞.

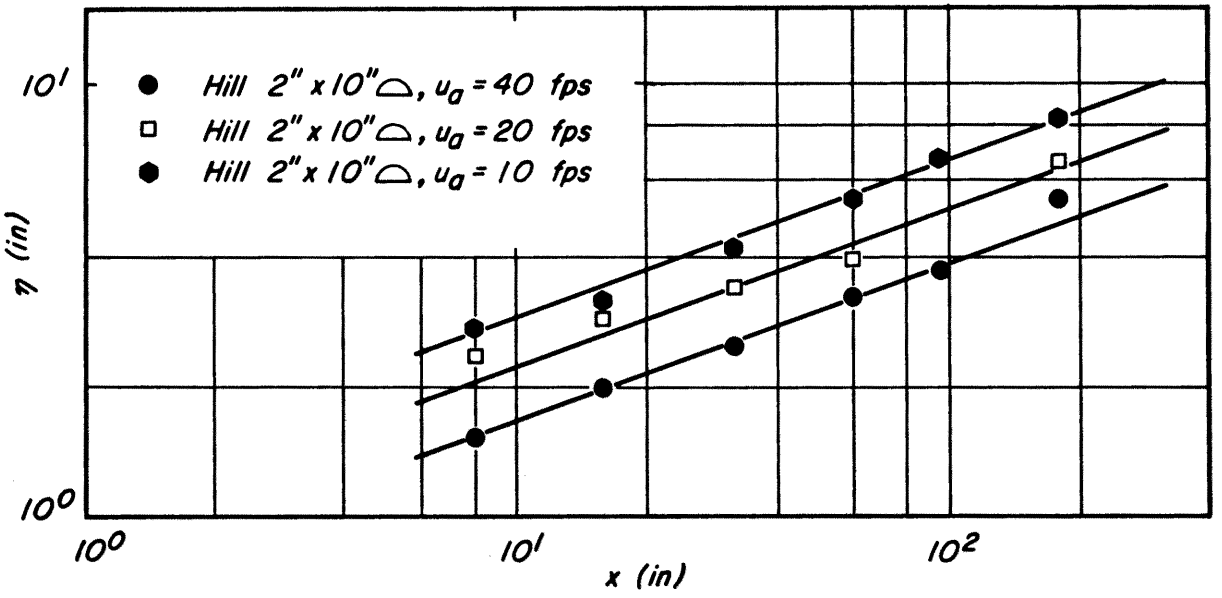

Fig. 22 Increase of η with x for different u_∞.

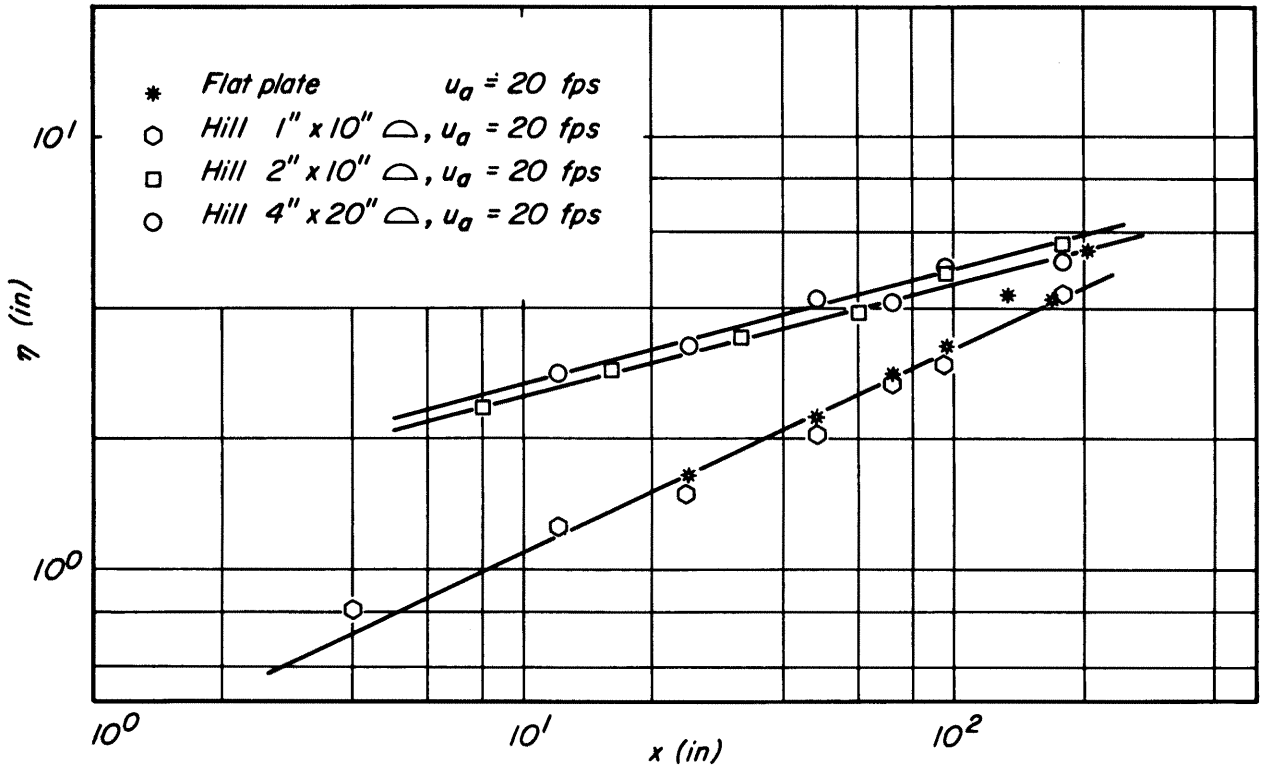

Fig. 23 Increase of η with x for different models.

APPENDIX 2

TABLES

TABLES

TABLE 2: PARAMETERS OF THE VELOCITY DISTRIBUTIONS 1: DISPLACEMENT THICKNESSES (in inches)

Hill 4" x 20"			U_a = 20 fps		Hill 2" x 10"			U_a = 40 fps		Hill 2" x 10"			U_a = 20 fps	
X (in)	Y = 7" w	Y = c	Y = 7" E	Average	X (in)	Y = 7" w	Y = c	Y = 7" E	Average	X (in)	Y = 7" w	Y = c	Y = 7" E	Average
12	2.67	4.33	2.67	3.22	8	2.19	3.28	2.20	2.56	8	2.32	3.26	2.41	2.66
24	2.41	4.03	2.49	2.98	16	2.08	3.25	2.21	2.51	16	2.36	3.37	2.41	2.71
48	2.20	3.61	2.24	2.68	32	2.09	3.05	2.20	2.45	32	2.29	3.33	2.06	2.57
72	2.26	3.55	2.26	2.69	60	2.06	3.20	2.23	2.50	60	2.21	3.19	2.15	2.52
96	2.40	3.58	2.09	2.69	96	2.24	3.25	2.16	2.55	96	2.51	3.27	2.30	2.69
180	2.83	3.52	2.44	2.93	180	2.45	3.44	2.60	2.83	180	2.85	3.57	2.62	3.01

Hill 2" x 10"			U_a = 10 fps		Hill 1" x 10"			U_a = 20 fps	
8	1.74	2.03	2.09	1.95	4	2.01	2.88	1.94	2.28
16	1.89	2.15	2.04	2.03	12	2.06	2.89	2.09	2.35
32	1.49	1.67	1.80	1.65	24	2.13	3.10	2.19	2.47
60	1.55	1.54	1.97	1.69	48	2.06	2.94	2.04	2.35
96	1.53	1.35	1.95	1.61	72	2.06	2.93	2.03	2.34
180	1.62	1.38	2.29	1.76	96	2.16	2.98	2.18	2.44
					180	2.47	3.30	2.44	2.74

PARAMETERS OF THE VELOCITY DISTRIBUTIONS 2: MOMENTUM THICKNESSES (in inches)

Hill 4" x 20"			U_a = 20 fps		Hill 2" x 10"			U_a = 40 fps		Hill 2" x 10"			U_a = 20 fps	
12	1.73	2.48	1.78	2.00	8	1.45	2.06	1.49	1.67	8	1.43	2.05	1.50	1.66
24	1.64	2.49	1.72	1.95	16	1.40	2.10	1.53	1.68	16	1.55	2.19	1.59	1.74
48	1.50	2.40	1.56	1.82	32	1.43	2.06	1.54	1.68	32	1.54	2.20	1.39	1.71
72	1.58	2.41	1.60	1.86	60	1.42	2.19	1.58	1.73	60	1.51	2.16	1.48	1.72
96	1.67	2.46	1.48	1.87	96	1.56	2.24	1.56	1.79	96	1.73	2.26	1.61	1.87
180	2.03	2.50	1.74	2.09	180	1.73	2.41	1.88	2.01	180	2.00	2.47	1.87	2.11

Hill 2" x 10"			U_a = 10 fps		Hill 1" x 10"			U_a = 20 fps	
8	1.00	1.11	1.22	1.11	4	1.36	1.95	1.32	1.54
16	1.12	1.24	1.30	1.22	12	1.39	1.96	1.45	1.60
32	1.00	1.10	1.22	1.11	24	1.44	2.10	1.51	1.68
60	1.06	1.05	1.36	1.16	48	1.41	2.00	1.41	1.61
96	1.06	0.93	1.39	1.13	72	1.41	2.00	1.40	1.60
180	1.18	1.00	1.63	1.27	96	1.50	2.06	1.51	1.69
					180	1.71	2.28	1.74	1.91

TABLE 3: VELOCITY DISTRIBUTION DATA

Hill 4" x 20" $U_a \approx 20$ fps

At X = 12"

Z (in)	U @ Y = 7" w	U @ Y = c	U @ Y = 7" E	Average Values U	Average Values U/U_∞
0.00	8.30	7.82	9.13	8.41	0.410
1.00	11.41	8.19	11.95	10.51	0.512
2.00	13.43	9.11	13.86	12.13	0.591
3.00	14.81	10.43	15.22	13.48	0.657
4.00	15.72	12.03	16.16	14.63	0.713
5.00	16.50	13.75	16.74	15.66	0.763
6.00	17.17	15.01	17.24	16.47	0.804
7.00	17.75	15.89	17.67	17.10	0.833
8.00	18.22	16.51	18.05	17.59	0.858
9.00	18.60	17.01	18.41	18.00	0.877
10.00	18.93	17.48	18.74	18.38	0.896
11.00	19.26	17.96	19.04	18.75	0.915
12.00	19.57	18.44	19.32	19.11	0.931
13.00	19.81	18.92	19.60	19.44	0.947
14.00	20.04	19.33	19.85	19.74	0.962
15.00	20.25	19.68	20.06	19.99	0.975
16.00	20.46	19.97	20.23	20.22	0.985
17.00	20.50	20.25	20.37	20.37	0.993
18.00	20.51	20.44	20.47	20.47	0.998
19.00	20.52	20.55	20.51	20.52	1.000
20.00	20.51	20.59	20.52	20.54	1.000
21.00	20.51	20.59	20.52	20.54	1.000
22.00	20.51	20.59	20.51	20.53	1.000
23.00	20.51	20.59	20.51	20.53	1.000
24.00	20.51	20.59	20.51	20.53	1.000

At X = 24"

Z (in)	U @ Y = 7" w	U @ Y = c	U @ Y = 7" E	Average Values U	Average Values U/U_∞
0.00	11.78	10.70	11.33	11.27	0.550
1.00	13.25	10.83	13.27	12.45	0.607
2.00	14.46	11.13	14.66	13.41	0.653
3.00	15.49	11.58	15.64	14.23	0.693
4.00	16.36	12.17	16.30	14.94	0.728
5.00	16.87	13.50	16.91	15.76	0.768
6.00	17.36	14.61	17.44	16.47	0.803
7.00	17.85	15.55	17.87	17.09	0.833
8.00	18.30	16.32	18.25	17.62	0.858
9.00	18.68	16.95	18.58	18.07	0.881
10.00	19.00	17.52	18.86	18.46	0.900
11.00	19.29	18.08	19.07	18.81	0.917
12.00	19.53	18.62	19.20	19.11	0.931
13.00	19.83	19.01	19.46	19.43	0.947
14.00	20.07	19.34	19.72	19.71	0.961
15.00	20.25	19.63	19.99	19.95	0.972
16.00	20.37	19.87	20.26	20.16	0.983
17.00	20.45	20.09	20.36	20.30	0.990
18.00	20.50	20.27	20.44	20.40	0.995
19.00	20.52	20.40	20.50	20.47	0.999
20.00	20.52	20.48	20.52	20.50	1.000
21.00	20.51	20.51	20.52	20.51	1.000
22.00	20.51	20.52	20.51	20.51	1.000
23.00	20.51	20.52	20.51	20.51	1.000
24.00	20.51	20.51	20.51	20.51	1.000

At X = 48"

Z (in)	U @ Y = 7" w	U @ Y = c	U @ Y = 7" E	Average Values U	Average Values U/U_∞
0.00	12.87	12.26	14.10	13.07	0.639
1.00	13.99	12.88	14.78	13.88	0.679
2.00	14.93	13.34	15.40	14.55	0.711
3.00	15.72	13.64	15.98	15.11	0.738
4.00	16.38	13.81	16.51	15.56	0.761
5.00	16.98	14.10	17.04	16.04	0.784
6.00	17.50	14.58	17.55	16.54	0.809
7.00	17.94	15.25	18.03	17.07	0.835
8.00	18.33	16.01	18.46	17.59	0.860
9.00	18.68	16.76	18.82	18.08	0.884
10.00	19.01	17.47	19.10	18.52	9.905
11.00	19.31	18.09	19.34	18.91	0.925
12.00	19.59	18.66	19.53	19.26	0.941
13.00	19.83	18.85	19.81	19.49	0.953
14.00	20.03	19.12	20.03	19.72	0.964
15.00	20.18	19.49	20.21	19.96	0.975
16.00	20.30	19.94	20.33	20.19	0.987
17.00	20.36	20.13	20.41	20.30	0.993
18.00	20.40	20.28	20.47	20.38	0.996
19.00	20.41	20.38	20.52	20.43	0.998
20.00	20.41	20.43	20.54	20.46	1.000
21.00	20.40	20.45	20.55	20.46	1.000
22.00	20.40	20.45	20.55	20.46	1.000
23.00	20.40	20.45	20.55	20.46	1.000
24.00	20.40	20.44	20.55	20.46	1.000

Hill 4" x 20" $U_a \approx 20$ fps

At X = 72"

Z (in)	U @ Y = 7" w	U @ Y = c	U @ Y = 7" E	Average Values U	Average Values U/U_∞
0.00	14.14	11.90	13.41	13.15	0.641
1.00	14.86	13.11	14.62	14.19	0.693
2.00	15.47	13.89	15.52	14.96	0.730
3.00	15.97	14.33	16.16	15.48	0.256
4.00	16.39	14.44	16.58	15.80	0.771
5.00	16.86	14.68	17.09	16.21	0.791
6.00	17.36	15.00	17.54	16.63	0.811
7.00	17.88	15.39	17.95	17.07	0.834
8.00	18.36	15.86	18.30	17.50	0.854
9.00	18.75	16.38	18.57	17.90	0.874
10.00	19.07	16.93	18.81	18.27	0.892
11.00	19.34	17.51	19.04	18.63	0.909
12.00	19.57	18.11	19.26	18.98	0.926
13.00	19.81	18.76	19.55	19.37	0.946
14.00	20.02	19.25	19.80	19.69	0.962
15.00	20.20	19.60	20.01	19.93	0.973
16.00	20.34	19.81	20.18	20.11	0.982
17.00	20.47	20.08	20.27	20.27	0.990
18.00	20.54	20.27	20.34	20.38	0.995
19.00	20.56	20.38	20.39	20.44	0.998
20.00	20.55	20.43	20.43	20.47	1.000
21.00	20.55	20.45	20.44	20.48	1.000
22.00	20.55	20.45	20.45	20.48	1.000
23.00	20.55	20.44	20.44	20.47	1.000
24.00	20.55	20.44	20.44	20.47	1.000

At X = 96"

Z (in)	U @ Y = 7" w	U @ Y = c	U @ Y = 7" E	Average Values U	Average Values U/U_∞
0.00	12.75	11.73	13.85	12.78	0.625
1.00	14.39	13.29	15.06	14.25	0.697
2.00	15.43	14.22	15.97	15.21	0.743
3.00	15.99	14.66	16.63	15.76	0.771
4.00	16.12	14.64	17.05	15.94	0.780
5.00	16.54	14.86	17.39	16.26	0.795
6.00	16.94	15.12	17.72	16.59	0.812
7.00	17.31	15.40	18.03	16.91	0.827
8.00	17.71	15.76	18.34	17.27	0.845
9.00	18.17	16.25	18.64	17.69	0.865
10.00	18.63	16.84	18.92	18.13	0.886
11.00	19.02	17.49	19.18	18.56	0.907
12.00	19.37	18.19	19.42	18.99	0.929
13.00	19.73	18.63	19.63	19.33	0.945
14.00	20.01	18.99	19.85	19.62	0.960
15.00	20.22	19.29	20.07	19.86	0.971
16.00	20.36	19.52	20.30	20.06	0.981
17.00	20.40	19.87	20.36	20.21	0.989
18.00	20.43	20.13	20.40	20.32	0.993
19.00	20.44	20.28	20.43	20.38	0.997
20.00	20.44	20.36	20.44	20.41	0.998
21.00	20.44	20.41	20.44	20.43	1.000
22.00	20.44	20.44	20.44	20.44	1.000
23.00	20.44	20.45	20.44	20.44	1.000
24.00	20.44	20.44	20.44	20.44	1.000

At X = 180"

Z (in)	U @ Y = 7" w	U @ Y = c	U @ Y = 7" E	Average Values U	Average Values U/U_∞
0.00	13.01	12.56	13.56	13.04	0.637
1.00	14.27	13.66	14.60	14.18	0.693
2.00	15.18	14.46	15.46	15.03	0.734
3.00	15.81	15.02	16.15	15.66	0.765
4.00	16.18	15.35	16.71	16.08	0.786
5.00	16.51	15.57	17.06	16.38	0.801
6.00	16.83	15.80	17.38	16.67	0.814
7.00	17.14	16.03	17.66	16.94	0.828
8.00	17.44	16.29	17.91	17.21	0.841
9.00	17.71	16.59	18.16	17.49	0.854
10.00	17.97	16.93	18.42	17.77	0.869
11.00	18.27	17.27	18.72	18.09	0.884
12.00	18.59	17.62	19.05	18.42	0.899
13.00	18.95	18.06	19.28	18.76	0.916
14.00	19.30	18.48	19.50	19.09	0.933
15.00	19.62	18.88	19.70	19.40	0.948
16.00	19.93	19.27	19.89	19.70	0.962
17.00	20.11	19.53	20.12	19.92	0.972
18.00	20.25	19.78	20.29	20.11	0.982
19.00	20.35	20.03	20.39	20.26	0.990
20.00	20.44	20.25	20.43	20.37	0.995
21.00	20.51	20.40	20.45	20.45	0.999
22.00	20.55	20.46	20.45	20.49	1.000
23.00	20.56	20.47	20.44	20.49	1.000
24.00	20.54	20.42	20.44	20.47	1.000

TABLE 3: VELOCITY DISTRIBUTION DATA (Continued)

Hill 2" x 10" U_a = 40 fps

At X = 8"

Z (in)	U @ Y = 7" W	U @ Y = c	U @ Y = 7" E	Average Values U	Average Values U/U∞
0.00	20.78	14.20	21.11	18.70	0.462
1.00	25.91	19.47	26.25	23.88	0.590
2.00	29.31	23.54	29.67	27.51	0.678
3.00	31.54	26.96	31.91	30.14	0.744
4.00	32.84	29.96	33.21	32.00	0.790
5.00	34.04	31.20	34.31	33.18	0.819
6.00	35.10	32.33	35.23	34.22	0.844
7.00	36.03	33.35	35.95	35.11	0.866
8.00	36.85	34.32	36.59	35.92	0.886
9.00	37.60	25.26	37.21	36.69	0.905
10.00	38.29	36.13	37.79	37.40	0.923
11.00	38.92	36.90	38.26	38.03	0.938
12.00	39.50	37.58	38.65	38.58	0.952
13.00	39.92	38.30	39.25	39.16	0.966
14.00	40.22	38.92	39.73	39.62	0.977
15.00	40.42	39.42	40.10	39.98	0.986
16.00	40.52	39.82	40.37	40.23	0.994
17.00	40.57	40.21	40.42	40.40	0.997
18.00	40.59	40.45	40.44	40.49	0.999
19.00	40.60	40.53	40.45	40.53	1.000
20.00	40.59	40.53	40.44	40.52	1.000
21.00	40.59	40.52	40.44	40.52	1.000
22.00	40.59	40.52	40.44	40.52	1.000
23.00	40.59	40.52	40.44	40.52	1.000
24.00	40.59	40.52	40.44	40.52	1.000

At X = 16"

Z (in)	U @ Y = 7" W	U @ Y = c	U @ Y = 7" E	Average Values U	Average Values U/U∞
0.00	23.32	20.75	23.47	22.51	0.557
1.00	27.03	22.03	27.16	25.41	0.629
2.00	29.74	23.91	29.91	27.85	0.690
3.00	31.70	26.26	31.96	29.97	0.743
4.00	33.04	28.97	33.44	31.82	0.788
5.00	34.24	30.58	34.43	33.08	0.820
6.00	35.26	31.94	35.26	34.15	0.846
7.00	36.12	33.08	35.94	35.05	0.868
8.00	36.85	34.09	36.50	35.81	0.888
9.00	37.48	35.03	36.97	36.49	9.904
10.00	38.06	35.89	37.41	37.12	9.920
11.00	38.61	36.68	37.86	37.72	0.934
12.00	39.13	37.39	38.31	38.28	0.949
13.00	39.54	37.99	38.76	38.76	0.961
14.00	39.87	38.56	39.17	39.20	0.971
15.00	40.13	39.10	39.53	39.59	0.981
16.00	40.31	39.61	39.85	39.92	0.989
17.00	40.32	39.94	40.08	40.11	0.993
18.00	40.33	40.16	40.24	40.24	0.997
19.00	40.33	40.26	40.33	40.31	1.000
20.00	40.33	40.30	40.34	40.32	1.000
21.00	40.33	40.30	40.34	40.32	1.000
22.00	40.33	40.29	40.33	40.32	1.000
23.00	40.33	40.29	40.33	40.32	1.000
24.00	40.33	40.29	40.33	40.32	1.000

At X = 32"

Z (in)	U @ Y = 7" E	U @ Y = c	U @ Y = 7" E	Average Values U	Average Values U/U∞
0.00	25.81	24.54	24.81	25.05	0.619
1.00	28.30	25.37	28.01	27.23	0.670
2.00	30.32	26.44	30.44	29.07	0.718
3.00	31.95	27.73	32.27	30.65	0.757
4.00	33.26	29.21	33.59	32.02	0.791
5.00	34.42	30.82	34.52	33.25	0.821
6.00	35.37	32.20	35.33	34.30	0.847
7.00	36.10	33.36	36.01	35.16	0.869
8.00	36.75	34.34	36.56	35.88	0.887
9.00	37.39	35.18	36.99	36.52	0.902
10.00	37.99	35.97	37.40	37.12	0.917
11.00	38.51	36.77	37.82	37.70	0.932
12.00	38.96	37.57	38.24	38.26	0.945
13.00	39.36	38.12	38.69	38.72	0.956
14.00	39.69	38.63	39.11	39.14	0.967
15.00	39.97	39.11	39.49	39.52	0.976
16.00	40.20	39.57	39.85	39.87	0.985
17.00	40.33	40.00	40.12	40.15	0.992
18.00	40.41	40.28	40.31	40.33	0.996
19.00	40.45	40.42	40.42	40.43	1.000
20.00	40.45	40.46	40.46	40.46	1.000
21.00	40.44	40.45	40.45	40.45	1.000
22.00	40.44	40.44	40.44	40.44	1.000
23.00	40.44	40.44	40.44	40.44	1.000
24.00	40.44	40.44	40.44	40.44	1.000

Hill 2" x 10" U_a = 40 fps

At X = 60"

0.00	26.24	23.94	26.73	25.64	0.633
1.00	28.73	26.00	28.27	27.90	0.690
2.00	30.63	27.47	30.71	29.60	0.731
3.00	32.04	28.44	32.05	30.84	0.762
4.00	33.03	28.96	33.02	31.67	0.782
5.00	34.21	30.03	34.08	32.77	0.810
6.00	35.21	31.14	34.97	33.77	0.834
7.00	36.04	32.30	35.67	34.67	0.857
8.00	36.77	33.45	36.30	35.51	0.877
9.00	37.43	34.54	36.87	36.28	0.896
10.00	38.03	35.51	37.36	36.97	0.914
11.00	38.56	36.33	37.82	37.57	0.928
12.00	39.03	37.02	38.23	38.09	0.942
13.00	39.48	37.63	38.65	38.59	0.954
14.00	39.85	38.22	39.05	39.04	0.965
15.00	40.11	38.80	39.45	39.45	0.975
16.00	40.29	39.35	39.83	39.82	0.984
17.00	40.37	39.75	40.05	40.06	0.989
18.00	40.43	40.04	40.23	40.23	0.995
19.00	40.45	40.23	40.36	40.35	0.998
20.00	40.45	40.34	40.43	40.41	1.000
21.00	40.44	40.41	40.45	40.43	1.000
22.00	40.44	40.46	40.45	40.45	1.000
23.00	40.44	40.46	40.45	40.45	1.000
24.00	40.44	40.43	40.44	40.44	1.000

At X = 96"

0.00	25.68	23.69	25.68	25.02	0.621
1.00	28.34	26.01	28.34	27.56	0.684
2.00	30.26	27.62	30.26	29.38	0.729
3.00	31.58	28.65	31.29	30.51	0.757
4.00	32.37	29.16	32.74	31.42	0.780
5.00	33.51	30.13	33.64	32.43	0.805
6.00	34.47	31.04	34.47	33.33	0.826
7.00	35.25	31.88	35.23	34.12	0.847
8.00	35.98	32.75	35.84	34.86	0.865
9.00	36.74	33.73	36.32	35.60	0.884
10.00	37.47	34.74	36.80	36.34	0.903
11.00	38.04	35.68	37.35	37.02	0.918
12.00	38.51	36.59	37.95	37.68	0.935
13.00	38.99	37.24	38.30	38.18	0.947
14.00	39.39	37.87	38.67	38.64	0.959
15.00	39.73	38.49	39.08	39.10	0.971
16.00	39.99	39.09	39.51	39.53	0.980
17.00	40.17	39.43	39.78	39.79	0.988
18.00	40.28	39.73	40.00	40.00	0.993
19.00	40.33	39.98	40.16	40.16	0.996
20.00	40.34	40.16	40.25	40.25	1.000
21.00	40.33	40.25	40.27	40.28	1.000
22.00	40.33	40.27	40.26	40.29	1.000
23.00	40.33	40.27	40.26	40.29	1.000
24.00	40.33	40.24	40.25	40.27	1.000

At X = 180"

0.00	25.11	23.33	25.31	24.58	0.610
1.00	27.97	25.78	28.16	27.30	0.678
2.00	30.06	27.63	30.22	29.30	0.727
3.00	31.54	28.99	31.66	30.73	0.762
4.00	32.49	29.92	32.56	31.66	0.786
5.00	33.19	30.62	33.44	32.42	0.805
6.00	33.92	31.30	34.13	33.12	0.821
7.00	34.66	31.96	34.64	33.75	0.838
8.00	35.40	32.62	35.01	34.34	0.853
9.00	36.10	33.32	35.40	34.94	0.868
10.00	36.73	34.07	35.88	35.56	0.882
11.00	37.30	34.87	36.47	36.21	0.898
12.00	37.83	35.71	37.16	36.96	0.918
13.00	38.37	36.43	37.62	37.47	0.930
14.00	38.83	37.13	38.02	37.99	9.943
15.00	39.22	37.80	38.35	38.46	0.955
16.00	39.53	38.44	38.61	38.86	0.964
17.00	39.77	38.98	39.01	39.25	0.974
18.00	39.98	39.39	39.34	39.57	0.982
19.00	40.14	39.65	39.59	39.79	0.988
20.00	40.26	39.84	39.80	39.97	0.992
21.00	40.33	40.02	39.98	40.11	0.994
22.00	40.35	40.18	40.11	40.21	0.998
23.00	40.35	40.29	40.17	40.27	1.000
24.00	40.32	40.35	40.18	40.28	1.000

TABLE 3: VELOCITY DISTRIBUTION DATA (Continued)

Hill 2" x 10" $U_a \approx$ 20 fps

At X = 8"

Z (in)	U @ Y = 7" w	U @ Y = c	U @ Y = 7" E	Average Values U	Average Values U/U∞
0.00	1.84	3.85	3.10	2.93	0.142
1.00	10.90	9.41	10.58	10.30	0.499
2.00	14.38	12.79	13.85	13.67	0.662
3.00	16.13	14.51	15.79	15.48	0.750
4.00	16.71	15.15	16.88	16.25	0.786
5.00	17.31	15.84	17.60	16.92	0.819
6.00	17.84	16.45	18.16	17.48	0.847
7.00	18.30	16.99	18.57	17.95	0.869
8.00	18.71	17.46	18.87	18.35	0.889
9.00	19.09	17.88	19.11	18.69	0.905
10.00	19.46	18.31	19.34	19.04	0.921
11.00	19.77	18.77	19.56	19.37	0.937
12.00	20.05	19.25	19.78	19.69	0.955
13.00	20.24	19.51	20.04	19.93	0.965
14.00	20.41	19.80	20.25	20.15	0.975
15.00	20.57	20.12	20.42	20.37	0.986
16.00	20.71	20.47	20.55	20.58	0.996
17.00	20.69	20.60	20.59	20.63	0.999
18.00	20.69	20.67	20.62	20.66	1.000
19.00	20.69	20.70	20.62	20.67	1.000
20.00	20.69	20.69	20.62	20.67	1.000
21.00	20.69	20.69	20.61	20.67	1.000
22.00	20.69	20.69	20.61	20.67	1.000
23.00	20.69	20.69	20.62	20.67	1.000
24.00	20.69	20.69	20.61	20.67	1.000

At X = 16"

Z (in)	U @ Y = 7" w	U @ Y = c	U @ Y = 7" E	Average Values U	Average Values U/U∞
0.00	9.14	9.67	10.78	9.86	0.478
1.00	12.31	10.89	12.40	11.87	0.576
2.00	14.33	12.16	13.86	13.45	0.653
3.00	15.65	13.48	15.21	14.78	0.718
4.00	16.45	14.84	16.46	15.92	0.772
5.00	17.08	15.68	17.31	16.69	0.810
6.00	17.63	16.36	17.95	17.31	0.840
7.00	18.10	16.90	18.40	17.80	0.864
8.00	18.54	17.36	18.73	18.21	0.884
9.00	18.96	17.79	19.01	18.59	0.902
10.00	19.34	18.16	19.27	18.92	0.917
11.00	19.67	18.46	19.50	19.21	0.932
12.00	19.96	18.70	19.70	19.45	0.944
13.00	20.22	19.14	19.92	19.76	0.959
14.00	20.40	19.53	20.13	20.02	0.971
15.00	20.50	19.88	20.32	20.23	0.981
16.00	20.53	20.18	20.50	20.40	0.990
17.00	20.58	20.32	20.57	20.49	0.994
18.00	20.61	20.44	20.61	20.55	0.998
19.00	20.62	20.54	20.62	20.59	1.000
20.00	20.62	20.60	20.62	20.61	1.000
21.00	20.62	20.62	20.61	20.62	1.000
22.00	20.61	20.62	20.61	20.61	1.000
23.00	20.61	20.62	20.61	20.61	1.000
24.00	20.62	20.61	20.62	20.62	1.000

At X = 32"

Z (in)	U @ Y = 7" w	U @ Y = c	U @ Y = 7" E	Average Values U	Average Values U/U∞
0.00	12.22	11.00	12.98	12.07	0.587
1.00	13.42	11.95	14.01	13.13	0.637
2.00	14.53	12.82	15.01	14.12	0.685
3.00	15.56	13.64	16.00	15.07	0.732
4.00	16.52	14.42	16.97	15.97	0.776
5.00	17.28	15.31	17.73	16.77	0.815
6.00	17.85	16.04	18.29	17.39	0.845
7.00	18.25	16.62	18.68	17.85	0.867
8.00	18.57	17.08	18.96	18.20	0.884
9.00	18.88	17.49	19.22	18.53	0.900
10.00	19.20	17.91	19.48	18.86	0.916
11.00	19.49	18.35	19.72	19.19	0.929
12.00	19.77	18.79	19.96	19.51	0.947
13.00	20.01	19.24	20.06	19.77	0.961
14.00	20.20	19.61	20.17	19.99	0.972
15.00	20.36	19.94	20.30	20.20	0.981
16.00	20.47	20.20	20.43	20.37	0.990
17.00	20.54	20.33	20.52	20.46	0.994
18.00	20.58	20.44	20.57	20.53	0.997
19.00	20.59	20.53	20.59	20.57	1.000
20.00	20.58	20.58	20.58	20.58	1.000
21.00	20.58	20.59	20.58	20.58	1.000
22.00	20.58	20.58	20.58	20.58	1.000
23.00	20.58	20.58	20.58	20.58	1.000
24.00	20.58	20.58	20.58	20.58	1.000

Hill 2" x 10" $U_a \approx$ 20 fps

At X = 60"

Z (in)	U @ Y = 7" w	U @ Y = c	U @ Y = 7" E	Average Values U	Average Values U/U∞
0.00	13.17	11.40	13.49	12.69	0.616
1.00	14.28	12.80	14.44	13.84	0.672
2.00	15.19	13.80	15.28	14.76	0.716
3.00	15.93	14.47	16.03	15.48	0.752
4.00	16.52	14.86	16.70	16.03	0.778
5.00	17.16	15.30	17.28	16.58	0.805
6.00	17.72	15.83	17.82	17.12	0.831
7.00	18.20	16.43	18.32	17.65	0.856
8.00	18.60	17.07	18.78	18.15	0.881
9.00	18.92	17.65	19.16	18.58	0.903
10.00	19.21	18.15	19.44	18.93	0.919
11.00	19.52	18.55	19.64	19.24	0.934
12.00	19.85	18.87	19.75	19.49	0.946
13.00	20.08	19.22	19.95	19.75	0.959
14.00	20.26	19.55	20.13	19.98	0.970
15.00	20.40	19.87	20.30	20.19	0.980
16.00	20.50	20.18	20.46	20.38	0.990
17.00	20.57	20.37	20.55	20.50	0.995
18.00	20.61	20.51	20.60	20.57	0.999
19.00	20.62	20.59	20.62	20.61	1.000
20.00	20.62	20.62	20.62	20.62	1.000
21.00	20.61	20.62	20.62	20.62	1.000
22.00	20.61	20.62	20.61	20.61	1.000
23.00	20.61	20.61	20.61	20.61	1.000
24.00	20.62	20.61	20.62	20.62	1.000

At X = 96"

Z (in)	U @ Y = 7" w	U @ Y = c	U @ Y = 7" E	Average Values U	Average Values U/U∞
0.00	12.96	12.14	13.77	12.96	0.628
1.00	14.01	13.33	14.68	14.01	0.769
2.00	14.90	14.15	15.42	14.82	0.718
3.00	15.64	14.66	16.01	15.44	0.748
4.00	16.25	14.90	16.46	15.87	0.770
5.00	16.81	15.31	16.96	16.36	0.793
6.00	17.30	15.79	17.45	16.85	0.817
7.00	17.71	16.31	17.94	17.32	0.840
8.00	18.07	16.88	18.39	17.78	0.862
9.00	18.41	17.45	18.78	18.21	0.882
10.00	18.76	17.96	19.11	18.61	0.902
11.00	19.14	18.41	19.40	18.98	0 921
12.00	19.53	18.80	19.66	19.33	0.937
13.00	19.90	19.21	19.86	19.66	0.953
14.00	20.17	19.43	20.04	19.88	0.964
15.00	20. 16	19.45	20.20	20.00	0.970
16.0	20.46	19.27	20.33	20.02	0.971
17.00	20.55	19.97	20.43	20.32	0.984
18.00	20.62	20.40	20.51	20.51	0.994
19.00	20.67	20.57	20.57	20.60	0.998
20.00	20.69	20.61	20.61	20.64	1.000
21.00	20.69	20.62	20.62	20.64	1.000
22.00	20.59	20.62	20.62	20.64	1.000
23.00	20.69	20.62	20.62	20.64	1.000
24.00	20.69	20.61	20.61	20.64	1.000

At X = 180"

Z (in)	U @ Y = 7" w	U @ Y = c	U @ Y = 7" E	Average Values U	Average Values U/U∞
0.00	12.31	11.43	12.56	12.10	0.588
1.00	13.75	12.79	14.22	13.59	0.660
2.00	14.77	13.81	15.36	14.65	0.711
3.00	15.45	14.56	16.09	15.37	0.746
4.00	15.84	15.07	16.47	15.79	0.767
5.00	16.21	15.51	16.81	16.18	0.786
6.00	16.63	15.90	17.15	16.56	0.804
7.00	17.09	16.24	17.51	16.95	0.823
8.00	17.51	16.54	17.85	17.30	0.840
9.00	17.83	16.84	18.17	17.61	0.855
10.00	18.13	17.17	18.47	17.92	0.870
11.00	18.51	17.55	18.75	18.27	0.886
12.00	18.93	17.97	18.99	18.63	0.904
13.00	19.31	18.39	19.39	19.03	0.924
14.00	19.60	18.82	19.70	19.37	0.941
15.00	19.83	19.23	19.93	19.66	0.954
16.00	19.98	19.64	20.07	19.89	0.966
17.00	20.21	19.92	20.17	20.10	0.976
18.00	20.38	20.16	20.28	20.27	0.984
19.00	20.51	20.36	20.43	20.43	0.992
20.00	20.57	20.50	20.54	20.54	0.997
21.00	20.59	20.59	20.59	20.59	1.000
22.00	20.58	20.63	20.59	20.60	1.000
23.00	20.58	20.63	20.59	20.60	1.000
24.00	20.58	20.60	20.57	20.58	1.000

TABLE 3: VELOCITY DISTRIBUTION DATA (Continued)

Hill 2" x 10" U_a = 10 fps

At X = 8"

Z (in)	U @ Y = 7" w	U @ Y = c	U @ Y = 7" E	Average Values U	Average Values U/U∞
0.00	4.46	4.37	4.77	4.53	0.402
0.50	4.73	4.51	4.53	4.59	0.407
1.00	5.49	4.91	4.87	5.09	0.451
1.50	6.57	5.50	5.70	5.92	0.525
2.00	7.85	6.24	6.84	6.98	0.620
2.50	8.60	7.41	7.70	7.90	0.700
3.00	9.16	8.28	8.31	8.58	0.761
3.50	9.57	8.95	8.71	9.08	0.805
4.00	9.85	9.44	8.94	9.41	0.834
4.50	10.13	9.79	9.24	9.72	0.861
5.00	10.37	10.09	9.51	9.99	0.886
5.50	10.59	10.35	9.76	10.23	0.907
6.00	10.78	10.57	9.98	10.44	0.926
6.50	10.95	10.77	10.18	10.63	0.943
7.00	11.11	10.94	10.37	10.81	0.958
7.50	11.24	11.11	10.54	10.96	0.971
8.00	11.34	11.23	10.69	11.09	0.984
8.50	11.40	11.30	10.81	11.17	0.991
9.00	11.44	11.33	10.91	11.23	0.996
9.50	11.45	11.34	11.00	11.26	1.000
10.00	11.43	11.32	11.06	11.27	1.000

At X = 16"

Z (in)	U @ Y = 7" w	U @ Y = c	U @ Y = 7" E	Average Values U	Average Values U/U∞
0.00	4.22	4.43	3.54	4.06	0.370
0.50	4.90	5.00	5.19	5.03	0.459
1.00	5.68	5.46	6.18	5.77	0.526
1.50	6.52	5.86	6.76	6.38	0.582
2.00	7.40	6.19	7.07	6.89	0.629
2.50	7.89	6.85	7.35	7.36	0.671
3.00	8.35	7.47	7.68	7.83	0.714
3.50	8.78	8.07	8.06	8.30	0.757
4.00	9.19	8.64	8.48	8.77	0.800
4.50	9.55	9.12	8.78	9.15	0.835
5.00	9.85	9.51	9.05	9.47	0.863
5.50	10.10	9.81	9.29	9.73	0.887
6.00	10.32	10.06	9.52	9.97	0.910
6.50	10.54	10.29	9.72	10.18	0.930
7.00	10.74	10.50	9.90	10.38	0.948
7.50	10.92	10.69	10.07	10.56	0.964
8.00	11.05	10.83	10.22	10.70	0.977
8.50	11.13	10.94	10.36	10.81	0.986
9.00	11.17	11.02	10.47	10.87	0.993
9.50	11.20	11.06	10.57	10.94	0.999
10.00	11.19	11.06	10.65	10.96	1.000

At X = 32"

Z (in)	U @ Y = 7" w	U @ Y = c	U @ Y = 7" E	Average Values U	Average Values U/U∞
0.00	6.45	5.38	6.76	6.20	0.564
0.50	6.98	6.73	6.84	6.85	0.623
1.00	7.44	7.43	6.97	7.28	0.663
1.50	7.83	7.68	7.15	7.55	0.687
2.00	8.17	7.52	7.37	7.69	0.700
2.50	8.58	7.83	7.65	8.02	0.730
3.00	8.94	8.18	7.94	8.35	0.760
3.50	9.26	8.55	8.25	8.69	0.791
4.00	9.54	8.95	8.57	9.02	0.821
4.50	9.79	9.32	8.81	9.31	0.847
5.00	10.03	9.65	9.05	9.58	0.873
5.50	10.27	9.97	9.29	9.84	0.896
6.00	10.48	10.26	9.52	10.09	0.920
6.50	10.65	10.51	9.75	10.30	0.938
7.00	10.79	10.72	9.97	10.49	0.956
7.50	10.92	10.88	10.16	10.65	0.970
8.00	11.03	11.00	10.31	10.78	0.983
8.50	11.13	11.07	10.44	10.88	0.992
9.00	11.19	11.11	10.53	10.94	0.997
9.50	11.22	11.12	10.60	10.98	1.000
10.00	11.22	11.11	10.65	10.98	1.000

Hill 2" x 10" U_a = 10 fps

At X = 60"

0.00	5.59	5.39	5.85	5.61	0.512
0.50	6.90	6.73	6.58	6.74	0.615
1.00	7.71	7.55	7.11	7.46	0.680
1.50	8.19	8.00	7.49	7.89	0.720
2.00	8.37	8.16	7.72	8.08	0.737
2.50	8.64	8.39	7.95	8.33	0.760
3.00	8.89	8.62	8.17	8.56	0.781
3.50	9.12	8.84	8.38	8.78	0.801
4.00	9.34	9.05	8.59	8.99	0.820
4.50	9.55	9.28	8.80	9.21	0.840
5.00	9.77	9.51	9.00	9.43	0.860
5.50	9.99	9.74	9.21	9.65	0.880
6.00	10.20	9.97	9.42	9.86	0.899
6.50	10.40	10.19	9.61	10.07	0.919
7.00	10.58	10.39	9.80	10.26	0.936
7.50	10.75	10.58	9.99	10.44	0.953
8.00	10.89	10.72	10.16	10.59	0.967
8.50	11.01	10.82	10.34	10.72	0.978
9.00	11.10	10.88	10.50	10.83	0.989
9.50	11.17	10.91	10.65	10.91	0.995
10.00	11.20	10.91	10.77	10.96	1.000

At X = 96"

0.00	3.50	5.03	6.79	5.11	0.469
0.50	6.58	6.84	7.32	6.91	0.634
1.00	8.01	7.88	7.67	7.85	0.721
1.50	8.64	8.43	7.86	8.31	0.763
2.00	8.66	8.60	7.91	8.39	0.771
2.50	8.87	8.81	8.03	8.57	0.786
3.00	9.07	9.01	8.18	8.75	0.804
3.50	9.24	9.20	8.34	8.93	0.820
4.00	9.40	9.37	8.52	9.10	0.836
4.50	9.59	9.59	8.69	9.29	0.854
5.00	9.77	9.79	8.87	9.48	0.871
5.50	9.93	9.97	9.04	9.65	0.886
6.00	10.09	10.15	9.22	9.82	0.901
6.50	10.26	10.31	9.40	9.99	0.917
7.00	10.42	10.47	9.58	10.16	0.934
7.50	10.58	10.60	9.76	10.31	0.946
8.00	10.73	10.70	9.94	10.46	0.961
8.50	10.86	10.78	10.13	10.59	0.973
9.00	10.98	10.84	10.30	10.71	0.984
9.50	11.08	10.88	10.46	10.81	0.993
10.00	11.14	10.90	10.60	10.88	1.000

At X = 180"

0.00	6.59	6.40	5.74	6.24	0.573
0.50	7.43	7.36	6.61	7.13	0.655
1.00	8.02	8.03	7.21	7.75	0.712
1.50	8.41	8.48	7.60	8.16	0.750
2.00	8.64	8.74	7.82	8.40	0.772
3.00	9.00	9.09	8.19	8.76	0.805
4.00	9.31	9.42	8.52	9.08	0.834
5.00	9.58	9.71	8.81	9.37	0.860
6.00	9.88	9.97	9.08	9.64	0.885
7.00	10.15	10.18	9.39	9.91	0.910
8.00	10.45	10.40	9.67	10.17	0.935
9.00	10.65	10.50	9.94	10.36	0.951
10.00	10.84	10.71	10.20	10.58	0.972
11.00	11.01	10.80	10.44	10.75	0.988
12.00	11.12	10.85	10.67	10.88	1.000

TABLE 3: VELOCITY DISTRIBUTION (Continued)

Hill 1" x 10" $U_a \approx 20$ fps

At X = 4"

Z (in)	U @ Y = 7" w	U @ Y = c	U @ Y = 7" E	Average Values U	Average Values U/U∞
0.00	12.65	10.77	12.38	11.93	0.570
1.00	14.40	12.87	14.46	13.91	0.665
2.00	15.67	14.30	15.92	15.30	0.732
3.00	16.57	15.24	16.93	16.25	0.777
4.00	17.17	15.78	17.55	16.83	0.804
5.00	17.77	16.33	18.09	17.40	0.832
6.00	18.31	16.84	18.53	17.89	0.856
7.00	18.81	17.33	18.89	18.34	0.877
8.00	19.22	17.79	19.19	18.73	0.895
9.00	19.53	18.24	19.48	19.08	0.913
10.00	19.80	18.68	19.78	19.42	0.928
11.00	20.09	19.09	20.08	19.75	0.945
12.00	20.37	19.49	20.37	20.08	0.961
13.00	20.59	19.86	20.55	20.33	0.971
14.00	20.75	20.17	20.70	20.54	0.982
15.00	20.86	20.43	20.81	20.70	0.990
16.00	20.92	20.62	20.89	20.81	0.994
17.00	20.92	20.78	20.91	20.87	0.998
18.00	20.92	20.88	20.92	20.90	0.999
19.00	20.92	20.92	20.92	20.92	1.000
20.00	20.92	20.92	20.92	20.92	1.000
21.00	20.92	20.92	20.92	20.92	1.000
22.00	20.92	20.92	20.92	20.92	1.000
23.00	20.92	20.92	20.92	20.92	1.000
24.00	20.92	20.92	20.92	20.92	1.000

At X = 12"

Z (in)	U @ Y = 7" w	U @ Y = c	U @ Y = 7" E	Average Values U	Average Values U/U∞
0.00	12.19	11.08	12.20	11.82	0.564
1.00	14.13	12.93	14.44	13.83	0.660
2.00	15.57	14.25	15.96	15.26	0.728
3.00	16.62	15.18	16.94	16.25	0.776
4.00	17.37	15.80	17.48	16.88	0.806
5.00	17.90	16.40	18.00	17.43	0.831
6.00	18.36	16.94	18.44	17.91	0.854
7.00	18.75	17.44	18.78	18.32	0.874
8.00	19.10	17.87	19.05	18.67	0.892
9.00	19.44	18.25	19.29	18.99	0.906
10.00	19.76	18.65	19.53	19.31	0.921
11.00	20.06	19.08	19.76	19.63	0.936
12.00	20.34	19.53	20.00	19.96	0.953
13.00	20.54	19.86	20.22	20.21	0.964
14.00	20.70	20.14	20.42	20.42	0.975
15.00	20.83	20.39	20.60	20.61	0.984
16.00	20.93	20.59	20.77	20.76	0.991
17.00	20.94	20.79	20.87	20.87	0.996
18.00	20.95	20.91	20.93	20.93	0.999
19.00	20.96	20.96	20.95	20.96	1.000
20.00	20.95	20.96	20.96	20.96	1.000
21.00	20.95	20.96	20.95	20.95	1.000
22.00	20.95	20.95	20.95	20.95	1.000
23.00	20.95	20.95	20.95	20.95	1.000
24.00	20.95	20.95	20.95	20.95	1.000

At X = 24"

Z (in)	U @ Y = 7" w	U @ Y = c	U @ Y = 7" E	Average Values U	Average Values U/U∞
0.00	12.18	10.87	12.03	11.69	0.558
1.00	13.96	12.66	14.20	13.61	0.649
2.00	15.32	13.94	15.66	14.97	0.714
3.00	16.36	14.86	16.60	15.94	0.761
4.00	17.15	15.46	17.12	16.58	0.791
5.00	17.75	16.10	17.76	17.20	0.821
6.00	18.28	16.64	18.29	17.74	0.847
7.00	18.72	17.10	18.71	18.18	0.868
8.00	19.10	17.53	19.05	18.56	0.885
9.00	19.45	17.98	19.31	18.91	0.902
10.00	19.74	18.42	19.54	19.23	0.918
11.00	20.00	18.83	19.77	19.53	0.932
12.00	20.22	19.21	20.00	19.81	0.945
13.00	20.46	19.58	20.17	20.07	0.959
14.00	20.66	19.91	20.34	20.30	0.970
15.00	20.82	20.22	20.52	20.52	0.980
16.00	20.93	20.49	20.69	20.70	0.988
17.00	20.95	20.74	20.83	20.85	0.995
18.00	20.95	20.90	20.92	20.92	0.998
19.00	20.95	20.96	20.95	20.95	1.000
20.00	20.95	20.96	20.96	20.96	1.000
21.00	20.95	20.96	20.96	20.96	1.000
22.00	20.95	20.95	20.95	20.95	1.000
23.00	20.95	20.95	20.95	20.95	1.000
24.00	20.95	20.95	20.95	20.95	1.000

Hill 1" x 10" $U_a \approx 20$ fps

At X = 48"

Z (in)	U @ Y = 7" w	U @ Y = c	U @ Y = 7" E	Average Values U	Average Values U/U∞
0.00	13.14	11.77	12.71	12.54	0.600
1.00	14.65	13.20	14.63	14.16	0.677
2.00	15.77	14.26	15.98	15.34	0.734
3.00	16.56	15.03	16.90	16.16	0.773
4.00	17.08	15.56	17.45	16.70	0.799
5.00	17.61	16.10	17.95	17.22	0.823
6.00	18.10	16.63	18.39	17.71	0.846
7.00	18.56	17.15	18.75	18.15	0.868
8.00	18.99	17.64	19.06	18.56	0.888
9.00	19.36	18.11	19.33	18.93	0.905
10.00	19.70	18.56	19.58	19.28	0.923
11.00	20.00	19.00	19.83	19.61	0.938
12.00	20.27	19.43	20.06	19.92	0.952
13.00	20.51	19.76	20.25	20.17	0.965
14.00	20.68	20.08	20.43	20.40	0.976
15.00	20.80	20.37	20.60	20.59	0.985
16.00	20.85	20.64	20.77	20.75	0.993
17.00	20.88	20.76	20.83	20.82	0.996
18.00	20.90	20.85	20.88	20.88	1.000
19.00	20.90	20.90	20.90	20.90	1.000
20.00	20.90	20.91	20.90	20.90	1.000
21.00	20.90	20.90	20.90	20.90	1.000
22.00	20.90	20.90	20.90	20.90	1.000
23.00	20.90	20.90	20.90	20.90	1.000
24.00	20.90	20.90	20.90	20.90	1.000

At X = 72"

Z (in)	U @ Y = 7" w	U @ Y = c	U @ Y = 7" E	Average Values U	Average Values U/U∞
0.00	12.87	11.72	13.24	12.61	0.602
1.00	14.70	13.19	14.73	14.21	0.678
2.00	15.96	14.32	15.89	15.39	0.735
3.00	16.78	15.17	16.80	16.25	0.776
4.00	17.22	15.79	17.50	16.84	0.804
5.00	17.76	16.31	18.07	17.38	0.829
6.00	18.25	16.81	18.54	17.87	0.853
7.00	18.67	17.29	18.91	18.29	0.873
8.00	19.05	17.75	19.20	18.67	0.891
9.00	19.38	18.18	19.46	19.01	0.907
10.00	19.67	18.59	19.69	19.32	0.922
11.00	19.93	18.98	19.89	19.60	0.936
12.00	20.15	19.36	20.07	19.86	0.948
13.00	20.37	19.72	20.24	20.11	0.960
14.00	20.57	20.03	20.42	20.34	0.971
15.00	20.74	20.31	20.58	20.54	0.981
16.00	20.88	20.54	20.75	20.72	0.989
17.00	20.92	20.73	20.84	20.83	0.995
18.00	20.93	20.85	20.90	20.89	0.998
19.00	20.94	20.92	20.93	20.93	1.000
20.00	20.94	20.94	20.94	20.94	1.000
21.00	20.94	20.94	20.94	20.94	1.000
22.00	20.94	20.94	20.94	20.94	1.000
23.00	20.94	20.94	20.94	20.94	1.000
24.00	20.94	20.94	20.94	20.94	1.000

At X = 96"

Z (in)	U @ Y = 7" w	U @ Y = c	U @ Y = 7" E	Average Values U	Average Values U/U∞
0.00	13.38	12.39	12.65	12.81	0.611
1.00	14.74	13.53	14.45	14.23	0.679
2.00	15.80	14.42	15.72	15.31	0.731
3.00	16.61	15.12	16.60	16.11	0.769
4.00	17.21	15.65	17.13	16.66	0.795
5.00	17.66	16.13	17.72	17.17	0.820
6.00	18.06	16.61	18.21	17.63	0.842
7.00	18.42	17.10	18.59	18.04	0.862
8.00	18.76	17.58	18.90	18.41	0.879
9.00	19.11	18.04	19.19	18.78	0.896
10.00	19.44	18.48	19.47	19.13	0.913
11.00	19.76	18.89	19.75	19.47	0.929
12.00	20.07	19.27	20.02	19.79	0.945
13.00	20.33	19.62	20.22	20.06	0.957
14.00	20.54	19.95	20.40	20.30	0.969
15.00	20.70	20.24	20.59	20.51	0.979
16.00	20.81	20.51	20.76	20.69	0.989
17.00	20.87	20.69	20.86	20.81	0.994
18.00	20.92	20.82	20.92	20.89	0.998
19.00	20.94	20.90	20.94	20.93	1.000
20.00	20.94	20.93	20.94	20.94	1.000
21.00	20.94	20.94	20.94	20.94	1.000
22.00	20.94	20.94	20.94	20.94	1.000
23.00	20.94	20.94	20.94	20.94	1.000
24.00	20.94	20.94	20.94	20.94	1.000

TABLE 3: VELOCITY DISTRIBUTION (Continued)

Hill 1" x 10" U_a = 20 fps

At X = 180"

Z (in)	U @ Y = 7" W	U @ Y = c	U @ Y = 7" E	Average Values U	Average Values U/U_∞
0.00	12.78	11.84	13.08	12.57	0.600
1.00	14.06	13.08	14.53	13.89	0.663
2.00	15.13	14.07	15.64	14.95	0.713
3.00	16.03	14.86	16.48	15.79	0.753
4.00	16.80	15.48	17.09	16.46	0.784
5.00	17.30	16.04	17.57	16.97	0.809
6.00	17.74	16.54	17.97	17.42	0.830
7.00	18.13	16.97	18.29	17.80	0.848
8.00	18.47	17.35	18.55	18.12	0.864
9.00	18.81	17.70	18.78	18.43	0.879
10.00	10.15	18.04	19.02	18.74	0.894
11.00	19.48	18.38	19.28	19.05	0.908
12.00	19.80	18.72	19.55	19.36	0.922
13.00	20.05	19.15	19.79	19.66	0.936
14.00	20.27	19.54	20.01	19.94	0.950
15.00	20.48	19.90	20.22	20.20	0.963
16.00	20.66	20.22	20.40	20.43	0.974
17.00	20.80	20.42	20.61	20.61	0.982
18.00	20.89	20.60	20.76	20.75	0.989
19.00	20.96	20.75	20.87	20.86	0.994
20.00	20.98	20.87	20.93	20.93	0.998
21.00	20.98	20.94	20.97	20.96	1.000
22.00	20.97	20.98	20.98	20.98	1.000
23.00	20.97	20.99	20.98	20.98	1.000
24.00	20.97	20.96	20.97	20.97	1.000

Flat Plate U_a = 20 fps

At X = 120"

Z (in)	U @ Y = c	U/U_∞
0.00	10.89	0.526
0.50	12.03	0.581
1.00	12.95	0.626
1.50	13.68	0.661
2.00	14.29	0.690
2.50	14.80	0.715
3.00	15.23	0.736
4.00	15.90	0.769
5.00	16.48	0.796
6.00	16.95	0.819
7.00	17.34	0.838
8.00	17.69	0.855
9.00	18.00	0.870
10.00	18.35	0.887
11.00	18.68	0.902
12.00	18.99	0.918
13.00	19.29	0.932
14.00	19.59	0.946
15.00	19.89	0.961
16.00	20.06	0.969
17.00	20.23	0.977
18.00	20.40	0.985
19.00	20.54	0.992
20.00	20.64	0.998
21.00	20.70	1.000

TABLE 4: PARAMETERS OF CONCENTRATION PROFILES

Flat Plate U_a = 10 fps

X (in)	y (in)	z (in)	λ @ $\frac{1}{2}C_{max}$ (in)	η @ $\frac{1}{2}C_{max}$ (in)	δ (in)	C_{max} (vertical) ppm x 10^4	C_{max} (horizontal) ppm x 10^4
36	c	Var.	1.84	-	-	0.087	-
68	c	Var.	2.35	-	-	0.0575	-
72	c	Var.	3.00	-	-	0.0372	-
96	c	Var.	3.65	-	-	0.0224	-
132	c	Var.	5.07	-	-	0.0109	-
168	c	Var.	5.95	-	-	0.0118	-
204	c	Var.	6.85	-	-	0.0084	-
24	Var.	1/8	-	1.65	-	-	0.087
48	Var.	1/8	-	2.34	-	-	0.056
72	Var.	1/8	-	2.83	-	-	0.035
96	Var.	1/8	-	3.32	-	-	0.0212
132	Var.	1/8	-	4.30	-	-	0.0107
168	Var.	1/8	-	4.20	-	-	0.0112
204	Var.	1/8	-	5.50	-	-	0.0085

Hill 2" x 10" U_a = 40 fps

8	c	Var.	2.05	-	16.16	0.0775	-
	Var.	1/8	-	1.515	-	-	0.0765
	Var.	2	-	1.315	-	-	0.0440
	Var.	2 1/2	-	1.500	-	-	0.0263
16	c	Var.	2.62	-	16.54	0.0440	-
	Var.	1/8	-	1.98	-	-	0.0400
	Var.	2	-	1.91	-	-	0.0272
	Var.	3	-	1.88	-	-	0.0180
32	c	Var.	3.68	-	17.41	0.0190	-
	Var.	1/8	-	2.44	-	-	0.0186
	Var.	3 1/2	-	2.55	-	-	0.0100
	Var.	4.65	-	2.55	-	-	0.0058
60	c	Var.	5.12	-	18.03	0.0098	-
	Var.	1/8	-	3.20	-	-	0.0098
	Var.	6	-	3.43	-	-	0.00395
	Var.	8	-	3.25	-	-	0.00140
96	c	Var.	6.20	-	18.24	0.00684	-
	Var.	1/8	-	3.63	-	-	0.00662
	Var.	7	-	4.00	-	-	0.00295
	Var.	9	-	3.87	-	-	0.00150
180	c	Var.	9.70	-	20.20	0.00292	-
	Var.	1/8	-	5.40	-	-	0.00289
	Var.	7	-	6.10	-	-	0.00220
	Var.	9	-	5.60	-	-	0.00160
	Var.	14	-	4.80	-	-	0.00040

Hill 4" x 20" U_a = 20 fps

X (in)	y (in)	z (in)	λ @ $\frac{1}{2}C_{max}$ (in)	η @ $\frac{1}{2}C_{max}$ (in)	δ (in)	C_{max} (vertical) ppm x 10^4	C_{max} (horizontal) ppm x 10^4
12	c	Var.	3.46	-	16.77	0.0610	-
	Var.	1/8	-	2.81	-	-	0.0612
	Var.	3	-	2.61	-	-	0.0363
	Var.	4 1/2	-	2.15	-	-	0.0150
24	c	Var.	4.23	-	17.38	0.0330	-
	Var.	1/8	-	3.27	-	-	0.0320
	Var.	3 3/4	-	3.15	-	-	0.0195
	Var.	5	-	2.97	-	-	0.0125
48	c	Var.	6.00	-	17.22	0.0157	-
	Var.	1/8	-	4.15	-	-	0.0155
	Var.	6	-	3.72	-	-	0.0078
	Var.	8	-	3.72	-	-	0.0042
72	c	Var.	7.38	-	17.50	0.0096	-
	Var.	1/8	-	4.05	-	-	0.0094
	Var.	7	-	4.975	-	-	0.00525
	Var.	10	-	3.82	-	-	0.00230
96	c	Var.	8.45	-	17.53	0.0073	-
	Var.	1/8	-	4.95	-	-	0.0072
	Var.	5 1/2	-	5.50	-	-	0.0052
	Var.	8 1/2	-	5.17	-	-	0.0036
180	c	Var.	11.5	-	19.55	0.00465	-
	Var.	1/8	-	5.05	-	-	0.00455
	Var.	11 1/2	-	6.72	-	-	0.00240
	Var.	15 1/2	-	5.55	-	-	0.00110

Hill 2" x 10" U_a = 20 fps

8	c	Var.	2.00	-	15.80	0.1120	-
	Var.	1/8	-	2.35	-	-	0.1100
	Var.	1 3/4	-	2.25	-	-	0.0650
	Var.	2 3/4	-	2.20	-	-	0.0293
16	c	Var.	2.53	-	16.54	0.0565	-
	Var.	1/8	-	2.85	-	-	0.057
	Var	2 1/2	-	2.85	-	-	0.0276
	Var.	3 3/4	-	2.60	-	-	0.0125
32	c	Var.	3.33	-	17.10	0.0310	-
	Var.	1/8	-	3.40	-	-	0.0305
	Var.	2	-	3.45	-	-	0.0220
	Var.	4	-	3.08	-	-	0.0122
	Var.	5 1/2	-	2.80	-	-	0.0055
60	c	Var.	4.80	-	16.70	0.0170	-
	Var.	1/8	-	3.90	-	-	0.0177
	Var.	3	-	4.17	-	-	0.0121
	Var.	5	-	4.10	-	-	0.0081
96	c	Var.	6.08	-	17.80	0.0098	-
	Var.	1/8	-	4.80	-	-	0.0097
	Var.	5	-	4.90	-	-	0.00595
	Var.	8 1/4	-	4.65	-	-	0.0028
180	c	Var.	9.30	-	19.00	0.0065	-
	Var.	1/8	-	6.55	-	-	0.00470
	Var.	8 1/2	-	6.52	-	-	0.00238
	Var.	12	-	6.38	-	-	0.00131

TABLE 4 (Continued)

Hill 2" x 10" U_a = 10 fps

X (in)	y (in)	z (in)	λ @ $\frac{1}{2}C_{max}$ (in)	η @ $\frac{1}{2}C_{max}$ (in)	δ (in)	C_{max} (vertical) ppm x 10^4	C_{max} (horizontal) ppm x 10^4
8	c	Var.	2.82	-	8.77	0.143	-
	Var.	1/8	-	2.70	-	-	0.132
	Var.	2 1/2	-	2.30	-	-	0.092
	Var.	3 1/2	-	1.85	-	-	0.032
16	c	Var.	2.92	-	9.18	0.080	-
	Var.	1/8	-	3.15	-	-	0.074
	Var.	2 3/4	-	2.75	-	-	0.0435
	Var.	4 1/2	-	2.46	-	-	0.0124
32	c	Var.	3.50	-	9.07	0.0418	-
	Var.	1/8	-	4.16	-	-	0.0408
	Var.	3 1/2	-	3.78	-	-	0.0207
	Var.	5	-	3.75	-	-	0.0107
60	c	Var.	4.36	-	9.69	0.0220	-
	Var.	1/8	-	5.42	-	-	0.0216
	Var.	4 1/2	-	4.60	-	-	0.0111
	Var.	7	-	4.12	-	-	0.0050
96	c	Var.	5.58	-	10.10	0.0146	-
	Var.	1/8	-	6.73	-	-	0.01435
	Var.	4	-	5.85	-	-	0.00955
	Var.	6	-	5.75	-	-	0.00705
180	c	Var.	7.30	-	12.05	0.00876	-
	Var.	1/8	-	8.30	-	-	0.00868
	Var.	7	-	7.55	-	-	0.00480
	Var.	10	-	7.05	-	-	0.00270

Hill 1" x 10" U_a = 20 fps

X (in)	y (in)	z (in)	λ @ $\frac{1}{2}C_{max}$ (in)	η @ $\frac{1}{2}C_{max}$ (in)	δ (in)	C_{max} (vertical) ppm x 10^4	C_{max} (horizontal) ppm x 10^4
4	c	Var.	0.69	-	15.69	0.816	-
	Var.	1/8	-	0.81	-	-	0.780
	Var.	3/4	-	0.785	-	-	0.353
	Var.	1 1/2	-	0.80	-	-	0.020
12	c	Var.	0.885	-	16.36	0.334	-
	Var.	1/8	-	1.24	-	-	0.3375
	Var.	7/8	-	1.315	-	-	0.1750
	Var.	1 7/16	-	1.25	-	-	0.0875
24	c	Var.	1.41	-	16.82	0.163	-
	Var.	1/8	-	1.49	-	-	0.159
	Var.	1 1/4	-	1.75	-	-	0.0895
	Var.	2	-	1.725	-	-	0.0475
48	c	Var.	2.28	-	16.60	0.0616	-
	Var.	1/8	-	2.02	-	-	0.06225
	Var.	2	-	2.36	-	-	0.03420
	Var.	3	-	2.42	-	-	0.02030
72	c	Var.	3.07	-	16.92	0.0234	-
	Var.	1/8	-	2.68	-	-	0.0257
	Var.	3	-	2.73	-	-	0.0168
	Var.	4 1/2	-	3.06	-	-	0.0085
96	c	Var.	3.80	-	17.00	0.0210	-
	Var.	1/8	-	2.96	-	-	0.02375
	Var.	4	-	3.48	-	-	0.0110
	Var.	6	-	3.40	-	-	0.0054
180	c	Var.	6.90	-	18.78	0.00792	-
	Var.	1/8	-	4.32	-	-	0.00812
	Var.	6	-	5.42	-	-	0.0050
	Var.	8	-	4.94	-	-	0.00335

TABLE 5: CONCENTRATION DISTRIBUTION DATA: VERTICAL

X (in)	Y (in)	ΔZ (in)	0	1	2	3	4	5	6	7	8	9	10	11	12	13	14	15	16	17	18	19	20
			Concentrations in PPM at Z = nΔZ, where n is equal to:																				
			Hill 4" x 20" U_a = 20 fps																				
12	0	0.5	617.0	572.0	552.0	502.0	432.0	412.0	367.0	302.0	222.0	152.0	114.0	69.0	36.0	18.0	8.0	-	-	-	-	-	-
24	0	0.5	332.0	299.0	279.0	269.0	254.0	239.0	219.0	199.0	179.0	152.0	121.0	89.0	59.0	40.0	26.0	16.0	17.0	7.0	4.0	-	-
48	0	1.0	158.0	130.0	122.0	115.0	105.0	90.0	80.0	61.0	40.0	29.0	16.0	8.0	5.0	-	-	-	-	-	-	-	-
72	0	1.0	96.5	91.0	84.0	81.0	75.0	67.0	62.0	52.0	42.0	32.0	22.0	17.0	12.0	7.0	3.0	-	-	-	-	-	-
96	0	1.0	73.2	67.0	63.0	59.0	57.0	54.0	51.0	45.0	39.0	33.0	26.0	21.0	15.0	10.0	5.0	2.0	0.5	-	-	-	-
180	0	2.0	46.5	43.0	42.0	37.0	33.0	28.0	22.0	15.0	9.0	5.0	2.0	1.0	0.5	0.5	0.5	-	-	-	-	-	-
			Hill 2" x 10" U_a = 40 fps																				
8	0	0.5	774.0	706.0	646.0	546.0	386.0	256.0	118.0	37.0	12.0	-	-	-	-	-	-	-	-	-	-	-	-
16	0	0.5	415.0	360.0	340.0	310.0	280.0	220.0	180.0	120.0	69.0	39.0	16.0	5.0	2.0	-	-	-	-	-	-	-	-
32	0	0.5	190.5	174.0	164.0	154.0	139.0	129.0	119.0	97.0	79.0	64.0	44.0	32.0	18.0	10.0	4.0	2.0	-	-	-	-	-
60	0	1.0	98.0	79.0	76.0	71.0	62.0	50.0	39.0	27.0	16.0	8.0	4.0	1.0	-	-	-	-	-	-	-	-	-
96	0	1.0	68.5	59.0	55.0	51.0	49.0	43.0	36.0	30.0	22.0	15.0	10.0	5.0	2.0	-	-	-	-	-	-	-	-
180	0	1.0	29.1	27.0	26.0	26.0	26.0	25.0	24.0	22.0	19.0	17.0	14.0	11.0	8.0	6.0	4.0	2.0	1.0	1.0	1.0	-	-
			Hill 2" x 10" U_a = 20 fps																				
8	0	0.5	1120.0	1006.0	886.0	766.0	586.0	376.0	221.0	116.0	60.0	15.0	8.0	-	-	-	-	-	-	-	-	-	-
16	0	0.5	567.0	534.0	474.0	424.0	336.0	309.0	219.0	154.0	104.0	60.0	33.0	18.0	9.0	-	-	-	-	-	-	-	-
32	0	0.5	315.0	291.0	271.0	241.0	221.0	201.0	173.0	151.0	119.0	94.0	74.0	54.0	39.0	24.0	13.0	7.0	4.0	-	-	-	-
60	0	1.0	173.0	152.0	138.0	120.0	102.0	82.0	62.0	43.0	26.0	15.0	10.0	6.0	2.0	-	-	-	-	-	-	-	-
96	0	1.0	99.5	89.0	80.0	73.0	66.0	60.0	51.0	41.0	32.0	23.0	16.0	9.0	6.0	-	-	-	-	-	-	-	-
180	0	1.0	45.2	43.0	41.0	40.0	36.0	35.0	32.0	30.0	28.0	24.0	20.0	16.0	13.0	10.0	7.0	6.0	4.0	1.0	-	-	-
			Hill 2" x 10" U_a = 10 fps																				
8	0	0.5	1430.0	1280.0	1300.0	1250.0	1124.0	925.0	579.0	320.0	169.0	48.0	6.0	-	-	-	-	-	-	-	-	-	-
16	0	0.5	830.0	750.0	685.0	643.0	577.0	488.0	382.0	286.0	200.0	126.0	70.0	33.0	15.0	6.0	-	-	-	-	-	-	-
32	0	0.5	419.0	383.0	357.5	322.5	297.0	275.0	244.0	210.0	172.0	137.0	107.0	80.0	58.0	38.0	25.0	15.0	8.0	3.0	-	-	-
60	0	1.0	218.5	191.5	163.0	143.0	119.0	93.0	68.5	46.5	29.0	15.0	7.0	2.0	-	-	-	-	-	-	-	-	-
96	0	1.0	145.5	132.2	119.4	106.5	93.0	80.0	67.5	54.5	43.0	32.0	22.5	14.5	8.0	4.8	3.5	-	-	-	-	-	-
180	0	1.0	87.2	82.0	76.0	69.0	62.8	57.0	51.3	46.0	39.0	32.6	26.5	20.7	15.6	11.6	8.3	5.1	2.8	0.8	-	-	-
			Hill 1" x 10" U_a = 20 fps																				
4	0	0.25	8160.0	7215.0	5650.0	3510.0	1570.0	650.0	200.0	50.0	5.0	-	-	-	-	-	-	-	-	-	-	-	-
12	0	0.25	3350.0	2785.0	2300.0	1875.0	1500.0	1130.0	780.0	480.0	250.0	120.0	60.0	20.0	10.0	-	-	-	-	-	-	-	-
24	0	0.25	1635.0	1490.0	1320.0	1160.0	1020.0	895.0	770.0	630.0	485.0	350.0	240.0	170.0	110.0	70.0	45.0	30.0	20.0	10.0	-	-	-
48	0	0.5	617.0	550.0	470.0	400.0	344.0	278.0	213.0	157.0	112.0	75.0	46.0	28.0	15.0	5.0	-	-	-	-	-	-	-
72	0	0.5	235.0	212.0	193.0	177.0	159.0	140.0	120.0	101.0	83.0	67.0	52.0	37.0	26.0	18.0	13.0	9.5	7.0	5.0	3.5	2.0	-
96	0	1.0	201.0	181.0	154.5	127.0	100.0	75.0	52.5	32.0	17.5	8.5	4.0	2.0	0.5	-	-	-	-	-	-	-	-
180	0	1.0	79.2	74.3	69.2	63.6	58.2	52.6	46.4	38.8	30.7	22.6	15.9	10.7	7.3	4.7	2.9	1.5	0.5	-	-	-	-
			Flat Plate U_a = 20 fps																				
12	0	0.25	500.0	1040.0	1940.0	2840.0	2940.0	247.0	1800.0	1030.0	520.0	250.0	100.0	50.0	30.0	-	-	-	-	-	-	-	-
24	0	0.25	875.0	960.0	1030.0	1050.0	1040.0	990.0	897.0	770.0	630.0	480.0	370.0	280.0	205.0	150.0	110.0	-	-	-	-	-	-
48	0	0.5	576.0	516.0	455.0	393.0	333.0	274.0	222.0	174.0	128.0	93.0	65.0	42.5	22.5	10.0	5.0	-	-	-	-	-	-
72	0	0.5	374.0	334.0	300.0	270.0	240.0	215.0	187.5	161.0	135.0	108.0	82.0	58.0	42.0	32.0	23.0	15.0	7.0	-	-	-	-
96	0	0.5	224.0	209.0	193.0	178.0	163.0	148.0	132.0	117.0	100.0	85.0	69.0	54.0	41.0	32.0	24.0	18.0	14.0	7.0	3.0	-	-
132	0	1.0	137.0	126.0	114.5	102.0	87.0	72.0	58.5	44.0	34.5	28.0	23.5	19.0	16.5	14.5	13.5	-	-	-	-	-	-
154	0	1.0	118.0	104.0	93.0	83.0	74.0	66.5	58.5	48.0	38.0	28.5	20.5	14.0	8.5	4.0	2.0	-	-	-	-	-	-
187	0	1.0	84.0	80.0	73.5	67.0	61.0	55.0	48.0	40.5	33.0	25.0	19.0	13.0	9.0	6.0	3.8	2.2	1.0	-	-	-	-

TABLE 6: CONCENTRATION DISTRIBUTION DATA: HORIZONTAL DISTRIBUTIONS

Hill 4" x 20" U_a = 20 fps

X (in)	Z (in)	Concentration in PPM at y (in inches) -9	-8	-7	-6	-5	-4	-3	-2	-1	0	+1	+2	+3	+4	+5	+6	+7	+8	+9
12	0.125	-	-	10.5	35.5	76.5	152.5	272.5	422.5	572.5	612.5	592.5	422.5	287.5	154.5	84.5	37.5	19.5	-	-
	3.00	-	-	-	7.5	44.5	74.5	152.5	232.5	307.5	362.5	312.5	247.5	152.5	75.5	26.5	7.5	-	-	-
	4.50	-	-	-	0.5	5.5	18.5	44.5	86.5	126.5	151.5	113.5	73.5	43.5	19.5	7.5	4.5	-	-	-
24	0.125	-	8.0	17.0	32.0	68.0	113.0	183.0	248.0	303.0	333.0	313.0	248.0	168.0	103.0	68.0	32.0	21.0	14.0	-
	3.75	-	1.5	4.5	15.5	30.5	63.5	111.5	156.5	186.5	196.5	181.5	151.5	101.5	61.5	31.5	16.5	9.5	5.5	-
	5.00	-	-	-	5.0	15.0	35.0	62.0	92.0	117.0	123.0	116.0	87.0	59.0	35.0	15.0	7.0	2.0	-	-
48	0.125	10.0	17.0	29.0	44.0	64.0	84.0	99.0	129.0	149.0	154.0	149.0	129.0	94.0	75.0	55.0	39.0	25.0	16.0	10.0
	6.00	-	2.0	6.0	12.0	24.0	36.0	48.0	58.0	68.0	80.0	73.0	58.0	50.0	35.0	22.0	14.0	7.0	4.0	-
	8.00	-	1.0	2.0	6.0	12.0	18.0	22.0	28.0	38.0	42.0	37.0	28.0	22.0	16.0	11.0	6.0	3.0	2.0	-
72	0.125	4.0	9.0	14.0	23.0	36.0	49.0	61.0	78.0	91.0	94.0	91.0	81.0	64.0	48.0	34.0	22.0	14.0	10.0	7.0
	7.00	6.0	8.0	12.0	17.0	24.0	34.0	42.0	44.0	51.0	53.0	51.0	44.0	42.0	36.0	25.0	20.0	14.0	9.0	6.0
	10.00	0.5	2.0	3.0	4.0	9.0	11.5	14.0	17.0	20.0	23.0	19.0	17.0	14.0	11.5	9.0	4.0	3.0	2.0	0.5
96	0.125	13.0	18.0	24.0	30.0	38.0	46.0	56.0	64.0	70.0	72.0	70.0	62.0	52.0	42.0	34.0	26.0	21.0	16.0	12.0
	5.50	9.0	12.0	19.0	24.0	32.0	39.0	44.0	49.0	51.0	52.0	51.0	48.0	43.0	36.0	29.0	22.0	16.0	12.0	8.0
	8.50	4.0	7.0	11.0	15.0	20.0	24.0	29.0	32.0	34.0	36.0	34.0	31.0	26.0	21.0	18.0	14.0	11.0	8.0	6.0
180	0.125	12.0	15.0	20.0	23.0	28.0	31.0	38.0	42.0	45.0	45.0	45.0	42.0	38.0	33.0	28.0	23.0	18.0	14.5	11.0
	10.75	7.0	9.0	12.0	16.0	18.0	20.0	22.0	22.0	23.0	24.0	23.0	22.0	20.0	19.0	16.0	13.0	11.0	8.0	7.0
	14.00	2.0	3.0	4.0	5.0	6.0	8.0	9.0	10.0	10.0	10.0	10.0	10.0	9.0	8.0	6.0	5.0	4.0	3.0	2.0

Hill 2" x 10" U_a = 40 fps

8	0.125	-	-	-	-	10.0	28.0	99.0	256.0	536.0	766.0	546.0	256.0	86.0	16.0	5.0	-	-	-	-
	2.00	-	-	-	-	-	2.0	17.0	98.0	283.0	443.0	293.0	98.0	15.0	4.0	-	-	-	-	-
	2.50	-	-	-	-	-	-	13.0	73.0	196.0	263.0	196.0	72.0	16.0	4.0	-	-	-	-	-
16	0.125	-	-	-	2.0	10.0	30.0	83.0	195.0	330.0	400.0	330.0	195.0	82.0	31.0	9.0	2.0	-	-	-
	2.00	-	-	-	-	3.0	15.0	51.0	124.0	224.0	274.0	224.0	129.0	52.0	15.0	1.0	-	-	-	-
	3.00	-	-	-	-	-	5.0	28.0	80.0	152.0	180.0	144.0	84.0	32.0	6.0	-	-	-	-	-
32	0.125	-	-	-	-	11.0	34.0	65.0	115.0	170.0	185.0	170.0	120.0	65.0	29.0	10.0	-	-	-	-
	3.50	-	-	-	-	4.0	19.0	38.0	65.0	94.0	100.0	93.0	65.0	37.0	17.0	4.0	-	-	-	-
	4.65	-	-	-	2.0	5.0	11.0	21.0	38.0	52.0	58.0	50.0	38.0	22.0	10.0	4.0	2.0	-	-	-
60	0.125	-	3.0	5.0	10.0	18.0	32.0	52.0	77.0	95.0	98.0	95.0	78.0	54.0	36.0	22.0	12.0	6.0	3.0	-
	6.00	-	2.0	3.0	5.0	9.0	16.0	23.0	31.0	36.0	40.0	36.0	31.0	24.0	16.0	10.0	6.0	3.0	2.0	-
	8.00	-	-	-	2.0	2.0	4.0	8.0	11.0	14.0	14.0	14.0	11.0	8.0	6.0	3.0	2.0	2.0	-	-
96	0.125	-	5.0	8.0	13.0	20.0	29.0	41.0	51.0	61.0	67.0	62.0	51.0	39.0	29.0	21.0	14.0	9.0	6.0	-
	7.00	-	2.0	4.0	6.0	10.0	14.0	19.0	24.0	27.0	30.0	27.0	24.0	21.0	16.0	11.0	7.0	4.0	2.0	-
	9.00	-	1.0	2.0	4.0	5.0	7.0	10.0	12.0	14.0	15.0	14.0	12.0	10.0	7.0	5.0	4.0	2.0	1.0	-
180	0.125	5.0	7.0	9.0	13.0	16.0	19.0	23.0	26.0	28.0	29.0	28.0	26.0	23.0	19.0	15.0	13.0	9.0	7.0	5.0
	7.00	5.0	7.0	9.0	11.0	14.0	16.0	18.0	20.0	21.0	22.0	21.0	20.0	18.0	16.0	14.0	11.0	9.0	7.0	5.0
	9.00	2.0	3.0	5.0	7.0	9.0	11.0	13.0	15.0	15.0	16.0	15.0	15.0	13.0	11.0	9.0	7.0	5.0	3.0	2.0

Hill 2" x 10" U_a = 20 fps

8	0.125	-	10.0	25.0	43.0	99.0	203.0	398.0	673.0	933.0	1093.0	923.0	653.0	353.0	153.0	67.0	43.0	25.0	15.0	-
	1.75	-	-	15.0	27.0	54.0	112.0	212.0	372.0	572.0	652.0	572.0	372.0	202.0	92.0	35.0	8.0	3.0	-	-
	2.75	-	-	2.0	8.0	18.0	40.0	80.0	150.0	240.0	290.0	250.0	170.0	90.0	35.0	15.0	6.0	2.0	-	-
16	0.125	7.0	11.0	23.0	44.0	89.0	154.0	261.0	391.0	541.0	571.0	541.0	411.0	271.0	146.0	86.0	41.0	16.0	3.0	-
	2.50	-	4.0	9.0	22.0	42.0	77.0	127.0	197.0	252.0	277.0	262.0	207.0	127.0	72.0	37.0	15.0	6.0	2.0	-
	3.75	-	1.0	2.0	5.0	15.0	26.0	50.0	83.0	115.0	125.0	115.0	83.0	50.0	26.0	14.0	5.0	1.0	-	-
32	0.125	5.0	14.0	27.0	49.0	77.0	120.0	175.0	245.0	295.0	305.0	285.0	245.0	175.0	113.0	77.0	49.0	27.0	14.0	9.0
	2.00	7.0	14.0	24.0	36.0	61.0	91.0	131.0	176.0	211.0	223.0	212.0	176.0	127.0	88.0	55.0	32.0	20.0	11.0	5.0
	4.00	-	2.0	5.0	12.0	22.0	41.0	63.0	91.0	114.0	122.0	112.0	89.0	61.0	37.0	18.0	10.0	4.0	2.0	-
60	0.125	14.0	22.0	33.0	48.0	64.0	87.0	117.0	142.0	165.0	182.0	168.0	147.0	111.0	82.0	60.0	44.0	30.0	19.0	13.0
	3.00	8.5	15.0	22.0	33.0	48.0	65.0	84.0	102.0	117.0	122.0	117.0	103.0	84.0	63.0	47.0	32.0	22.0	14.0	10.0
	5.00	3.2	7.0	12.0	19.0	30.0	44.0	56.0	69.0	79.0	81.0	79.0	71.0	56.0	43.0	30.0	20.0	11.5	5.5	3.0
96	0.125	8.0	14.0	22.0	34.0	46.0	58.0	70.0	82.0	91.0	97.0	92.0	82.0	70.0	59.0	44.0	35.0	24.0	17.0	12.0
	5.00	7.0	11.0	15.0	21.0	29.0	36.0	45.0	52.0	58.0	60.0	58.0	52.0	45.0	37.0	30.0	21.0	16.0	13.0	9.0
	8.25	3.0	4.0	6.0	9.0	13.0	17.0	20.0	24.0	27.0	28.0	27.0	24.0	20.0	17.0	13.0	9.0	6.0	4.0	3.0
180	0.125	13.0	17.0	21.0	26.0	32.0	34.0	39.0	43.0	46.0	47.0	46.0	43.0	40.0	34.0	32.0	26.0	21.0	16.0	13.0
	8.50	6.0	9.0	11.0	14.0	17.0	19.0	21.0	23.0	23.0	23.0	23.0	22.0	20.0	18.0	16.0	13.0	10.0	7.0	5.0
	12.00	3.0	5.0	6.0	7.0	9.0	11.0	11.0	12.0	13.0	13.0	13.0	12.0	11.0	10.0	9.0	7.0	6.0	5.0	3.0

TABLE 6: CONCENTRATION DISTRIBUTION DATA: HORIZONTAL DISTRIBUTIONS (Continued)

Hill 2" x 10" U_a = 10 fps

X (in)	Z (in)	Concentration in PPM at y (in inches) -9	-8	-7	-6	-5	-4	-3	-2	-1	0	+1	+2	+3	+4	+5	+6	+7	+8	+9
8	0.125	-	12.0	23.0	62.0	170.0	336.0	550.0	910.0	1186.0	1321.0	1210.0	930.0	590.0	360.0	210.0	134.0	100.0	-	-
	2.50	-	-	3.0	28.0	72.0	156.0	305.0	582.0	850.0	921.0	845.0	522.0	286.0	162.0	94.0	50.0	21.0	10.0	-
	3.50	-	-	-	1.0	10.0	26.0	67.0	146.0	252.0	321.0	264.0	150.0	80.0	43.0	23.0	12.0	-	-	-
16	0.125	-	6.0	27.0	75.0	150.0	256.0	400.0	573.0	702.0	741.0	700.0	530.0	388.0	264.0	158.0	86.0	44.0	20.0	-
	2.75	-	-	-	25.0	46.0	100.0	184.0	290.0	387.0	431.0	395.0	303.0	206.0	134.0	86.0	53.0	29.0	10.0	-
	4.50	-	-	-	3.0	10.0	22.0	48.0	80.0	108.0	126.0	110.0	75.0	48.0	30.0	18.0	10.0	-	-	-
32	0.125	-	45.0	67.0	101.0	150.0	213.0	277.0	335.0	386.0	410.0	387.0	342.0	282.0	217.0	158.0	107.0	64.0	31.0	-
	3.50	-	11.0	20.0	35.0	61.0	96.0	136.0	172.0	196.0	207.0	199.0	174.0	137.0	100.0	70.0	47.5	32.0	23.0	-
	5.00	-	6.0	15.0	27.0	40.0	58.0	77.0	92.0	102.0	106.0	98.0	80.0	58.0	38.0	23.0	15.0	9.0	5.0	-
60	0.125	-	57.0	77.5	100.0	123.0	148.0	175.0	197.0	211.0	216.0	209.0	192.0	167.5	140.0	115.0	91.5	70.0	52.5	-
	4.50	-	18.0	25.0	35.0	48.0	64.0	82.0	97.0	107.0	111.0	106.5	96.0	80.0	65.0	51.0	39.0	27.0	17.5	-
	7.00	-	6.0	8.0	12.5	18.0	25.0	33.0	41.5	47.5	50.0	47.0	42.0	35.0	27.5	20.0	15.0	10.0	7.0	-
96	0.125	32.0	48.0	65.5	86.0	103.0	116.4	127.0	135.5	141.6	143.5	141.0	134.7	125.0	113.0	98.0	81.5	68.0	53.8	41.8
	4.00	23.8	31.0	38.2	46.3	55.0	65.0	75.0	85.5	93.0	95.5	92.2	85.0	76.6	66.0	55.0	46.0	37.0	29.0	22.0
	6.00	17.0	21.5	27.0	33.5	40.5	48.5	57.0	65.3	69.2	70.5	69.0	65.0	57.0	48.0	40.0	33.5	27.5	22.0	16.8
180	0.125	34.5	46.0	56.5	64.8	71.5	77.3	81.5	84.5	86.2	86.5	86.0	84.0	81.0	76.2	70.5	64.0	56.0	47.0	38.0
	7.00	20.2	23.5	27.0	30.2	33.8	37.5	41.0	44.2	47.0	48.5	47.0	44.5	41.0	36.7	32.5	28.3	24.6	21.0	17.8
	10.00	9.5	11.5	13.6	16.0	18.4	21.0	23.5	25.5	27.0	27.5	26.8	25.6	23.6	21.2	18.4	15.7	13.2	11.0	9.0
		Hill 1" x 10" U_a = 20 fps																		
4	0.125	-	-	-	-	-	-	20.0	430.0	3000.0	7800.0	2950.0	300.0	10.0	-	-	-	-	-	-
	0.75	-	-	-	-	-	-	-	150.0	1320.0	3545.5	1140.0	50.0	-	-	-	-	-	-	-
	1.50	-	-	-	-	-	-	-	-	50.0	200.0	60.0	-	-	-	-	-	-	-	-
12	0.125	-	-	-	-	-	10.0	100.0	565.0	2170.0	3373.0	2220.0	570.0	40.0	5.0	-	-	-	-	-
	0.875	-	-	-	-	-	-	40.0	360.0	1170.0	1773.0	1175.0	350.0	25.0	-	-	-	-	-	-
	1.438	-	-	-	-	-	-	25.0	130.0	580.0	876.0	560.0	150.0	15.0	-	-	-	-	-	-
24	0.125	-	-	-	-	35.0	60.0	160.0	490.0	1160.0	1593.0	1200.0	445.0	120.0	25.0	-	-	-	-	-
	1.25	-	-	-	-	10.0	35.0	120.0	375.0	730.0	898.0	720.0	310.0	90.0	10.0	-	-	-	-	-
	2.00	-	-	-	-	-	10.0	65.0	195.0	370.0	478.0	370.0	180.0	45.0	5.0	-	-	-	-	-
48	0.125	-	-	1.0	9.0	30.0	80.0	170.0	323.0	507.0	622.5	520.0	305.0	140.0	53.0	15.0	6.0	1.0	-	-
	2.00	-	-	-	7.5	22.5	59.0	121.0	210.0	310.0	342.5	310.0	203.0	110.0	46.0	13.5	2.0	-	-	-
	3.00	-	-	-	5.0	14.0	31.0	68.0	135.0	187.0	202.5	185.0	126.0	70.0	30.0	10.0	2.0	-	-	-
72	0.125	-	2.0	6.0	14.0	39.0	74.0	119.0	171.0	229.0	257.0	229.0	166.0	99.0	53.5	26.0	12.5	6.0	1.0	-
	3.00	-	1.0	3.0	8.0	18.0	40.0	75.0	119.0	156.0	168.0	156.0	120.0	72.0	39.0	20.0	10.0	3.0	-	-
	4.50	-	-	2.0	6.0	12.5	25.0	41.0	61.0	77.5	85.0	78.0	62.0	44.0	28.0	14.0	6.0	2.0	-	-
96	0.125	1.0	3.5	9.0	21.0	45.0	79.0	122.5	174.0	220.0	237.5	216.0	162.5	110.0	67.5	37.0	19.0	11.0	7.0	4.0
	4.00	1.0	3.5	8.0	15.0	27.5	46.5	69.0	89.0	103.5	110.5	104.0	87.0	64.0	42.5	26.0	14.0	7.5	3.0	1.0
	6.00	-	1.0	3.0	7.0	13.0	22.0	32.0	43.0	51.0	53.5	50.0	41.0	30.0	19.0	10.0	5.0	2.0	-	-
180	0.125	5.5	10.0	16.0	23.5	33.0	43.6	56.0	68.0	77.5	81.0	77.2	68.0	56.8	44.8	34.0	25.0	17.0	10.5	5.0
	6.00	7.0	11.0	16.0	21.6	28.0	34.7	41.0	45.5	49.0	50.0	49.0	45.0	40.0	33.6	27.4	21.7	17.0	13.0	10.0
	8.00	4.0	6.0	9.0	12.7	16.4	20.5	24.7	29.0	32.5	33.5	32.8	29.8	25.6	20.6	16.3	12.8	9.5	7.0	5.5

TABLE 6: CONCENTRATION DISTRIBUTION DATA: HORIZONTAL DISTRIBUTIONS (Continued)

Flat Plate U_a = 20 fps

X (in)	Z (in)	Concentration in PPM at y (in inches) -9	-8	-7	-6	-5	-4	-3	-2	-1	0	+1	+2	+3	+4	+5	+6	+7	+8	+9
12	0.25	-	-	-	-	-	-	-	-	270.0	920.0	270.0	-	-	-	-	-	-	-	-
	0.50	-	-	-	-	-	-	-	60.0	620.0	1690.0	730.0	90.0	-	-	-	-	-	-	-
	1.50	-	-	-	-	-	-	-	40.0	700.0	2180.0	880.0	50.0	-	-	-	-	-	-	-
24	0.125	-	-	-	-	-	-	33.0	193.0	618.0	868.0	593.0	173.0	34.0	8.0	-	-	-	-	-
	2.00	-	-	-	-	-	13.0	64.0	247.0	537.0	677.0	497.0	202.0	58.0	-	-	-	-	-	-
	3.00	-	-	-	-	-	16.0	35.0	88.0	181.0	226.0	166.0	79.0	32.0	19.0	-	-	-	-	-
48	0.125	-	-	-	-	18.0	40.0	134.0	292.0	464.0	562.0	482.0	302.0	134.0	45.0	4.0	-	-	-	-
	3.00	-	-	-	-	3.0	38.0	87.0	151.0	210.0	234.0	201.0	131.0	68.0	50.0	5.0	-	-	-	-
	4.00	-	-	-	-	5.0	13.0	53.0	78.0	120.0	130.0	116.0	76.0	54.0	33.0	-	-	-	-	-
72	0.125	-	-	2.0	5.0	21.0	59.0	121.0	199.0	289.0	349.0	289.0	209.0	125.0	51.0	17.0	4.0	-	-	-
	3.00	-	-	2.0	10.0	22.0	49.0	89.0	135.0	178.0	196.0	176.0	135.0	88.0	43.0	20.0	7.0	-	-	-
	4.00	-	-	3.0	6.0	16.0	36.0	65.0	98.0	131.0	141.0	131.0	101.0	61.0	34.0	14.0	6.0	-	-	-
96	0.125	-	4.0	10.0	18.0	34.0	60.0	99.0	139.0	183.0	212.0	187.0	142.0	92.0	53.0	26.0	12.0	3.0	-	-
	3.00	-	-	4.0	11.0	24.0	44.0	72.0	97.0	119.0	129.0	116.0	94.0	64.0	41.0	22.0	11.0	5.0	-	-
	4.00	-	-	3.0	8.0	14.0	22.0	32.0	42.0	53.0	57.0	51.5	43.0	32.5	22.0	13.5	8.0	4.0	-	-
132	0.125	17.0	20.0	24.0	35.0	50.0	68.0	91.0	138.0	142.0	161.0	145.0	120.0	90.0	67.0	49.0	36.0	27.0	20.0	15.0
	5.50	17.0	19.0	23.0	29.0	36.0	43.0	52.0	60.0	65.0	68.0	66.0	60.0	52.0	42.0	33.0	26.0	22.0	19.0	17.0
	7.50	15.0	16.0	19.0	23.0	27.0	30.0	35.0	39.0	42.0	43.0	41.0	39.0	34.0	29.0	24.0	21.0	18.0	17.0	15.0
154	0.125	9.0	13.0	21.0	29.0	42.0	57.0	75.0	95.0	107.0	112.0	107.0	92.0	72.0	57.0	46.0	36.0	27.0	14.0	10.0
	6.00	-	10.0	12.0	20.0	26.0	36.0	42.0	49.0	56.0	58.5	57.0	50.0	42.0	36.0	27.0	21.0	16.0	12.0	-
	8.00	-	5.0	7.0	11.0	16.0	20.0	25.0	29.0	33.0	37.0	33.0	28.0	23.0	20.0	16.0	11.0	7.0	5.0	-
187	0.125	8.0	13.0	18.0	29.0	38.0	49.0	61.0	72.0	82.0	85.0	83.0	70.0	56.0	41.0	31.0	24.0	17.0	12.0	8.0
	7.00	7.0	10.0	14.0	18.0	21.0	27.0	31.0	35.0	38.0	41.0	40.0	35.0	31.0	26.0	21.0	16.5	14.0	10.0	7.0
	10.00	4.0	6.0	7.0	9.0	11.0	12.0	16.5	18.0	19.0	20.0	19.0	18.0	15.0	12.0	11.0	9.0	7.0	6.0	4.0

APPENDIX 3.

"DIFFUSION FROM A GROUND LEVEL LINE SOURCE INTO THE DISTURBED BOUNDARY LAYER FAR DOWNSTREAM FROM A FENCE"

NOTATION

a	Coefficient in Elliott's law for the inner boundary layer	(-)
A	Coefficient in the velocity distribution law for the outer layer	(-)
b	Constant relating mean Lagrangian vertical velocity to the shear velocity	(-)
B	Numerical factor	(-)
c	Local concentration	(cm^3/cm^3)
c_{max}	Maximum or ground level concentration	(cm^3/cm^3)
D	Coefficient in the velocity distribution law for the inner layer	(-)
G	Volume flow rate of diffusing gas per unit width of line source	(cm^3/sec cm)
h	Fence height	(cm)
H	Height of source from the ground	(cm)
$I_1;I_2$	Integrals in the determination of ground level concentrations	(-)
k	Karman's constant	(-)
L	Distance of reattachment point from fence	(cm)
m	Exponent in Elliott's law for the inner boundary layer	(-)
t	Time	(sec)
u	Local velocity	(cm/sec)
u_{*i}	Shear velocity of inner layer	(cm/sec)
u_{*o}	Shear velocity of outer layer	(cm/sec)
u_a	Ambient velocity	(cm/sec)
x	Horizontal distance from the source	(cm)
x'	Ratio δ'/δ	(-)
$\bar{x}$	Horizontal distance of the center of gravity of a diffusion cloud from the source	(cm)
x_o	Virtual diffusion origin upstream of source	(cm)
X	Horizontal distance from the fence	(cm)
y	Vertical distance from the wall	(cm)
$\bar{y}$	Distance of the center of gravity of a diffusion cloud from the wall	(cm)
z_o	Roughness height	(cm)
α	Exponent in concentration distribution law	(-)
λ	Distance y at which $c = 1/2\ c_{max}$	(cm)
ν	Kinematic viscosity	(cm^2/sec)

NOTATION - Continued

δ	Boundary layer thickness	(cm)
δ_o	Thickness of the undisturbed boundary layer at X = 0	(cm)
δ'	Thickness of inner boundary layer	(cm)
ρ	Density of air	(gm/cm^3)
τ_o	Wall shearing stress	(g/cm^2)

DIFFUSION FROM A GROUND LEVEL LINE SOURCE INTO THE DISTURBED BOUNDARY LAYER FAR DOWNSTREAM FROM A FENCE

by

Erich J. Plate
Fluid Dynamics and Diffusion Laboratory
Colorado State University

ABSTRACT

The concentration field is discussed which exists far downstream from a line source of ammonia gas emitting continuously into the boundary layer along a smooth flat plate. The boundary layer is obstructed by an impermeable and sharp edged fence which extends over the whole width of the plate at a short distance downstream from the source. The basis of discussion is a set of experimental data which was obtained in a wind tunnel.

The flow field downstream from the fence exhibits three different zones of velocity distributions. These zones are indicated and a velocity distribution law is given based on the assumption that the disturbed boundary layer consists of two parts: an outer layer for which the parameters of the distribution law depend on the boundary layer thickness and on the geometry of the disturbing fence, and an inner layer for which the velocity distribution law depends on the roughness of the floor.

The vertical distributions of concentrations downstream from the fence follow a similarity law whose shape corresponds to that found in undisturbed boundary layers. The similarity parameters reflect strongly the presence of the fence. The characteristic length λ is found to increase exponentially with the fence height. The characteristic length, the similarity law, and the velocity distribution law, are used to calculate the maximum ground concentrations at large distances downstream from the fence where the presence of the boundary layer edge limits the growth of the diffusion plume to that of the boundary layer.

DIFFUSION FROM A GROUND LEVEL LINE SOURCE INTO THE DISTURBED BOUNDARY LAYER FAR DOWNSTREAM FROM A FENCE

INTRODUCTION

The atmospheric boundary layer hardly ever corresponds to the aerodynamic flow along a flat plate with uniform roughness. Changes of roughness along the approach distance, and topographic features of small or large dimensions, cannot fail to show their influence in the local flow characteristics, and therefore, also in the distribution of concentrations of any matter which happens to be present in the atmosphere. Very little is known about the flow in a boundary layer which is disturbed by a topographic feature and even less about diffusion in such a flow field.

In order to provide a body of experimental data, against which hypotheses concerning diffusion of gas in a disturbed boundary layer can be tested, the experiments reported herein were undertaken. As a first experimental set up, the obstacle chosen consisted of a sharp edged flat plate placed perpendicular to the direction of flow, and extending over the whole width of the test section of a low speed wind tunnel. This type of obstacle shall be called a fence. The physical situation corresponds somewhat to the atmospheric flow over wind breaks or snow fences, but other types of obstacles can be expected to behave similarly.

The diffusion plume was emitted continuously from a line source placed at some distance upstream from the fence at ground level, as is indicated in Fig. 1. The floor of the wind tunnel test section represents the lower boundary of the flow field on which the boundary layer is forming. The basic variable for the present study of the diffusion field was the height of the fence.

DIFFUSION IN A BOUNDARY LAYER WITHOUT FENCE

An analytical description of the mean concentration distribution of a contaminating gas, downstream from a continuous source, requires a determination of the probability distribution for finding contaminants at a given point in space downstream from the source. This probability distribution is related to the velocity field because it denotes the

relative number of elementary parcels of contaminating gas which have traveled from the vicinity of the source to the space point considered. Clearly, the path of travel is the time integral of the instantaneous velocities of the parcels with contaminating gas. If the gas only marks rather than modifies the velocity field of the carrier fluid, then the velocities of the parcel are the Lagrangian velocities of the turbulence field of the carrier fluid. This view of turbulent diffusion, due to Taylor (1921), indicates immediately the difficulties inherent in each analytical description of a turbulent diffusion process, because even the determination of the mean concentration requires the averaging of a large number of realizations of the Lagrangian turbulence field.

Owing to the complexitites encountered, either in analytically predicting or in measuring Lagrangian velocities, one usually circumvents the problem of determining the complete probability distributions of the diffusion field, and attempts to specify only some of its simpler moments on the basis of physical arguments.

At a given distance downstream from the source, the first moment of the vertical concentration distribution is the distance $\bar{y}$ of the center of gravity of the concentration distribution from the flow boundary. Its determination in a flow of homogeneous turbulence with constant mean velocity in which the "boundary" is only a mathematical plane parallel to the mean flow direction is a trivial matter, i.e., $\bar{y} = 0$ for reasons of symmetry. In the case of a concentration distribution downstream from a source located at the boundary and emitting into the turbulent boundary layer along the boundary, the problem becomes more complex. An approach to the determination of $\bar{y}$ has been suggested by Batchelor (1959). It is based on the concept of "Lagrangian Similarity" and relates mean Lagrangian velocity components to mean Eurlerian (and therefore easily measurable) velocity components of the boundary layer. The mean vertical Lagrangian velocity is set equal to bu_{*i} where b is a constant (about 0.1, after Cermak (1963)) and u_{*i} is the shear velocity based on the wall shear stress τ_o , i.e. , $u_*^2 = \frac{\tau_o}{\rho}$. The mean horizontal velocity is set equal to the velocity of the center of gravity of the diffusion cloud. It is found from a power law for the velocity distribution (Ellison, 1959)), or from a logarithmic velocity distribution law.

$$\frac{u}{u_{*i}} = \frac{1}{k} \ln \frac{y}{z_o}. \qquad (1)$$

With Eq. 1, it is found that

$$\bar{y} - y_o = \int_{t_o}^{t} b u_{*i} \, dt = u_{*i} b \, (t - t_o)$$

$$\bar{x} - x_o = \int_{t_o}^{t} \frac{u_{*i}}{k} \ln \frac{\bar{y}(t)}{z_o} \, dt. \qquad (2)$$

The simultaneous solution of Eqs. 1 and 2 is easily accomplished by eliminating t ; however, an uncertainty arises in the appropriate definition of the initial conditions. For a source at zero elevation, the logarithmic law is no longer valid at the source. For an elevated source, the configuration of the source, as well as the exit velocity of the gas, introduce initial conditions which cannot properly be accounted for in the simple model. One must, therefore, specify by some other reasoning the initial conditions which will then become that at $\bar{y} = y_o$, $\bar{x} = x_o$. In the case of a ground level source, y_o corresponds approximately to the roughness height z_o . In the case of an elevated source, y_o corresponds to H , the height of the source from the ground. However, as Cermak (1963) has shown, the effect of the initial conditions does not extend very far.

The solution of Eqs. 1 and 2 can be written, for large values of $\bar{y}/z_o$

$$bk \frac{\bar{x} - x_o}{z_o} = \frac{\bar{y}}{z_o} \log \frac{\bar{y}}{z_o} - \frac{\bar{y}}{z_o} \qquad (3)$$

where x_o is given by the initial conditions.

The Lagrangian similarity hypothesis cannot serve, in its present form, to predict more than the first moment of the concentration distribution. However, in those cases where the concentration distribution obeys a similarity law, a single length parameter and the function describing the similarity law are sufficient to fully specify the concentration distribution. The reference length must then be proportional to the first

moment. Such similarity laws are observed for concentrations emitted from a line source at ground level. Wieghardt (1948) and Poreh and Cermak (1964), among others, show evidence that the distribution of temperature and of mass concentration, emitted respectively from a line source of heat and of ammonia, are represented by a similarity distribution of the form

$$\frac{c(x,y)}{c_{max}(x)} = e^{-B\left(\frac{y}{\bar{y}(x)}\right)^{\alpha}} \qquad (4)$$

where the exponent α was found to be about 1.6 to 1.8. In this equation, $c(x,y)$ stands for concentration (or temperature excess), $c_{max}(x)$ is the concentration (or temperature excess) at ground level at some distance x, and B is a numerical factor. It was found convenient by Poreh and Cermak (1964) to use instead of $\bar{y}(x)$ the parameter $\lambda(x)$, which is defined as that vertical distance at which the concentration in the two-dimensional concentration plume is reduced to one-half its value at the boundary for given x, as is indicated in Fig. 1. With this choice of the length parameter, the coefficient B becomes equal to $\ln 2$.

The Lagrangian similarity hypothesis based on Eqs. 1 and 2 will fail to give useful results in the neighborhood of the source, and in that region downstream from the source where the diffusion cloud has spread so far that it reaches the edge of the boundary layer. Poreh and Cermak (1964) have investigated the different regions of diffusion conditions (see Fig. 1). In the course of their investigation, they found it advantageous to separate the diffusion field into regions of validity of different types of geometry and the local velocity gradients near the source, are of predominate influence; a second zone in which the diffusion cloud spreads out according to the law:

$$\lambda(x) = 0.076\, x^{0.8}, \qquad (5)$$

where both $\lambda(x)$ and x are given in cm, and a final region in which the diffusion parameter λ becomes proportional to the boundary layer thickness δ. The factor of proportionality between λ and δ in the final region is about 0.64.

It will now be shown that Eq. 3 agrees well with Eq. 5, if $x = \bar{x}$ and $\bar{y}$ is replaced by λ, except for the factor of proportionality. In Fig. 2, the ratio $\bar{y} / z_o$ has been plotted on double logarithmic paper against $bk \frac{\bar{x} - x_o}{z_o}$ as calculated from Eq. 3. It is evident that for $\bar{y} / z_o > 100$ the curve can be represented well by an equation of the form

$$\left(bk \frac{\bar{x} - x_o}{z_o} \right)^{0.8} = 1.09 \frac{\bar{y}}{z_o} . \qquad (6)$$

Since z_o is a small number (of the order of 0.001 to 0.01 for smooth surfaces), a ratio $\bar{y} / z_o = 100$ corresponds to small heights $\bar{y}$ (of the order of 0.1 to 1 cm). Therefore, for practical purposes the logarithmic Eq. 3 can be replaced by Eq. 6.

If $x_o << \bar{x}$, then it follows from Eq. 5 and Eq. 6 that for the data of Poreh and Cermak (1964), with $\lambda \approx \bar{y}$ and k = Karman's constant = 0.38

$$0.076 = \frac{z_o}{1.09} \cdot \left(\frac{bk}{z_o} \right)^{0.8} , \text{ or } b^{0.8} z_o^{0.2} = 0.180 .$$

Poreh and Cermak (1964) have not given a value of z_o which therefore must be estimated. For a smooth surface, $z_o \approx 13 \frac{\nu}{u_{*i}}$ where u_{*i} = shear velocity = $\sqrt{\frac{\tau_o}{\rho}}$ and ν = kinematic viscosity. Cermak (1963), who used the same data as Poreh and Cermak (1964), found an average z_o value of about $1.5.10^{-3}$ cm, which leads to a value of $b = 0.66$. This is higher than the value of 0.1 given by Cermak (1963).

The fact that the exponent in Eq. 4 is equal to 0.8 is of considerable interest. The same exponent is found when the growth of a turbulent boundary layer along a smooth surface is determined from Blasius' velocity distribution law (see Schlichting (1960)). An exponent of 0.8 was also found by Elliott (1958) for his model of the growth of an internal boundary layer which starts at the discontinuity in roughness between two adjacent surfaces of uniform, but unequal roughness. Boundary layers and diffusion clouds of two-dimensional mean flows, are thus found to obey the same growth laws. It seems thus that the exponent 0.8 is a

characteristic for the propagation of disturbances in an equilibrium layer, and can be analyzed with methods like the ones proposed by Townsend (1965 a and b).

FINAL ZONE DIFFUSION IN A FENCE-DISTURBED BOUNDARY LAYER

A fence which takes up an appreciable portion of the undisturbed boundary layer causes a large increase in turbulent energy which is generated along the separation stream line. This energy is decaying further downstream, and the disturbed boundary layer is no longer an equilibrium layer. The different energy structure is responsible for an initially very rapid growth of the diffusion cloud, but the vertical extent of the cloud increases at a slower rate than $x^{0.8}$. As will be shown, this is what happens for the experimental data of this study. However, there exists another reason why the growth of the diffusion cloud does not follow Eq. 5.

Poreh and Cermak (1964) have shown that far downstream from the source the boundary layer edge limits the growth of a diffusion cloud. Outside of the boundary layer, the turbulence level is very low, all diffusion is essentially by molecular action only. Consequently, only little gas (or heat) is lost to the flow region outside of the boundary layer and for this final diffusion zone, the length scale for the concentration distribution law becomes proportional to the boundary layer thickness. The same development can be found in a boundary layer which is disturbed by a fence.

In the remainder of the paper, it shall be shown that the final zone diffusion is indeed governing the experimental results of this study. In the final zone, it is possible to calculate the ground level concentration if the velocity distribution law, the development of the boundary layer thickness, and the concentration distribution law are known. The determination of the ground level concentration in the final diffusion zone is the objective of the following investigations.

EXPERIMENTAL PROCEDURES

The experiments were performed in an noncirculating low-speed wind tunnel, which was formerly located in the Fluid Mechanics and Diffusion Laboratory of Colorado State University. An air velocity of about 2.7 m/sec was used for the diffusion experiments. Fence heights of 1.27, 2.54, 3.81 and 5.08 cm were studied. The line source of gas was located at a distance of 9 m downstream from the test section entrance and 0.46 m upstream from the fence. The fence consisted of angle iron pieces with machined sharp edges.

No reliable measurements of the velocity distributions were taken during the time of the concentration measurement. The measurements suffice, however, to show the development of the outer edge of the boundary layer. After these measurements, the wind tunnel was torn down. The velocity field downstream from a fence was, later on, investigated by Plate (1966), in a new wind tunnel, over a wide range of variables, and the discussion of the velocity distributions is based on the later results. The velocity distributions were measured with a pitot static tube in conjunction with an electronic micromanometer (Transonics Equibar Type 120) which was calibrated periodically against a water manometer (Flow Corporation Type MM 2).

The gas consisted of anhydrous ammonia, which was emitted continuously from a 4 ft. long line source at ground level. The source produced a mean concentration field which was nearly two-dimensional, except near the wind tunnel walls.

Concentrations were measured by passing air-gas mixtures, withdrawn continuously from the wind tunnel at the desired point by means of a vacuum pump, through a known volume of hydrochloric acid, which absorbed the ammonia over a fixed period of time, usually one minute. An addition of Nessler's Reagent to the sample gave a brown discoloration which, in a colorimeter, yielded a light absorbtion proportional to the concentration of ammonia trapped in the sample over a given period of time. The procedure is accurate within ± 20% at readings of 500 ppm. An uncertainty of the data of about ± 30 ppm has to be expected for all readings. Measurements of low

concentrations are, therefore, very unreliable. The sampling system has been described by Malhotra and Cermak (1964). Poreh and Cermak (1964) gave the details of the source and of the wind tunnel.

VELOCITY DISTRIBUTIONS IN THE DISTURBED BOUNDARY LAYER

The velocity field downstream from the fence is distorted by the presence of the fence. One can distinguish the different flow zones indicated in Fig. 3. These flow zones are separated by suitable blending regions.

At some distance upstream from the fence, the boundary layer is unaffected by the presence of the fence and behaves like an undisturbed boundary layer along a smooth flat plate. At a short distance in front of the fence, the boundary layer separates and a separation bubble with a closed circulation is formed. The separation streamline reattaches on the front of the fence, at a point close to the fence edge. At the fence edge the flow separates again, this time forming a much longer separation zone. Reattachment takes place at $X = L$ and along the plate for $X > L$ a new inner boundary layer is developing which gradually thickens. The outer portion of the boundary layer in this region remains essentially unchanged, except for an outward displacement. With further increase in distance, the blending region between the inner and outer layer increases in width, and there is some experimental evidence that at some large value of X the blending profile has spread over the whole boundary layer, and determines the velocity distribution in the redeveloped boundary layer. Ultimately, only the increased boundary layer thickness remains as an indication of the distortions which the flow field suffered by the fence. In this context, this complicated flow development can be described only qualitatively. A detailed investigation of the flow field downstream from a fence will be given elsewhere (Plate (1966)).

The flow region near separation is governed by both the velocity field and the pressure field which is created by the retardation and acceleration of the fluid near the fence. Downstream from reattachment, the pressure again becomes constant, and, from then on, one may expect that the boundary layer develops in the form of an outer displaced equilibrium

layer and an inner equilibrium boundary layer (Townsend (1965 a)). Since equilibrium layers in wall shear flows obey to a good approximation, logarithmic velocity distribution laws, the velocity distributions are best presented in a semi-logarithmic plot. Examples are shown in Fig. 4. In this figure, dimensionless velocities obtained by dividing the local velocity u by the ambient velocity u_a were plotted against the dimensionless distances y/δ, where δ is the height of the outer boundary layer. δ has been defined as the distance at which the local velocity has a magnitude of $0.98\ u_a$. Small adjustments in δ were made in order to bring the outer parts of the velocity profiles for all distances X into good agreement. As is readily seen, each profile consists of two well defined logarithmic parts, separated by a blending region the height of which increases with increasing distance X.

In order to obtain an expression for the velocity distribution of the total boundary layer, one must obtain suitable equations which describe the velocity distributions in the inner and the outer layer. For the outer layer, the velocity profile can be described by a type of velocity defect law

$$\frac{u - 0.98\ u_a}{u_{*o}} = \frac{1}{k} \ln \frac{y}{\delta} \qquad (7)$$

where u_{*o} is the shear velocity of the outer layer. The quantity u_{*o} reflects the effect of the fence on the shear stress in the outer part of the boundary layer. The outer profile develops as if a rough boundary had existed at some distance upstream from the location of the reattachment point. This "equivalent rough boundary" has a friction coefficient defined by $c_f = \frac{2u_{*o}^2}{u_a^2}$, which must depend on the fence characteristics. The coefficient c_f is dependent on an empirical parameter A, defined by Plate (1966) through the relation $c_f = 0.0544\ A^2$. Experimental data of Plate (1966) have been used to show the dependency of the coefficient A on the ratio of h/δ_o in Fig. 5, where δ_o is the thickness of the undisturbed boundary layer at the location of the fence (i.e., before the fence has been placed into the boundary layer).

For the inner profile, the assumption can be made that the shear stress at the floor is equal to that of the flow before the fence is introduced (Plate (1966) . This assumption is required in order to assign a finite magnitude to the drag which is introduced by the fence. Thus, the profile can be described by the inner velocity distribution law or the wall law, for boundary layers on smooth flat plates

$$\frac{u}{u_{*i}} = \frac{1}{k} \ln y + D , \qquad (8)$$

where the term D has to be determined from the joining condition that at the edge of the inner boundary layer, at $y = \delta'$, the inner profile velocity equals that of the outer profile. The shear velocity u_{*i} can be calculated from standard curves, for example, Schlichting (1960) p. 504. Thus, with A given by Fig. 5, and the profiles of the inner and outer boundary layer determined by Eqs. 7 and 8, the velocity distribution of the whole boundary layer is known if the laws are given which determine the growth of the inner boundary layer, and of the outer boundary layer.

The edge δ' of the inner boundary layer can be found by extending the straight lines in Fig. 4 until inner and outer profile intersect. This distance δ' corresponds to that distance from the floor of the intersection betweeen inner and outer profile, which is found when any discontinuity at the surface of a flat plate is causing a change in the boundary conditions for the boundary layer. Problems of this kind have been treated recently by numerous authors, among them: Townsend (1965, a and b), Taylor (1962), Dyer (1963), and Elliott (1958). Perhaps representative of the results is the simple formula of Elliott

$$\frac{\delta'}{z_o} = a \left(\frac{x}{z_o} \right)^m \qquad (9)$$

where x is the distance downstream from the line of discontinuity, m is a (constant) exponent, about 0.8, as was already mentioned, and a is a function of the ratio of the upstream roughness lengths z_{01} to the downstream roughness length z_{02} .

For the case of a boundary layer which is disturbed by a fence, the inner boundary layer starts at reattachment, and in order to find a law

which correspond to Eq. 9, one has to subtact L from the distance X. For this purpose, the length L, from the fence to the reattachment point has to be found. Experimental results of Nagabhushanaiah (1962) indicate that $L/h = 12.5$, where h = height of fence, independent of velocity and fence height. This result was used for the present data, and δ' was plotted against $X - L$ in Fig. 6. The data scatter very much, a well defined straight line through each set of data points cannot be found. It is apparent, however, that the exponent would be considerably lower than 0.8, a value of 0.5 appears more reasonable. There are two possible reasons for this. First, the exponent of 0.8 is valid only for equilibrium boundary layers, i.e. boundary layers in which at any point turbulent energy generation equals turbuelnt energy dissipation. Even though the mean velocity distribution laws for both of the parts of the boundary layer downstream from the fence have the appearance of equilibrium layers, the flow actually is not in equilibrium because the turbulent energy first increases very rapidly and then decays with distance X.

A second explanation can be given by considering the limitations which the height of the outer boundary layer imposes on the growth of the inner boundary layer. This effect leads to a constant ratio δ'/δ, and such a constant is indeed found. The limitations imposed by the small thickness δ are more serious than those due to neglecting the turbulence decay, because most of the data of Fig. 4, and therefore also the velocities pertaining to the concentration distributions, show these limitations, as can be seen from Fig. 4. For large values of X, the intersection of the inner and outer velocity profile is found at $\frac{u}{u_a} = 0.75$. This empirical result implies that δ'/δ = constant, with the constant given from the law of the outer profile

$$\frac{u}{u_a} = \frac{u}{u_{*o}} \sqrt{\frac{c_f}{2}} = 0.75 \longrightarrow \frac{1}{k} \sqrt{\frac{c_f}{2}} \ln \frac{\delta'}{\delta} = -0.23$$

$$\text{or} \quad \frac{\delta'}{\delta} = e^{-\frac{0.124}{\sqrt{c_f}}} \tag{10}$$

Eq. 10 makes it possible to obtain the velocity distribution law for the disturbed boundary layer, at large distances from the fence,

from a knowledge of the wall shear stress and of the boundary layer thickness. Since at $y = \delta'$ both Eqs. 7 and 8 are valid, D is found from the conditions:

$$\frac{u_{*i}}{k} \ln \delta' + u_{*i} D = \frac{u_{*o}}{k} \ln \frac{\delta'}{\delta} + 0.98 u_a$$

and with $k = 0.38$ one finds the velocity distribution law for the total boundary layer, expressed in terms of u_a :

$$y < \delta \cdot e^{-\frac{0.124}{\sqrt{c_f}}} : \frac{u}{u_a} = \frac{u_{*i}}{k u_a} \ln \frac{y}{\delta} + 0.75 + 0.23 \frac{u_{*i}}{u_{*o}}$$

$$y > \delta \cdot e^{-\frac{0.124}{\sqrt{c_f}}} : \frac{u}{u_a} = \frac{u_{*o}}{k u_a} \ln \frac{y}{\delta} + 0.98 . \qquad (11)$$

Since the shear velocity u_{*i} corresponds to that found at X with an undisturbed boundary layer, and since u_{*o} is determined by the ratio of h/δ_o , the velocity distribution law is fully specified at large distances X , if δ is known.

Empirically, δ is given by Fig. 7 . Large increses of δ with fence height are found. The strong growth of the boundary layer is probably due to the fact that the ratio of the boundary layer thickness δ_o (= 13 cm) of the undisturbed flow to fence height h is fairly small. One must expect that the boundary layer would experience a much reduced growth rate if this ratio is increased.

CONCENTRATION DISTRIBUTIONS IN THE DISTURBED BOUNDARY LAYER

The parameters of the concentration distributions are tabulated in Table 1. Examples of concentration distributions of the ammonia gas in the disturbed boundary layer are shown in dimensionless form in Fig. 8. The length coordinate y has been made dimensionless by dividing it through λ . The concentrations have been divided by the ground level concentration c_{max} . Except for the data corresponding to short distances X , the results confirm a similarity law for the concentrations in the disturbed boundary layer. For small x , the profiles show smaller changes near the floor. It is found that in the separation bubble, the

vertical concentrations are essentially constant, with a magnitude given by the concentrations near the separation streamline.

The similarity profiles for large distances X can be expressed well by Eq. 4. However, an exponent α of 1.6, fits the data better than the value of 1.8 found by Malhotra and Cermak (1964). The exponent α was first obtained by a computer using a method of least squares, but the data at large values of y/λ introduced too strong a bias on the computer calculations. Therefore, the exponent was determined from a graphical presentation of Eq. 4, as is shown in the example of Fig. 9.

With the concentration distributions expressed through Eq. 4, one must determine the scale parameters λ and c_{max} in order to fully

TABLE 1

h (cm)	X (cm)	$\frac{\lambda u_a c_{max}}{G}$	u_a (m/sec)	λ (cm)	c_{max} (-) 10^6	c_{max}/G (sec cm/cm^3) $.10^3$
1.27	46	2.73	2.74	3.7	657	2.7
	92		2.74	5.2	532	1.92
	137		2.74	6.0	346	1.67
	228		2.74	6.3	309	1.58
	318		2.65	9.3	263	1.12
	408		2.79	10.3	229	0.95
2.54	92	2.83	2.89	6.3	350	1.56
	137		2.85	7.5	290	1.33
	228		2.74	9.8	245	1.05
	318		2.79	13.0	178	0.78
	408		2.85	12.2	153	0.82
3.81	46	2.89	2.94	8.5	518	1.15
	92		2.74	8.5	327	1.24
	137		2.74	10.6	281	1.00
	228		2.74	11.7	224	0.91
	318		2.67	15.2	179	0.73
5.08	46	2.94	2.74	12.9	458	0.84
	92		2.86	13.1	242	0.78
	137		2.67	14.0	219	0.79
	228		2.71	15.0	153	0.71
	318		2.71	20.0	123	0.54
	408		2.71	22.0	120	0.49

specify the concentration distribution. In the following discussion, the growth of λ shall be related for the final zone to the growth of the boundary layer thickness δ . The velocity and concentration distribution laws, δ as function of X , and the total diffused mass are then used to calculate the decrease of ground level concentration with distance.

In agreement with experimental results of other investigators, for example Poreh and Cermak (1964), the length scale λ should be a function of x , where x is the distance from the source. However, when the effect of the fence on the flow is taken into consideration, it is realized that the strong shear at the sharp edge of the fence generates such a high turbulence level that all spreading that had taken place before the diffusion cloud reached the fence edge is insignificant compared to that which occurs downstream from the fence. Therefore, the diffusion cloud should behave somewhat like a diffusion cloud emitted from an elevated line source, with an elevation of the order of the fence height and located at $X = 0$. For this reason, λ was plotted against X in Fig. 10 .

The fence height strongly influences the initial growth of the diffusion cloud. In the logarithmic presentation of Fig. 10, curves corresponding to increased fence heights are shifted parallel to the curve for zero fence height, with equal increments in height causing equal logarithmic increments in λ . This implies that λ increases exponentially with the fence height. A sharp edged fence is, therefore, a very efficient device for rapidly spreading out gas clouds.

With increasing distances X , the diffusion cloud grows slower than according to a power law with an exponent of 0.8 . It is not certain whether this is attributable only to the decaying turbulence level, because, for the present data, the growth of the diffusion cloud is restricted by the edge of the boundary layer. In order to illustrate this point, the ratio λ/δ was noted down on each of the data points, and it is seen that the data reach a ratio of λ/δ of about 0.68 already at fairly short distances X .

With the length scale λ proportional to δ, the ground level concentrations can be calculated by considering the mass conservation equation

$$G = \int_0^{\infty} u \cdot c \, dy \qquad (12)$$

where G is the gas discharge of the line source per unit width and unit time. The upper limit of the integral can be replaced by δ without great error. Inserting the similarity laws for velocity and concentration distributions, Eqs. 11 and 4 into Eq. 12, yields:

$$G = \delta u_a c_{max} \left[\int_0^{\frac{\delta'}{\delta}} e^{-\ln 2 \left(\frac{y}{\lambda}\right)^{1.6}} \left\{ \frac{u_{*i}}{k u_a} \ln \frac{y}{\delta} + 0.75 + 0.23 \frac{u_{*i}}{u_{*o}} \right\} d\left(\frac{y}{\delta}\right) \right.$$

$$\left. + \int_{\frac{\delta'}{\delta}}^{1} e^{-\ln 2 \left(\frac{y}{\lambda}\right)^{1.6}} \left\{ \frac{u_{*o}}{k u_a} \ln \frac{y}{\delta} + 0.98 \right\} d\left(\frac{y}{\delta}\right) \right]$$

For the final zone, $\delta'/\delta = x'$ is given by Eq. 10, and $\lambda = 0.68\,\delta$. In terms of these variables, Eq. 12 becomes:

$$G = \delta u_a c_{max} \left\{ \frac{u_{*o}}{k u_a} \left[I_1'(x') \left(\frac{u_{*i}}{u_{*o}} - 1 \right) + I_1'(1) \right] + 0.23 \left(\frac{u_{*i}}{u_{*o}} - 1 \right) I_2(x') + 0.98\, I_2(1) \right\} \qquad (13)$$

where

$$I_1'(x') = \int_0^{x'} e^{-1.29 \left(\frac{y}{\delta}\right)^{1.6}} \ln \frac{y}{\delta} \, d\left(\frac{y}{\delta}\right) = 0.435\, I_1(x')$$

and

$$I_2(x') = \int_0^{x'} e^{-1.29 \left(\frac{y}{\delta}\right)^{1.6}} d\left(\frac{y}{\delta}\right) .$$

The integrals I_1 and I_2 have been determined numerically and are plotted in Fig. 11.

From Eq. 13, the ground level concentrations were calculated. It was found that for the experimental data the effect of u_{*i} was very small. Since u_{*i} was not known, values of $G/\delta\, u_a\, c_{max}$ were calculated with u_{*i} ranging from 8.5 to 11.6 cm/sec. The variation in $G/\delta\, u_a\, c_{max}$ was found to be less than 1% over this range of u_{*i}-values, while it changed from 0.50 to 0.54 with increase in the fence heights considered. The ground level concentration was calculated from the results by using experimental values of u_a and λ as given in Table 1. The results are compared with the experimentally found c_{max} values in Fig. 12. Except for the highest concentrations, which are found at short distances X, the agreement of the experimental data with the calculated data is good. All the data fall within the band given by the likely error of $\pm$ 30 ppm. It is thus demonstrated that the final zone diffusion is well represented by the distribution law Eq. 4, the development of the boundary layer thickness, and the velocity distribution law Eq. 11.

ACKNOWLEDGMENTS

Financial support for this study has been given by the Agricultural Research Service under Contract No. 12-14-100-45 46 (41) and by the U. S. Army, Fort Huachuca, under Grant No. DA-SIG-36-039-62-G24. H. Shokouh, A. A. Quraishi and R. D. Marshall helped with gathering the experimental data. Valuable comments by Dr. J. Deardorff are gratefully acknowledged.

BIBLIOGRAPHY

Batchelor, G. K., (1959), "Note on the diffusion from sources in a turbulent boundary layer" Unpublished.

Cermak, J. E., (1963), "Lagrangian similarity hypothesis applied to diffusion in turbulent shear flow", J. Fluid Mech., Vol. 15 Pt. 1, pp. 49-64.

Dyer, A. J., (1963), "The adjustment of profiles and eddy fluxes", Quart. J. Roy. Met. Soc., Vol. 89, pp. 276-280.

Elliott, W. P., (1958), "The growth of the atmospheric internal boundary layer", Trans. Am. Geophy. Union, Vol. 39, pp. 1048-1054.

Ellison, T. H., (1959), "Turbulent diffusion", Science Progress, Vol. 47, pp. 495-506.

Malhotra, R. C., and J. E. Cermak (1964), "Mass diffusion in neutral and unstably stratified boundary layer flows", Int. J. Heat and Mass Transfer, Vol. 7, pp. 169-186.

Nagabhushanaiah, H. S., (1961), "Separation flow downstream of a plate set normal to a plane boundary", Ph. D. Dissertation, Civil Engr. Dept., Colorado State University, Fort Collins, Colorado.

Plate, E. J., (1966), "Ein Beitrag zur Berechnung von Austauschvorgängen in der durch eine Wand gestorten bodennahen Luftschicht." Doctoral dissertation, Department of Civil Engineering, Technische Hochschule Stuttgart, Stuttgart, Germany.

Poreh, M., and J. E. Cermak (1964), "Study of diffusion from a line source in a turbulent boundary layer", Int. J. Heat and Mass Transfer, Vol. 7, pp. 1083-1095.

Schlichting, H., (1960), "Boundary layer theory", Fourth edition, McGraw-Hill, New York, N. Y.

Taylor, G. I., (1921), "Diffusion by continuous movement", Proc. London Math Soc., Vol. 20, pp. 196-212.

Taylor, R. J., (1962), "Small scale advection and the neutral wind profile", J. Fluid Mech., Vol. 13, pp. 529-539.

Townsend, A. A., (1965a), "Self preserving flow inside a turbulent boundary layer", J. Fluid Mech., Vol. 22, pp. 773-797.

Townsend, A. A., (1965b), "The response of a turbulent boundary layer to abrupt changes in surface conditions", J. Fluid Mech, Vol. 22, pp. 799-822.

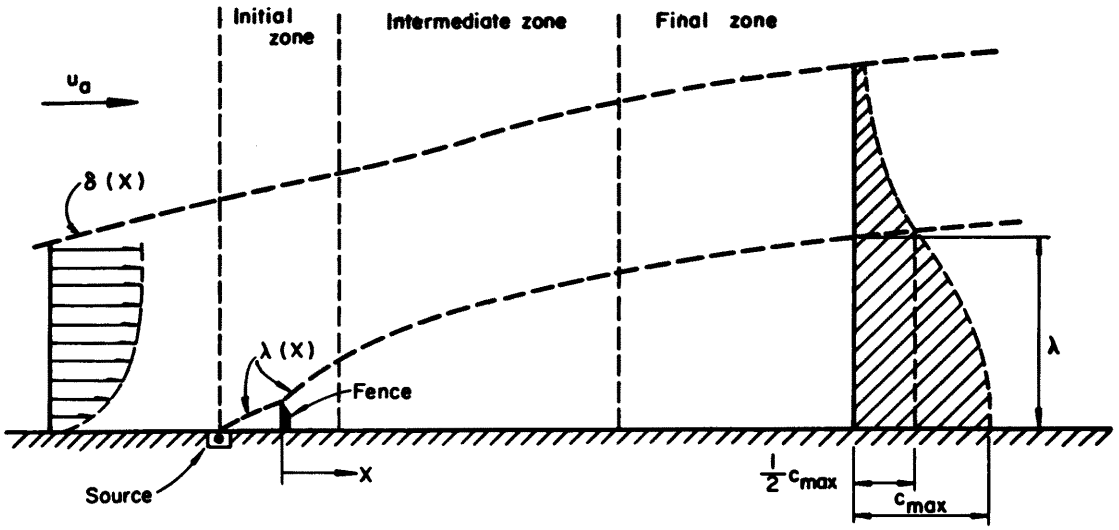

FIG. 1 THE ZONES OF DIFFUSION IN A DISTURBED BOUNDARY LAYER

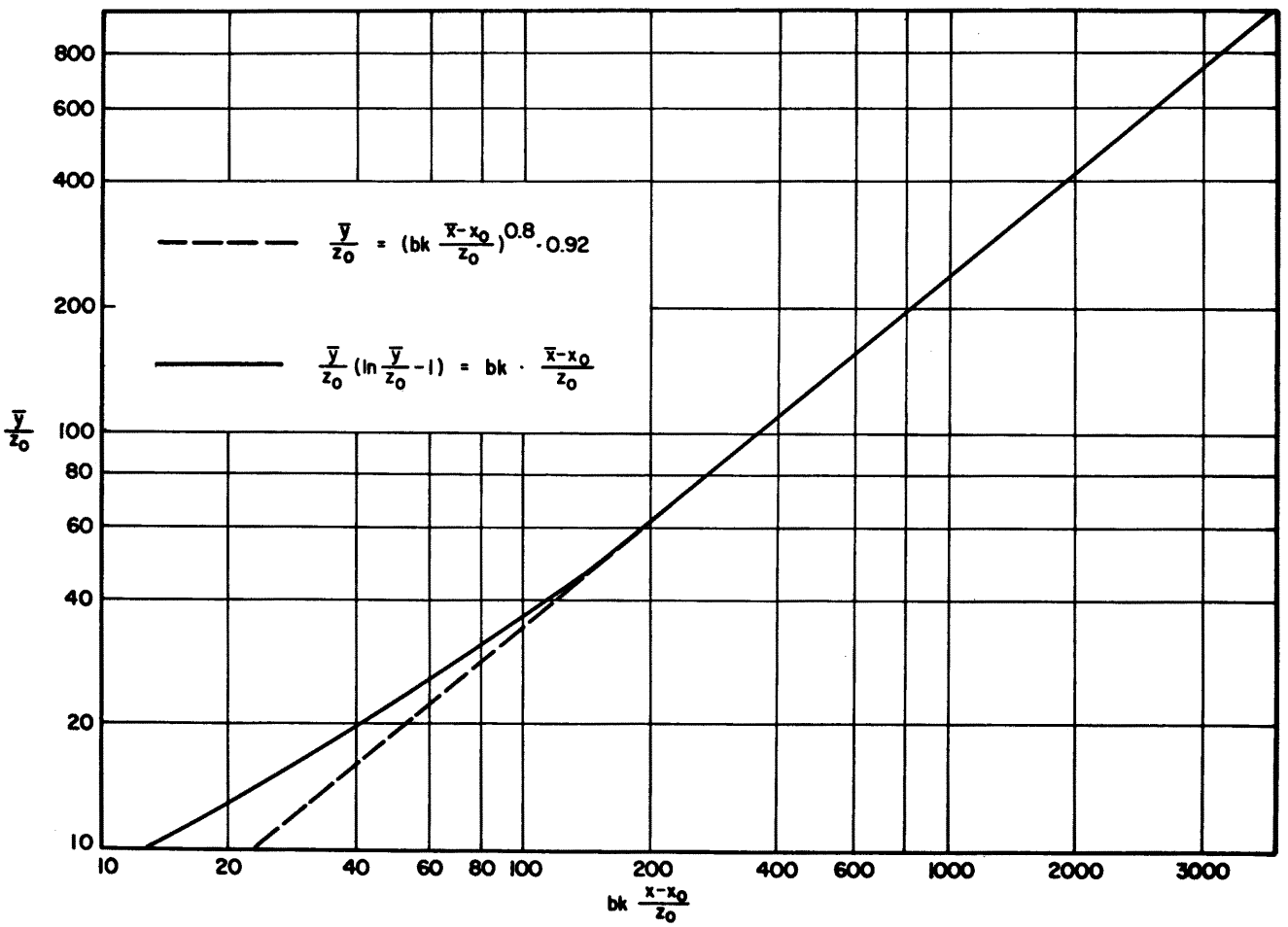

FIG. 2 THEORETICAL GROWTH OF DIFFUSION LENGTH SCALE WITH DISTANCE.

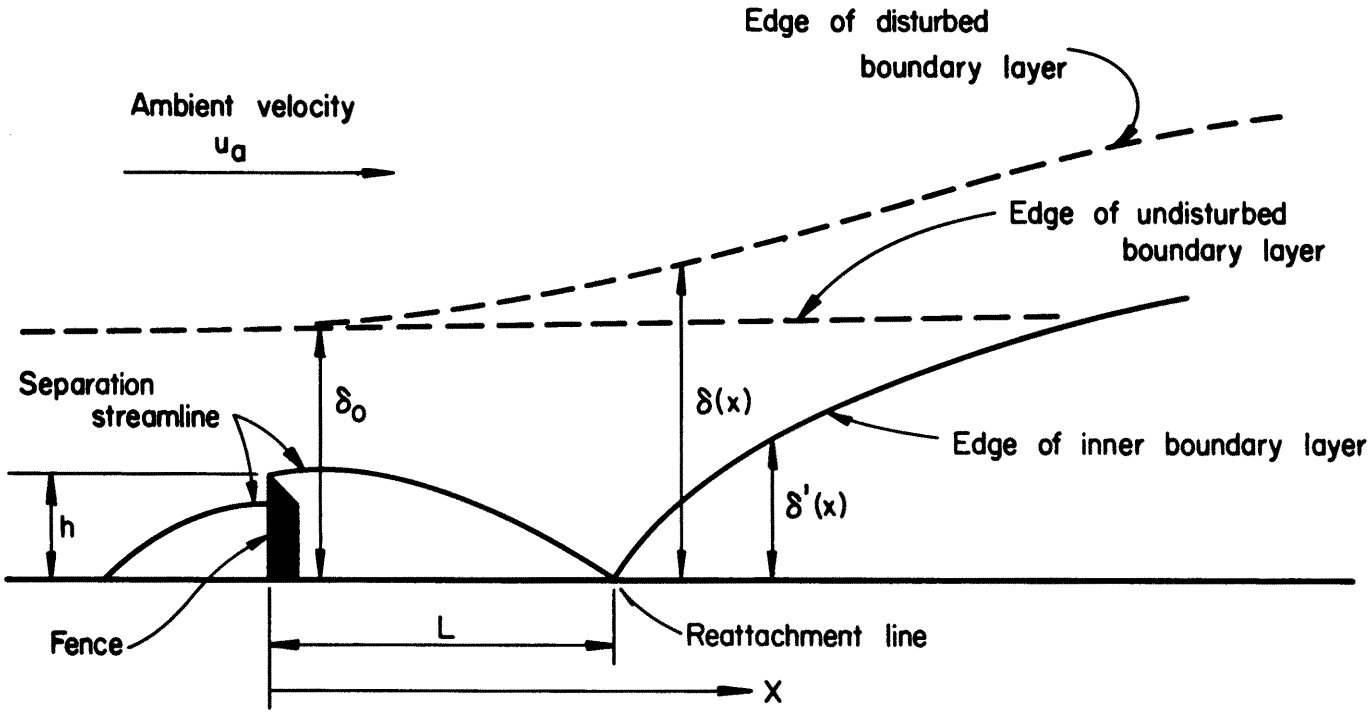

FIG. 3 FLOW REGIONS OF THE DISTURBED BOUNDARY LAYER

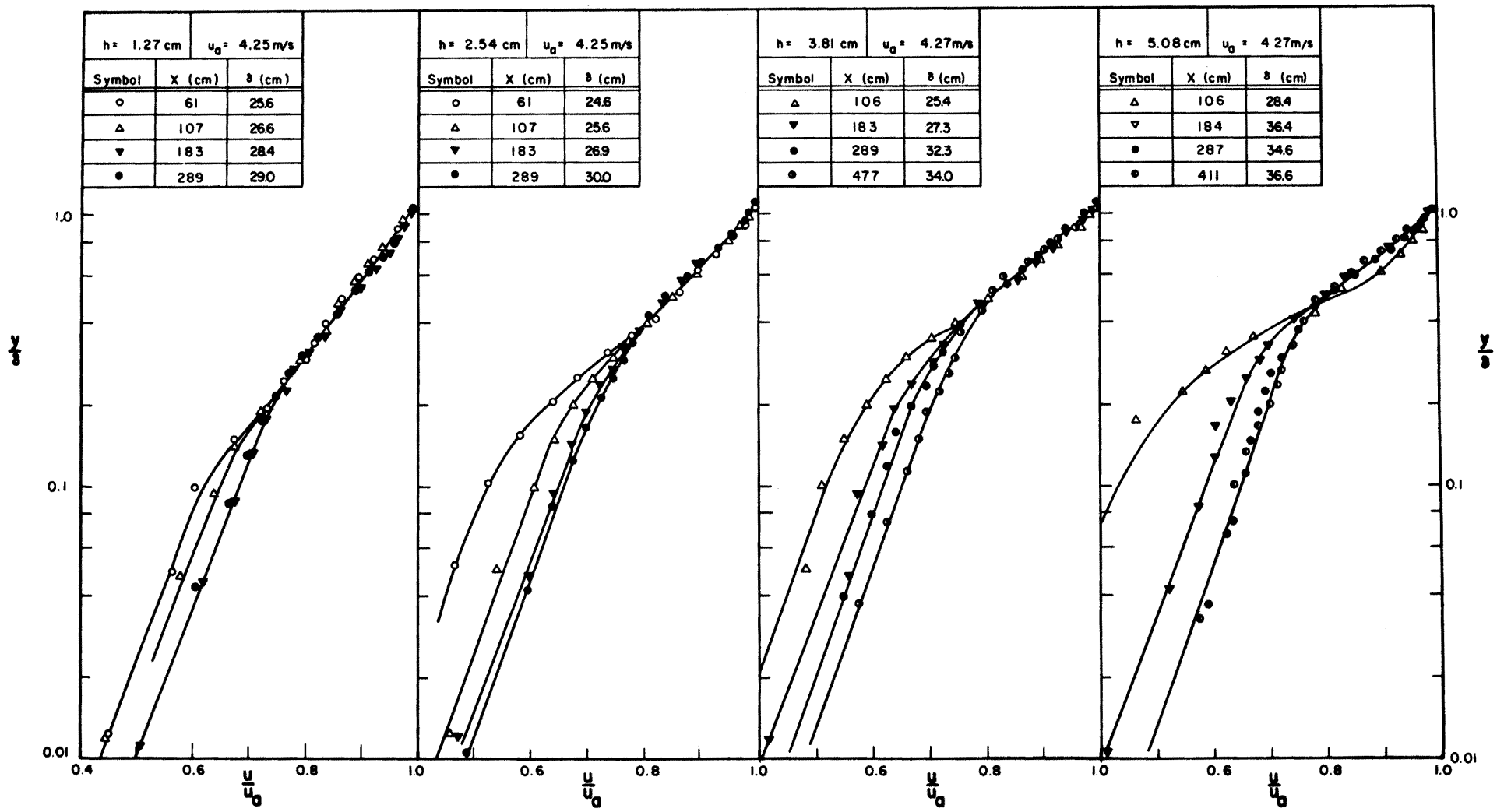

FIG. 4 DIMENSIONLESS VELOCITY DISTRIBUTIONS

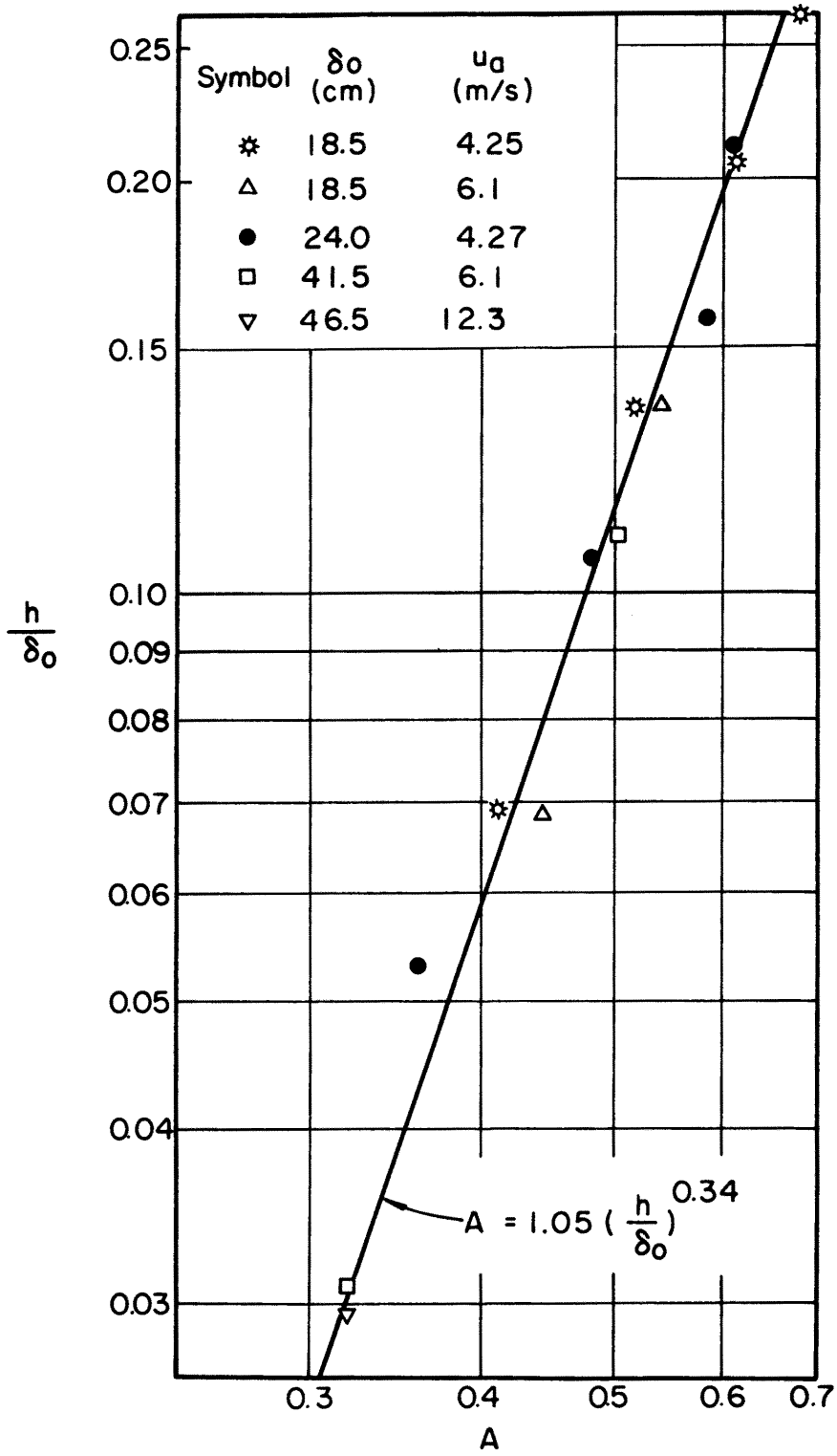

FIG. 5 A AS FUNCTION OF $\frac{h}{\delta_o}$

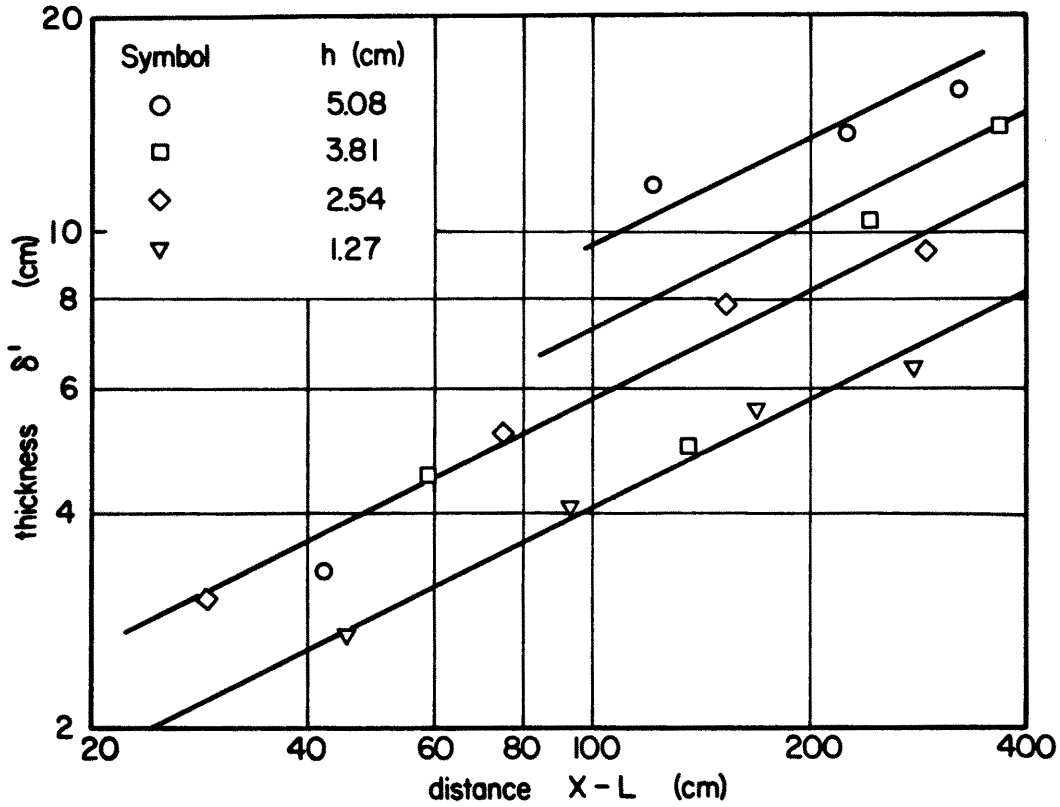

FIG. 6 THE GROWTH OF THE INNER BOUNDARY LAYER

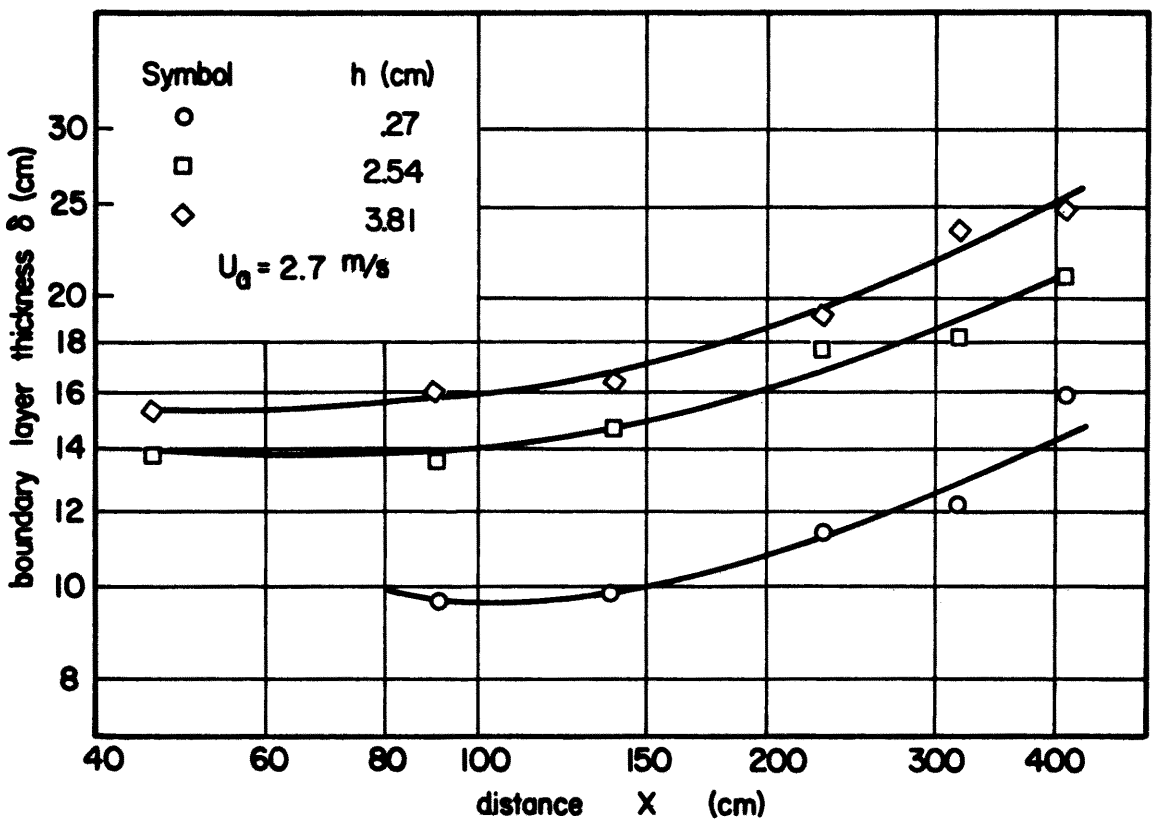

FIG. 7 BOUNDARY LAYER THICKNESS δ AS FUNCTION OF X

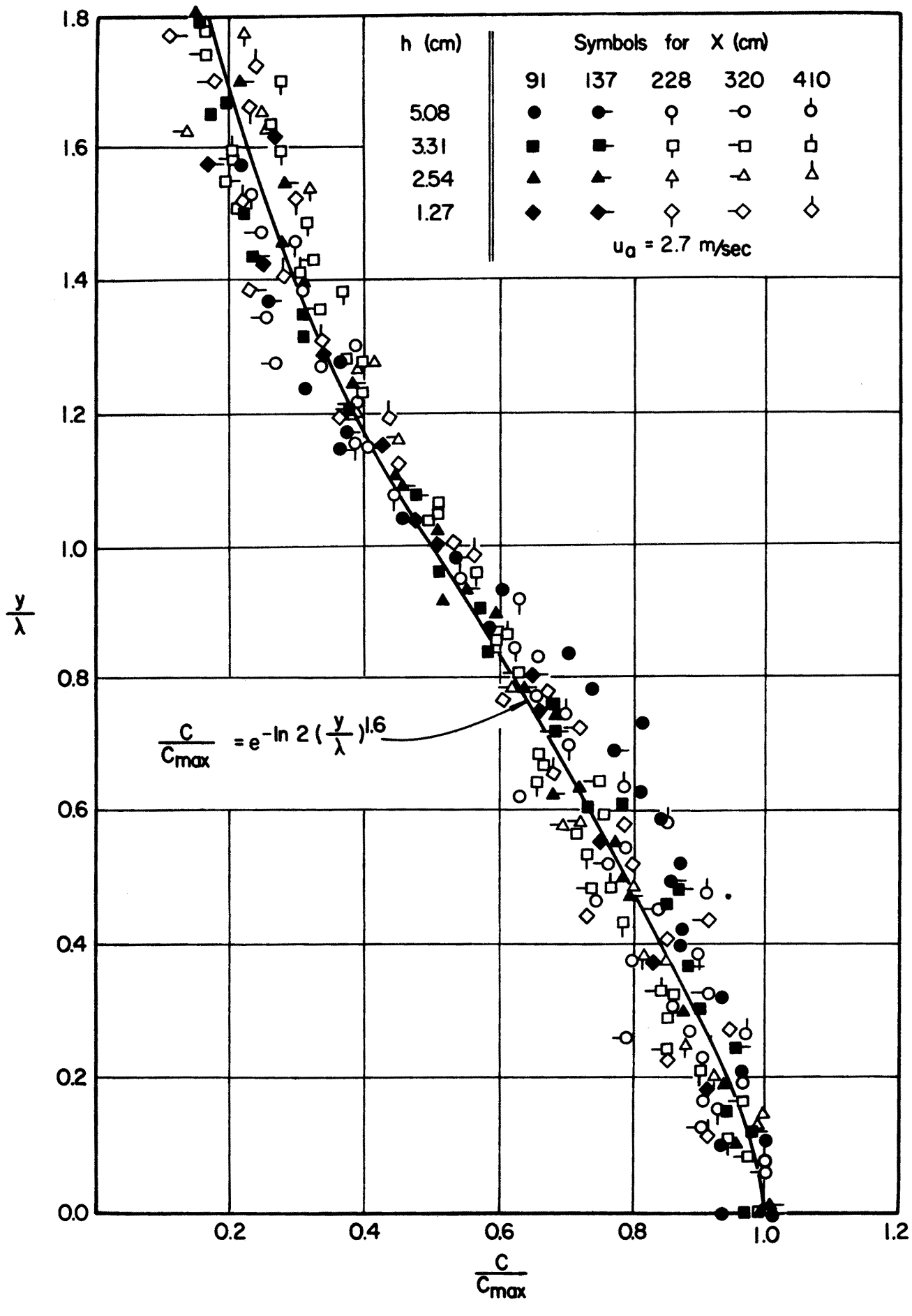

FIG. 8 DIMENSIONLESS CONCENTRATION PROFILES.

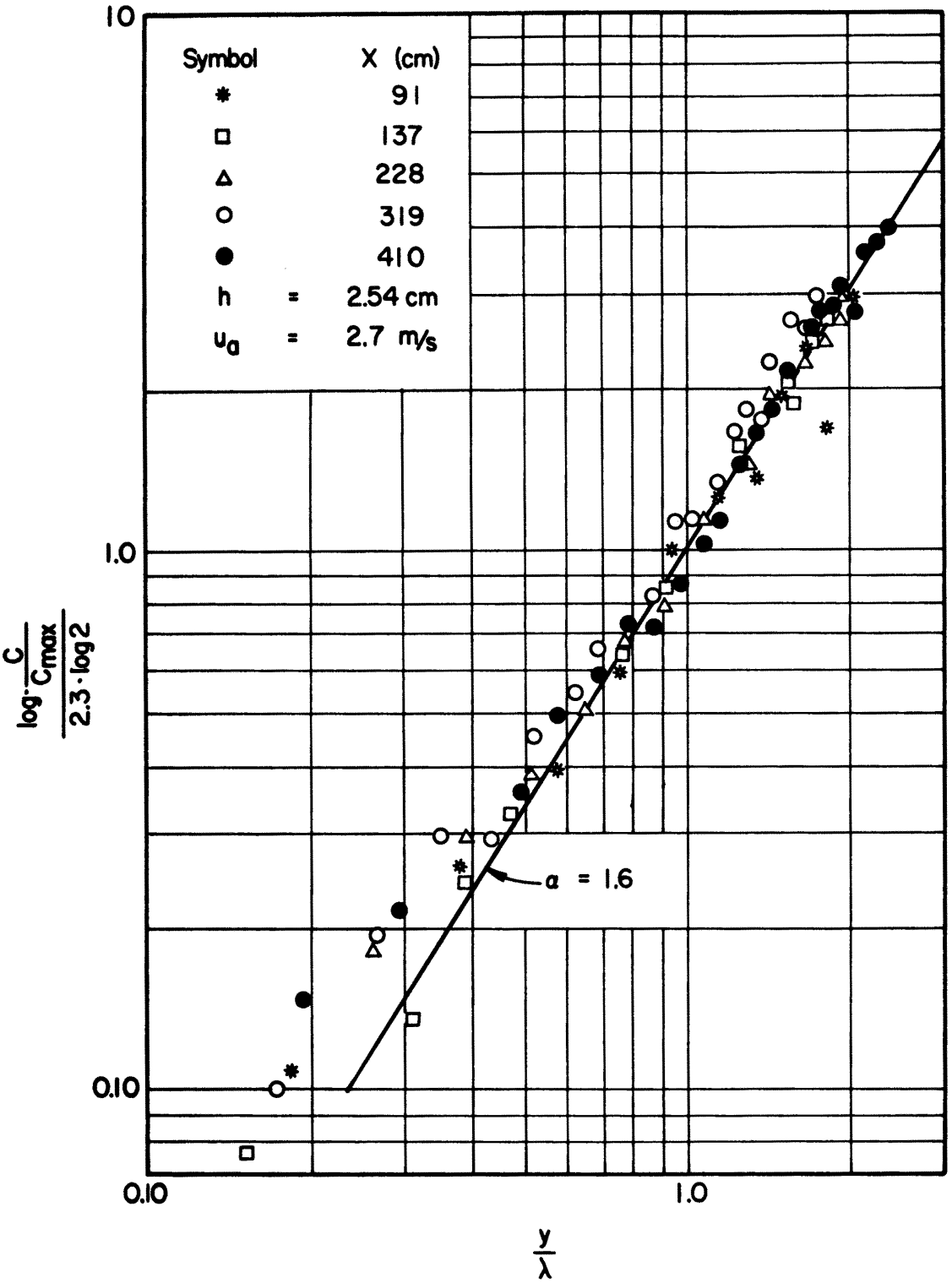

FIG. 9 EXAMPLE FOR THE DETERMINATION OF THE EXPONENT α.

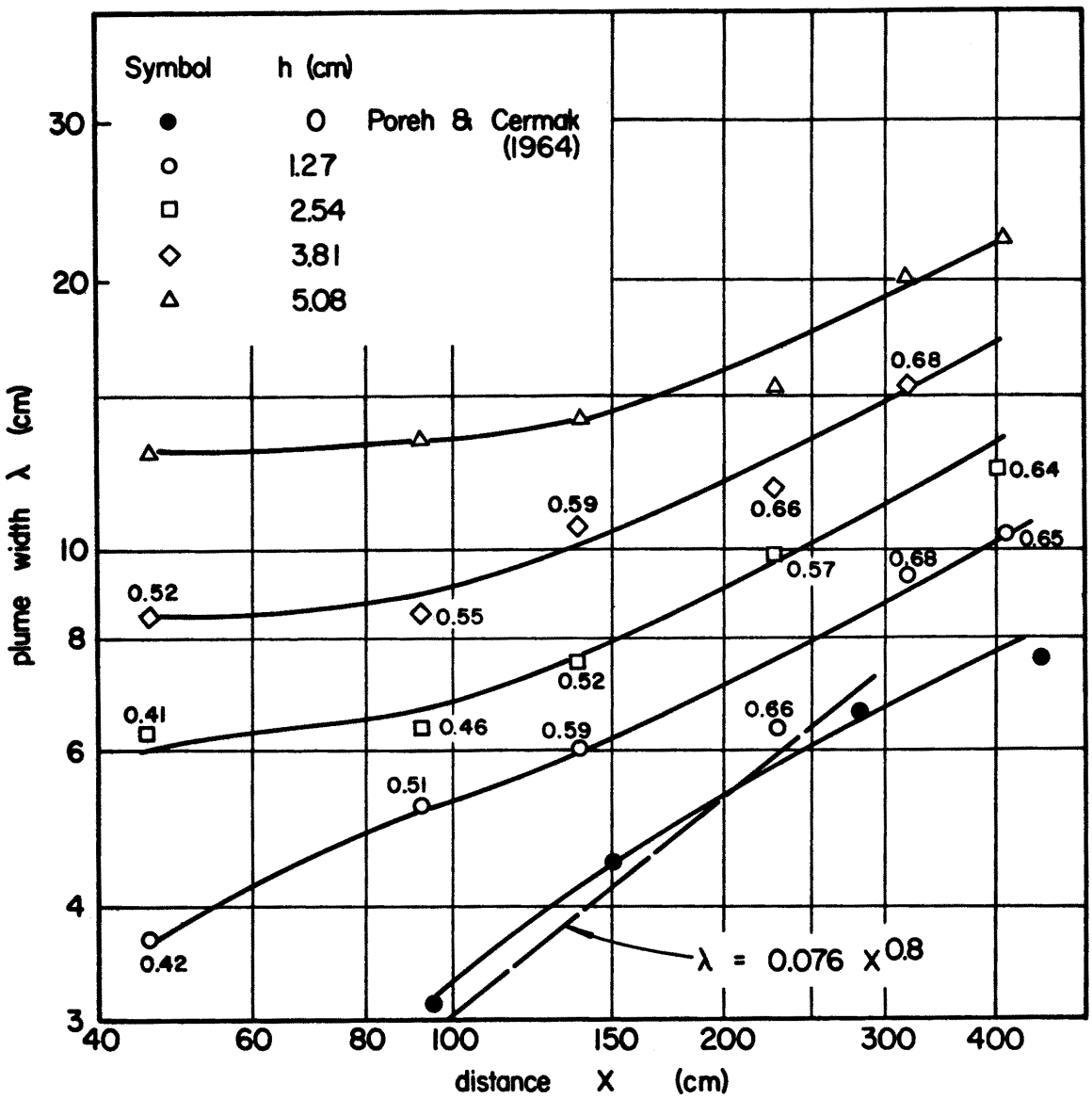

FIG. 10 THE PLUME WIDTH λ AS FUNCTION OF X.

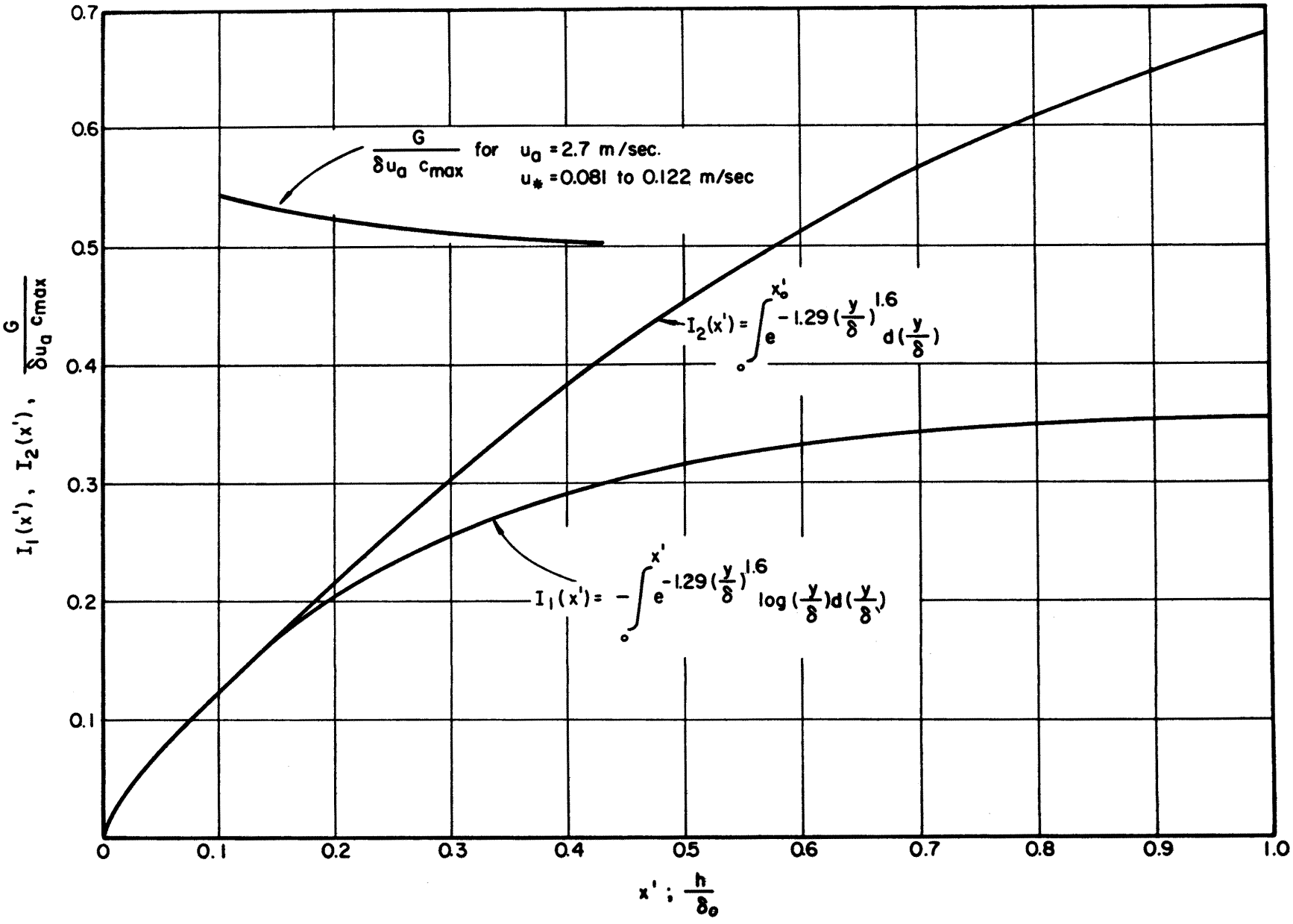

FIG. 11 FUNCTIONS FOR CALCULATING THE GROUND CONCENTRATIONS

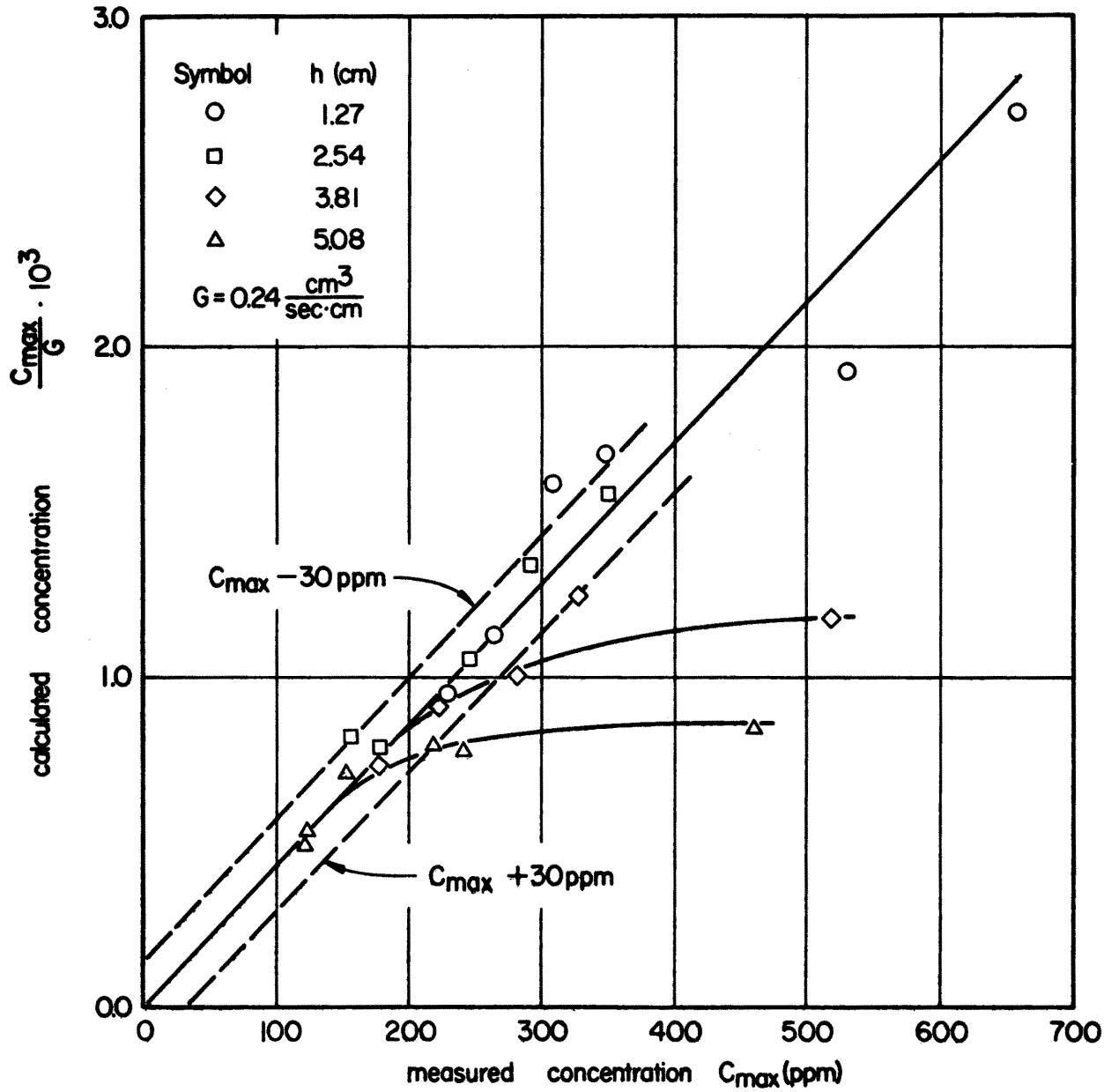

FIG. 12 COMPARISON OF CALCULATED AND MEASURED MAXIMUM CONCENTRATION.